Department of Electrical and Computer Engineering

Centre for Smart Grid and Sustainable Power systems

On Line Condition Monitoring of Wind Turbine Generators

Abdulwahed Almokhtar Salem

This thesis is presented for the

Degree of Doctor of

Philosophy

Of

Curtin University

August 2016

Contents

List of Figures

List of Tables

Abbreviations

HAWTs *Horizontal –axis wind turbines*

IEA *International energy association*

IEC *International Electrotechnical Commission*

CM *Condition monitoring*

CMSs *Condition monitoring systems*

CM WTs *Condition monitoring of Wind turbines*

WECSs *Wind turbine conversion systems*

WRSG *Wound- rotor Synchronous generators*

DFIG *Doubly fed induction generator*

OCMSs *on line condition monitoring systems*

SCIGs *Squirrel cage induction generators*

IPS *Instantaneous power spectrum*

MCW *Morlet continuous wavelet*

DWT *Discrete wavelet transform*

STATCOM *Static synchronous compensator*

DWT *Discrete wavelet transform*

CWT *Continuous wavelet transform*

IMs *Induction machines*

CMFDS *Condition monitoring fault diagnoses scheme*

HSS *High speed stage*

LSS *Low speed stage*

COT *Computed order tracking*

AMFM *Amplitude modulation and frequency modulation*

MED Minimum entropy deconvolution.

FFT Fast Fourier transform

TSA Time signal averaging

ISOVG International Standards Organisation Viscosity Grade

Declaration

I certify that

- All the work has been done in this thesis is my own work unless acknowledged.
- The outcome of this thesis has not been submitted to any other institute for any academic degree.

Signature: ……..

Date: ……

Acknowledgements

The completion of a PhD thesis is a challenging undertaking, and without the guidance, support and suggestions I have received, it would not have been achievable. I would like to express my most sincere appreciation to all the people who helped me attain my goal.

I would like to thank my supervisor, Associate Professor Ahmed Abu-siada, and Co-Supervisor, Professor Syed Islam, Electrical Engineering Department, for their support and encouragement, which motivated me to finish this work.

I would like to thank Associate Professor, Ian Howard, Mechanical Engineering Department, for his visits to the power laboratory and his valuable suggestions regarding the test rig setup.

I would also like to thank all the power laboratory technicians for their help during the research period.

Finally, I would like to thank my wife, for her patience in my absence and her continuous encouragement and support. I am so grateful for my children, "Raghd, Haroon and Roaa," and I look forward to making up for any lost time upon completion of my study.

Dedication

To my parents, Almokhtar and Elshikha, for their endless love and support throughout my life, and to my dearest wife and children, for their support and patient of my absence during the course of my study.

Journal Papers

I. A. Salem, A. Abu-Siada, and S. Islam, "Condition Monitoring Techniques of the Wind Turbines Gearbox and Rotor," International Journal of Electrical Energy, vol. 2, pp. 53-56, 2014.

II. Salem, Abdulwahed, A. Abu-Siada, and S. Islam. "Application of Order Analysis to Diagnose Fatigue within Wind Turbine Gearbox." Technology and Economics of Smart Grids and Sustainable Energy 2.1:3, (2017).

III. Salem, Abdulwahed, Ahmed Abu-Siada, and Syed Islam. "Improved condition monitoring technique for wind turbine gearbox and shaft stress detection." IET Science, Measurement & Technology (2017).

IV. A. Salem, A. Abu-siada, and S. Islam, "Improved Condition Monitoring Technique to Detect Incipient Mechanical Faults of Wind Turbine Drivetrain," IEEE Transactions on Energy Conversion, special issue on Modeling and Advanced Control of Wind Turbines/Wind Farms, 2016. (Extended abstract accepted)

V. A. Salem, A. Abu-Siada, and S. Islam, "Impact of Gearbox Oil Contamination on the Performance of the Wind Turbine Drivetrain," International Journal on Renewable Energies and Power Quality, vol. 14, pp. 230-234, 2016.

Conference Papers

I. A. Salem, A. Abu-Siada, and S. Islam, "Condition Monitoring Techniques of the Wind Turbines Gearbox and Rotor," presented at the International Journal of Electrical Energy, Paris, 2014. (Selected for the journal).

II. A. Salem, A. Abu-Siada, and S. Islam, "Impact of Gearbox Oil Contamination on the Performance of the Wind Turbine Drivetrain," presented at the International Conference on Renewable Energies and Power Quality, Madrid, 2016. (selected for the journal)

Abstract

Condition monitoring (CM) has been widely used to detect mechanical and electrical faults of wind turbine (WT) in order to avoid any potential catastrophic failures, reduce operation and maintenance costs, and enhance the reliability and availability of the equipment. Although several studies concerning wind turbine condition monitoring can be found in the literatures, it is still a challenge to adopt a reliable and cost effective technique to protect wind turbines from severe mechanical stress due to the harsh weather conditions they are exposed. Although statistical studies show that gearbox failure rate is low, the resulting downtime and cost for replacement or repair is substantial. For these reasons and due to the global significant increase in wind energy conversion systems (WECS), a reliable and cost effective condition monitoring technique is essential to maintain the availability and improve the reliability of wind turbines (WTs).

In order to investigate the fault detection accuracy of the common signal processing techniques, this study employs an improved technique to monitor and compare the condition of the wind turbine gearbox based on gearbox vibration and shaft torque signatures. Based on Practical Measurement, and conducted on a test rig that emulates real wind turbine operation, a system was developed to analyse the behaviour of a wind turbine under various mechanical fault levels. Shaft torque and mechanical vibration signals were detected using high resolution sensors and analysed using two signal processing techniques: 1) wavelet and 2) order analyses. The impact of chosen fault levels on the wind turbine drivetrain was also investigated.

Both signal processing techniques were then compared, based on their sensitivity to detect incipient fault conditions. In the test rig, the model based control technique was applied using voltage slider, whereby a current was injected through the induction generator stator terminals to control the torque. This emulated real fault conditions on the wind turbine blades, including ice accumulation, wind share, and gust wind. The applied technique

successfully and effectively improved detection accuracy when monitoring drivetrain mechanical stress, including gearbox and shaft.

This thesis also compares two different types of lubrication oil, which are tested during the monitoring process of fault detection, as well as several lubrication oil contamination scenarios that are applied on the test rig gearbox. The results show that oil viscosity and purity have a significant impact. In order to further clarify the conditions of the wind turbine, in terms of healthy or faulty, a fuzzy logic model was introduced to the case studies in this thesis. Based on the condition of the wind turbine, a reliable asset management decision was also proposed.

Chpater 1 Introduction

1.1 **Background**

Due to the day-to-day increase in load demand, and the harmful environmental impact of fossil fuel-based electricity generation, the global trend is currently focusing on generating electricity from clean renewable resources such as wind.

From as early as the 19th century, small capacity wind turbines were developed in some European countries, including Germany, Denmark, and Belgium. The most common wind turbine type, during that time, was a turbine with two blades [1].

Due to recent degradation and cost increase of conventional fossil fuel, along with the global trend to decrease the greenhouse effect, clean energy production from renewable sources has been given much consideration over the last few decades. Most notably, there has been a rapid increase in wind energy conversion system (WECS), which means that various condition monitoring and fault diagnosis techniques have been developed to detect incipient mechanical and electrical faults and mitigate any catastrophic failures to wind turbines.

Improvement to the mechanical strain of wind turbines is achieved by applying direct control to the induction generator electromagnetic torque [2]. Failure of specific wind turbine components, such as blades, gearbox, breaking system and tower, may lead to a catastrophic failure jeopardising the whole investment [3, 4]. Many techniques have been published in the literature that monitor the wind turbine. Condition monitoring of the drivetrain is essential to explore incipient faults, allowing effective maintenance and reliability improvement. Various gearbox failures have been investigated in the literature [4].

Over the last three decades in Australia, renewable energy generation has grown rapidly. Based on the Clean Energy Australia report published in 2014, wind energy represents about 31% of the total renewable energy generations as shown in Figure 1.1 and Table 1 [2].

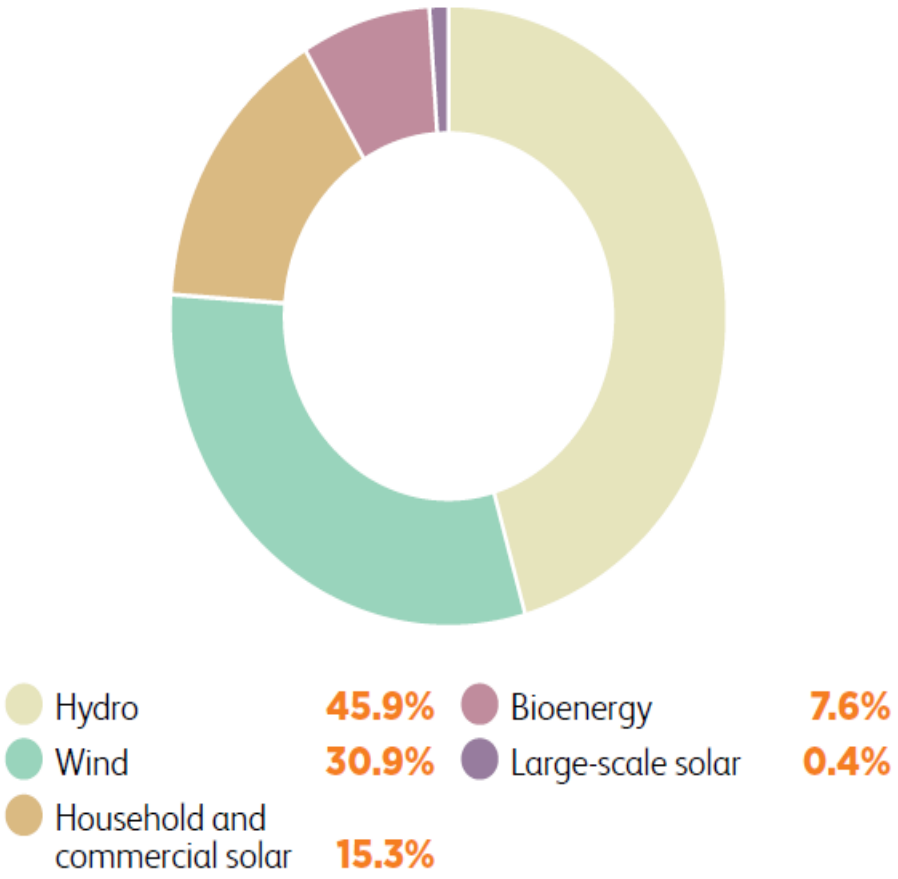

Figure 1.1 Estimated energy contribution of each technology to renewable generation [5].

Table 1.1 Renewable energy generation 2014, Australia [5].

Technology	Generation (GWh)	Percent of renewable generation	Percent of total generation	Equivalent number of households powered
Hydro	14,555	45.9%	6.19%	2,049,900
Wind	9777	30.9%	4.16%	1,377,000
Household and commercial solar <100 kW	4834	15.3%	2.06%	680,900
Bioenergy	2400	7.6%	1.02%	338,000
Large-scale solar5	118	0.4%	0.05%	16,700
Geothermal	0.50	0.002%	0.00%	70
Marine	0.04	0%	0.00%	6
TOTAL	31,684	100%	13.47%	4,462,600

Wind turbine has become a vital renewable energy source worldwide because of its harmless environmental impact and low cost when compared with other renewable energy technologies of the same capacity [6]. Figure 1.2 shows the historical development of wind turbines between 1980, where the tower height was just 15m and turbine capacity was a few kilowatts, and 2020, where tower height is expected to be more than 200m with a wind turbine capacity of up to 20 MW [7].

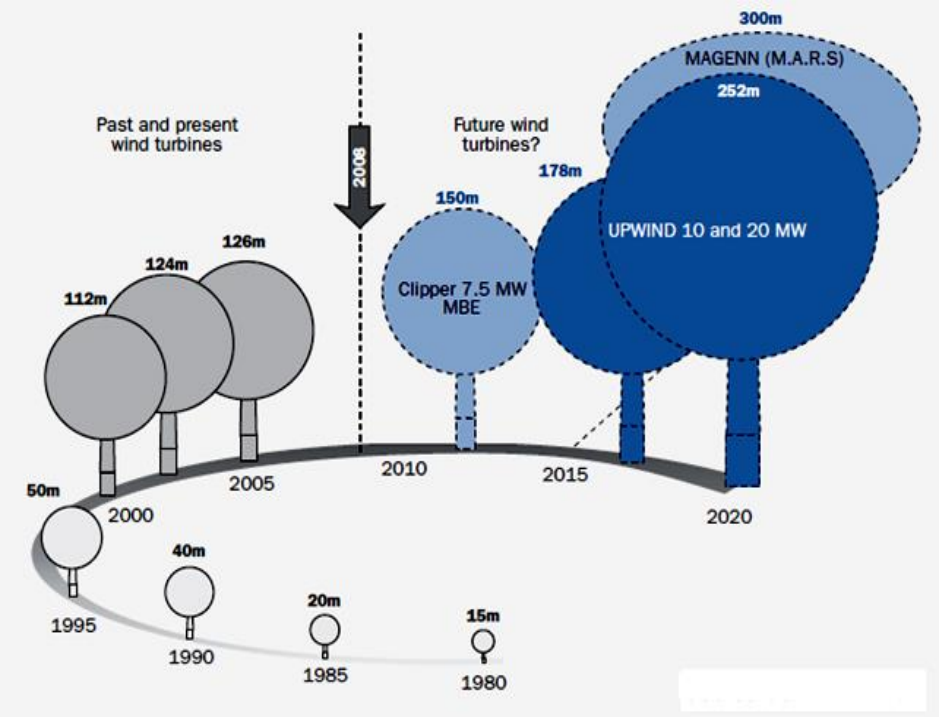

Figure 1.2 Construction development in wind turbine sizes [7].

Late models of wind turbine come in two configurations, depending on the rotor operating principles: 1) horizontal –axis wind turbines (HAWTs) and 2) vertical –axis wind turbines (VAWTs). HAWTs with a three blade configuration are more common [8]. A turbine's optimum performance relies on the blade taper angle and the height of the turbine on the tower.

There is a constant need for the reduction of operational and maintenance costs of Wind Energy Conversion Systems (WECSs). This motivates utilities and wind turbine stakeholders to adopt various condition monitoring techniques to detect incipient faults and to facilitate a proactive response, avoiding any catastrophic failure to the turbine, minimising downtime, and maximising productivity. Occasional malfunction of specific parts (such as blades, gearbox, tower, braking system, etc.) can result not only in high repairing / replacement expenses, but may also lead to a catastrophic failure that endangers the surrounding environment. For these reasons, adopting a reliable condition monitoring technique to detect

incipient faults in the various components of the wind turbine, as shown in Figure 1.3, is essential.

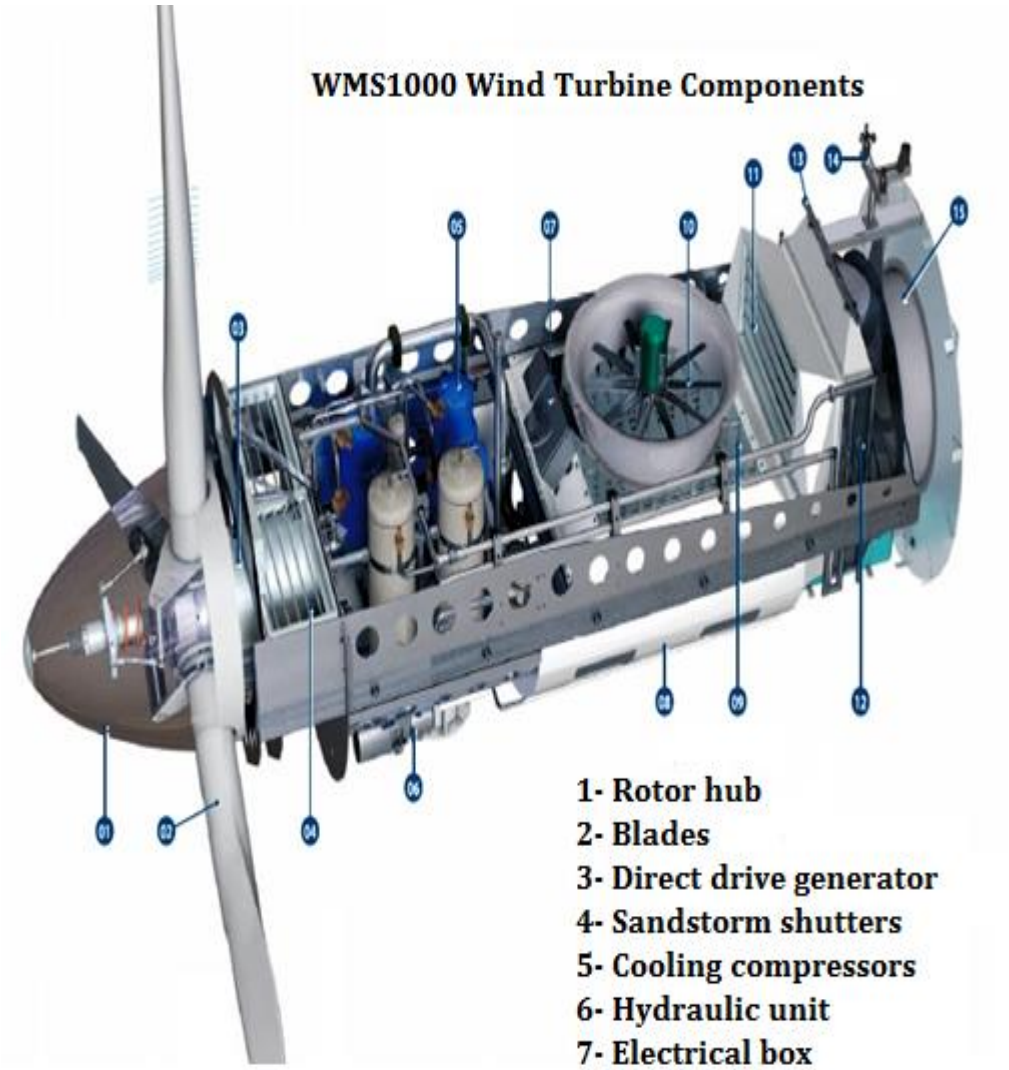

Figure 1.3 Wind Turbine Components

1.2 Contribution and Research Objectives

This thesis aims to introduce an improved online condition monitoring technique for wind turbine drivetrains. In this regard, a scaled down test rig was developed to emulate real wind turbine operation. High

resolution sensors were used to capture the drivetrain vibrations and torque signatures during normal and faulty operating conditions. The captured signals were analysed using signal processing techniques in order to identify and quantify incipient faults in real time. The key objectives of this research are to:

1. Carry out an extensive literature review for determining which state-of-the-art techniques are available for wind turbine condition monitoring and to identify the most common electrical and mechanical faults that wind energy conversion systems may exhibit.
2. Develop a prototype test rig model to investigate the effect of various mechanical and electrical faults on the measured vibration and torque signatures for real time fault detection.
3. Employ an online signal processing technique for fault detection and for analysis of wind turbine mechanical type faults.
4. Propose effective mitigation techniques for the investigated faults and provide a reliable asset management decision based on the wind turbine operating condition.

1.3 Thesis Organisation

- **Chapter -1**

This chapter provides an overview of wind turbine components, the scope of the work, and the main objectives of the thesis.

- **Chapter -2**

An extensive literature review in Chapter 2 reveals the various condition monitoring techniques currently used in wind turbine systems. The chapter also describes the crucial components of a wind turbine.

- **Chapter -3**

In this chapter, the commonly used signal processing and analysis techniques — such as Fourier transform, Wavelet and order analysis -— for

machinery condition monitoring systems are introduced. The advantages and limitations of each signal processing technique are also highlighted and discussed.

- **Chapter -4**

  This chapter details the components of the test rig and explains how various faults are implemented to mimic real wind turbine faults.

- **Chapter -5**

  Chapter 5 presents the main outcomes of the laboratory-based setup measurements. The results are analysed and compared during normal operating conditions and during various faults.

- **Chapter -6**

  In this final chapter, the main conclusion drawn from this research work is summarised. This is followed by recommendations for future work.

Chapter 2 Condition Monitoring of Wind Turbines Failure and Diagnoses

2.1 Introduction

Wind speed is a key aspect in terms of how electricity is generated by the wind turbine. The higher the wind tower, the greater the energy harvest, and even a small change in wind speed can cause a substantial difference in the amount of generated electricity. This is attributed to the non-linear correlation between generated power and wind speed [9]. Figure 2.1 shows the key components of the wind turbine (WT), along with the energy conversation system [10]. The diagram illustrates the overall principal of the wind turbine and the supervisory control system.

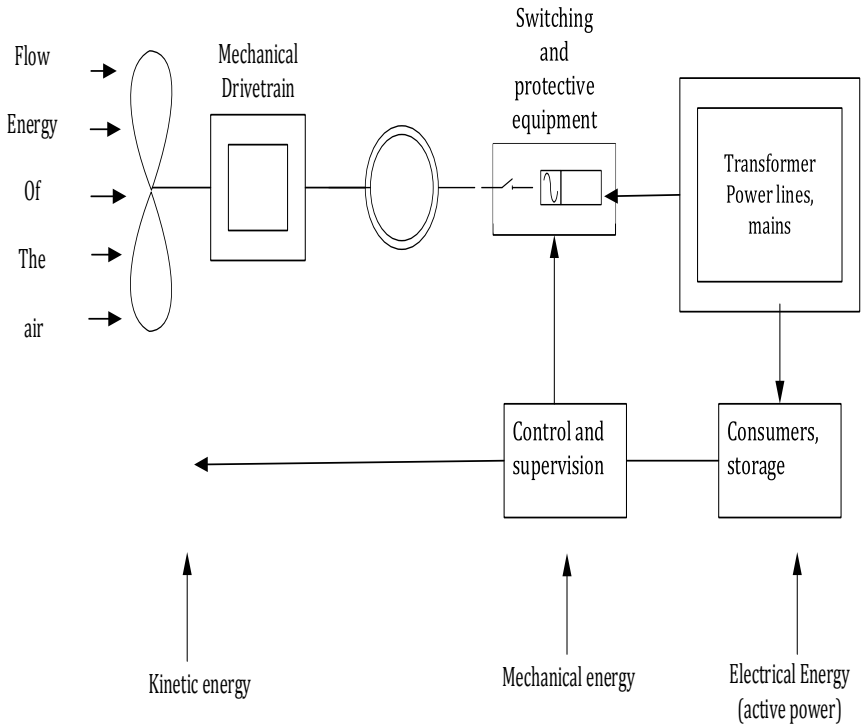

Figure 2.1 Functional chain and conversion stages of a wind energy conversion convertor.

2.2 Power Characteristics of a Wind Turbine

The International Energy Association (IEA) in collaboration with the International Electrotechnical Commission (IEC) recommend improvements to a wind turbine's power curve based on the formal standard (IEC61400-12) of measurement [7].

The conventional power curve, correlating to the mechanical power P_M generated by wind speed v_w (as shown in Figure 2.4), is characterised by three wind speeds, namely: 1) cut-in wind speed, 2) rated wind speed, and 3) cut-out wind speed [8]. These speeds are defined below:

- *Cut-in wind speed*: is measured from the commencement of the turbine's operation until it starts to deliver power.
- *Rated wind speed*: is the speed corresponding to rated output power.
- *Cut-out wind speed:* is the highest level of wind speed at which a turbine should operate, and when a turbine should be stopped to protect it from severe wind damage.

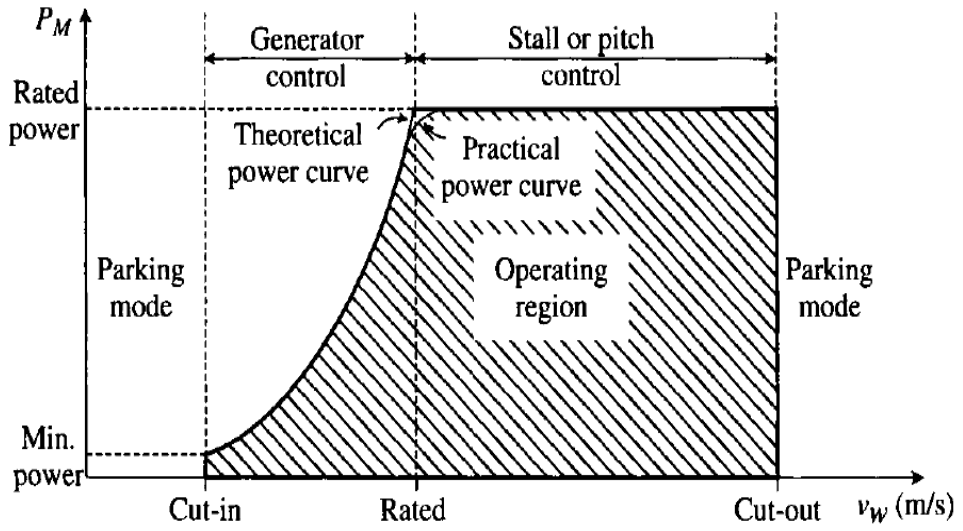

Figure 2.2 Qualitative turbine mechanical power versus wind speed curve[8].

The WT at the cut-in stage captures a wind speed that allows blade movement. When the wind speed increases, a variable speed controller is required, while the captured power at the rated stage is controlled by the blades' aerodynamic system. This procedure of action requires different mechanism steps to achieve passive stall, active stall and pitch control [11].

2.3 Wind Turbine Function and Structure

2.3.1 Tower

A high tower is a key element in wind turbine structure and represents about 20% of the overall cost of the WT structure [12]. The output power of the WT's generator rotor increases with the height of the tower, and is also dependent on the proper location of the WT. For example, at inland sites, due to harsh weather conditions (dust accumulation, Birds wastes), where the degree of surface roughness is high, wind speeds increase slowly with the height of the tower. This is compared to shore-based locations, where surface roughness is low and wind speed is also low.

A WT tower can be a steel lattice type or a concrete type. It can also be a free-standing steel tubular tower or a guyed steel tubular tower. Figure 2.3 shows the modern tower, from base to top, and where the nacelle is to be placed [11]. Safety protected ladders, measuring approximately 60-70 metres, are fitted to the top of each platform. For towers higher than 80 m, special safety ladders or climbing lifts are required. The tower includes a transformer, which requires quite a large space at the base. Air conditioning maintains a reasonable temperature inside the tower base room, and a dehumidifying and filtering system is also necessary when avoiding corrosion complications.

2.3.2 Strength and Stiffness Design

In the design stage of the tower, it is essential to calculate tower stiffness and strength to ensure the tower's fatigue strength can withstand massive wind speeds that fluctuate throughout the operational life of the wind turbine (20-30 years).

2.3.2.1 Breaking strength

The static load of the tower is determined by the tower-head weight, the tower's material weight, and the aerodynamic rotor thrust. In load cases, which required the breaking strength for the tower to be tested, the tower's highest bending moment was determined with rotors ''without blade pitch control (stall-controlled turbines) or when the worst rotor blade position'' was demanded [11].

2.3.2.2 Stiffness

The stiffness calculation is based on the first specific natural bending frequency and with respect to other frequencies, such as torsion frequency, that relate to the yaw system dynamics of the wind turbine as a whole.

2.3.2.3 Fatigue Strength

The propulsive force that the WT rotor faces during operation, and as a result of the wind speed variation, has a significant impact on the fatigue lifespan of the tower and, in particular, the slender towers. Purely static stress analysis is commonly required by the building authorities for conventional buildings, but is not appropriate for the tower design of a wind turbine [12].

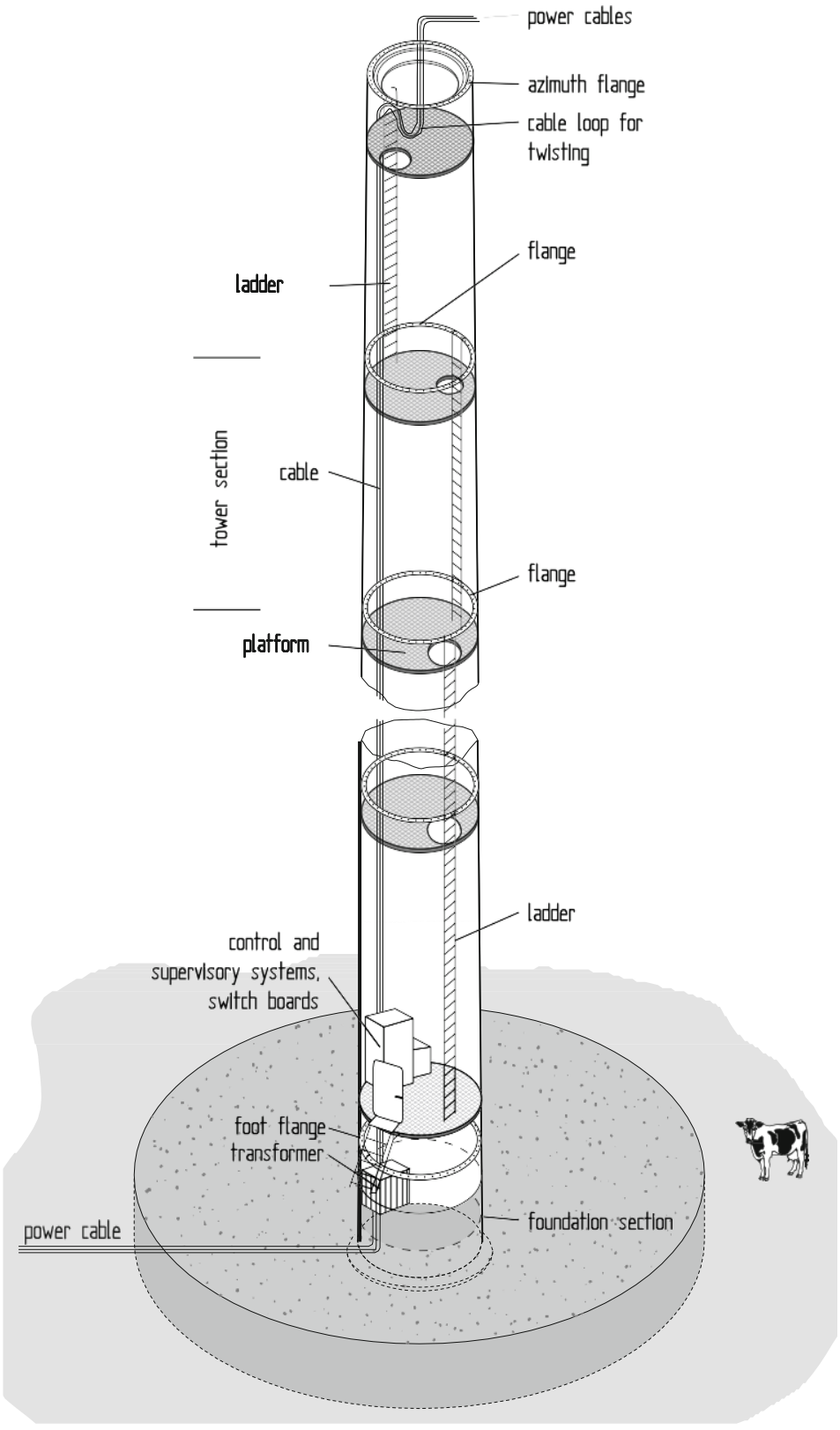

Figure 2.3 Steel tubular tower with installations of a large wind turbine [12].

2.4 Condition Monitoring System (CMS)

To avoid any catastrophic failure to the WT, it is essential to adopt a reliable condition monitoring technique, which ensures timely and proper maintenance. The Condition Monitoring Fault Diagnoses Scheme (CMFDS) gives the operator time and opportunity to prepare the necessary parts prior to the cut-down stage of the machine. The main components of a WT's Online Condition Monitoring System (OCMS) include data acquisition, sensors, fault detection and a diagnosis approach [13]. According to [14], there are two types of condition monitoring techniques currently used in the industry: 1) continuous and 2) periodic. The first scheme continuously monitors the machine and activates all necessary alarms whenever a fault occurs. This method however is expensive and may lead to the mix-up of raw data and noise signals, which can in turn lead to an incorrect diagnosis.

Although several publications can be found in the literatures proposing several methodologies for OCMSs [15-19], investigation is still under way as modern wind turbines become more equipped with a variety of condition monitoring systems (including main and sub-main fault diagnosis systems [20-22].

According to [23], a number of tasks are essential for a successful CMS:

1. Transduction measurement (sensing of primary variables).
2. Data acquisition.
3. Processing and identifying measured data.
4. Fault diagnostics and decision making.

Figure 2.4 shows the main monitoring tasks of which a CMS comprises.

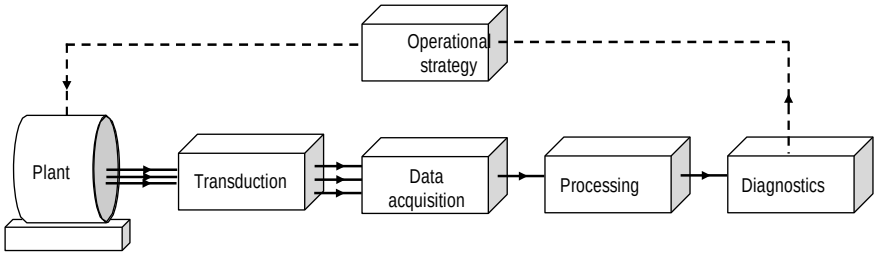

Figure 2.4 Main monitoring tasks [23]

2.4.1 Condition Based Maintenance (CBM)

A Condition Based Maintenance (CBM) approach employs high quality vibration sensors, temperature sensors and torque transducers in order to monitor the condition of the turbine's health and allow a proper maintenance plan to be put in place if any of the measured parameters exceed the pre-known threshold limits. By using a CBM programme, the failure cause is eliminated at an early stage and the unit's productivity, reliability and availability is enhanced.

2.4.2 Wind Turbine Reliability

The journey of WT reliability starts at the manufacturing stage and continues throughout the operational life span of the turbine. Improved reliability of the asset can be achieved by avoiding unreliable suppliers, cheap spares (bearings), careless transportation, and wear and tear to the machine.

Condition monitoring alone does not improve reliability. A pro-active approach must be taken to identify the the cause of the failure, resulting in

improved safety, the prevention of catastrophic failures, and a future maintenance plan that is based on a reliable, condition-based program.

2.5 Fault Diagnosis

Fault diagnoses and the detection of the failure mode is a fundamental aspect of any successful maintenance procedure. Different failures modes require different detection techniques and diagnoses strategies to eliminate any potential failures, sustain the maintenance budget and avoid any expensive downtime. A gearbox failure, due to lack of proper CM for wind turbine 3 years of age, has been reported to cost $426,000 (Canadian dollars ,2004) [24]. Despite the variety of diagnoses techniques currently used by industry, further research is required to improve the quality of measuring sensors, data acquisition, and data analyses.

2.6 Wind Turbine Generators (WTGs)

An assessment of wind energy conversion system technology demonstrates the need to moderate the generator's configuration in order to accommodate life requirements [8]. A categorisation of commonly used wind turbine generators (especially the larger sizes) is shown in Figure 2.5. According to the structure and operating fundamentals of a wind turbine generator, they are divided into two main types: 1) Induction Generators (IGs) and 2) Synchronous Generators (SGs). The Wound Rotor Synchronous Generator (WRSG) is shared between the (IGs) and (SGs) and fed through a slip ring or a brushless electromagnetic field exciter. A Doubly Fed Induction Generator (DFIG) is the most common generator within the wind turbine generator industry [25].

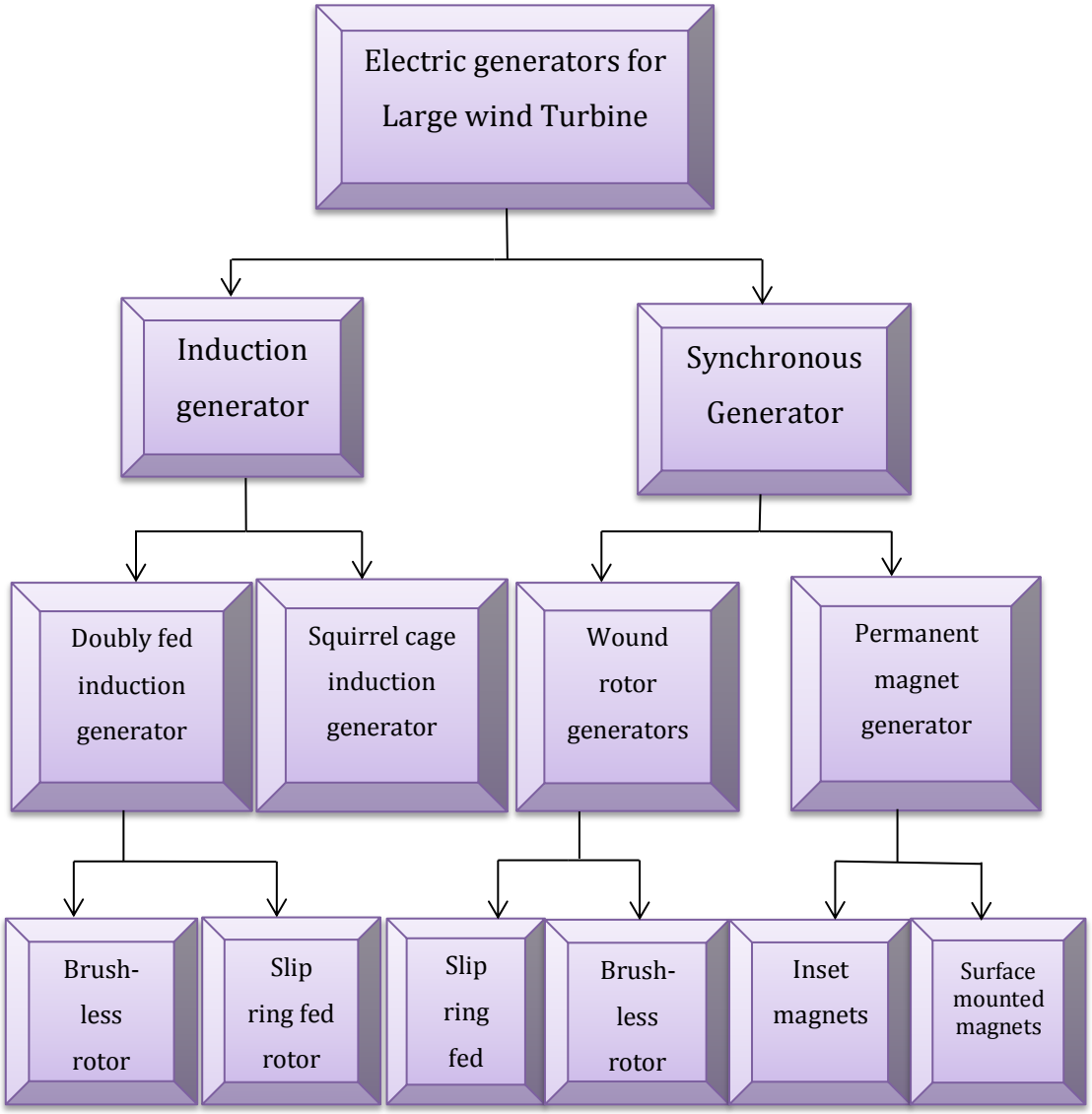

Figure2.5 Categorisation of commonly used generators in large wind turbines

The WRSG has received wide attention in practical wind energy conversion technology due to its high number of poles and capability to perform at low wind speed. Permanent Magnet Synchronous Generators (PMSGs) have been also used in the wind energy industry and have two common types: 1) surface mounted and 2) inset magnets. The main operating principle in this kind of generator is that the magmatic flux of the rotor is generated through permanent magnets. Another type of generator

used in the wind power market is the Squirrel Cage Induction Generator (SCIG). The rotor bars of this generator are shorted together leaving no option to connect with external circuits [8]. Figure 2.6 illustra3tes the configuration and structure of the different WT generators based on their connection to the grid.

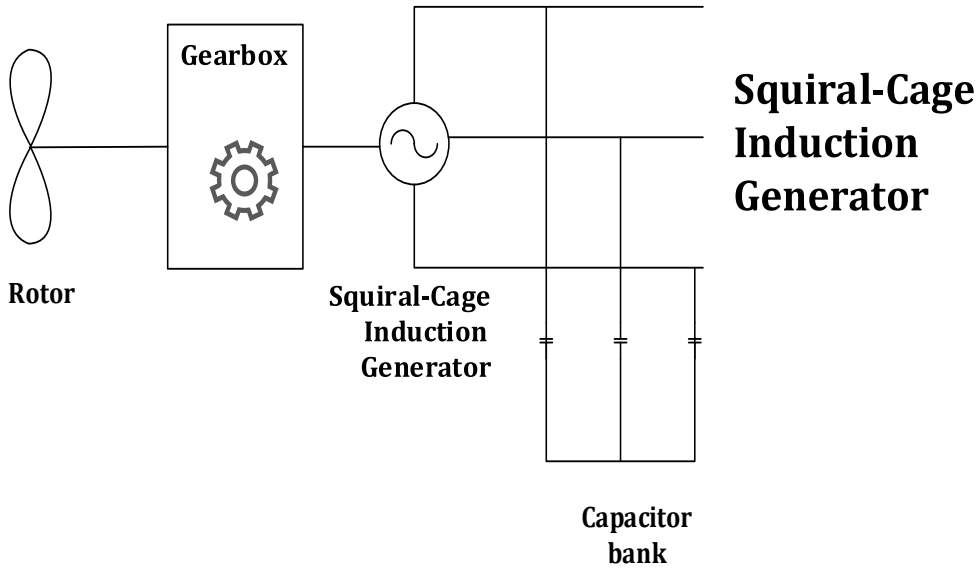

(a)

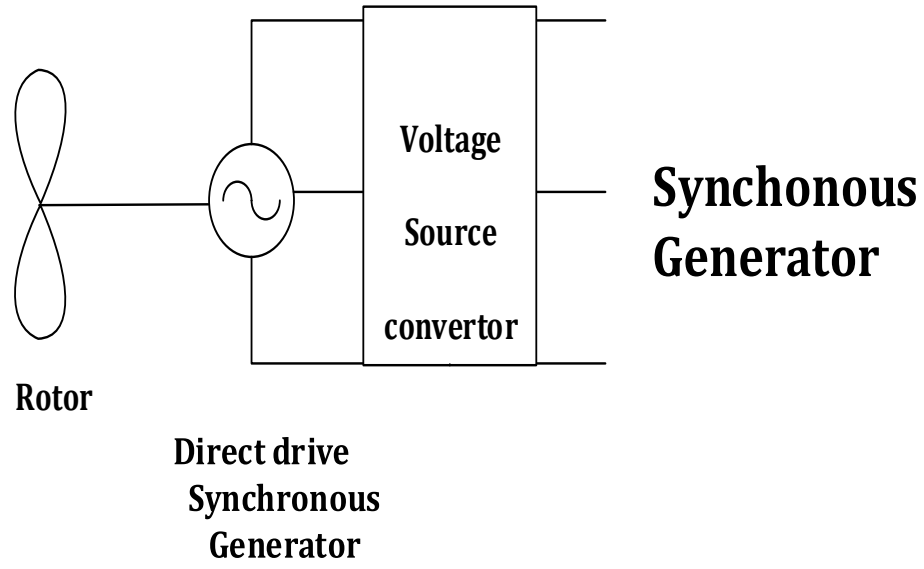

(b)

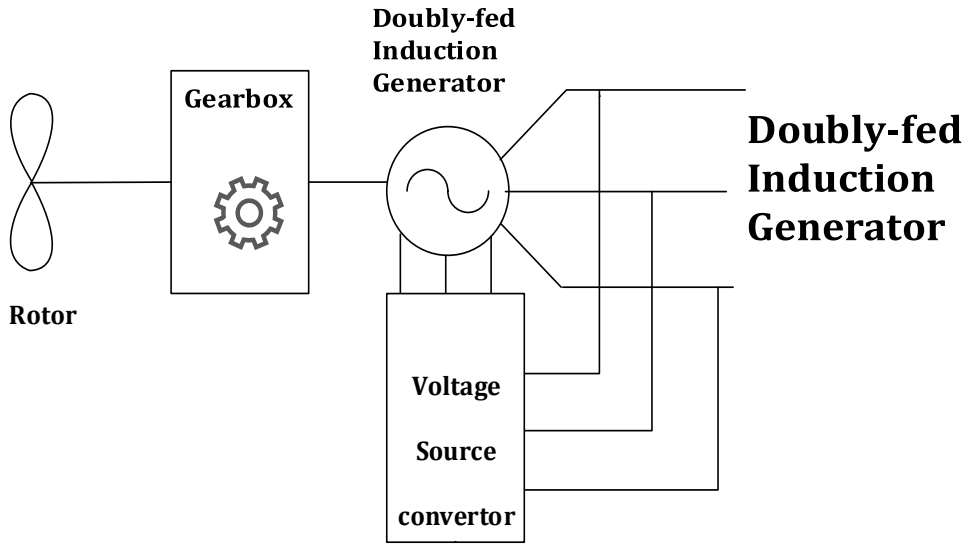

(c)

Figure 2.6 Different wind turbine generator structures and their connections (a) Squirrel-Cage Induction Generator (b) Synchronous Generators (c) Doubly-Fed Induction Generator.

2.7 Wind Turbine Gearbox

One of the most expensive and critical components in a wind turbine is the gearbox, which connects the low speed shaft to the high speed shaft according to the gear ratio. Failure of this crucial component may have determinate impacts on wind energy conversion systems in terms of the continuity of power supply, especially in islanded areas where the majority of power demand is supplied by wind farms. As such, adoption of an effective condition monitoring technique for the wind turbine gearbox is essential to avoid any catastrophic failure to the gearbox and hence maintain system reliability. Figure 2.7 illustrates the mechanism and complicity design of the WT gearbox.

Figure 2.7 Wind turbine gearbox [26].

A planetary gearbox is commonly used with wind turbines because of its excellent design tolerance. This kind of gearbox has multiple speed stages and is connected to the generator through the high speed stage.

As reported in [27], most WT failures modes (59%) involve the gear system. Another study [28] reports that about 19.1% of failures are related to the transmission system.

All grid faults are followed by electromagnetic transient torque which causes the gearbox to experience fatigue and massive stress that, in turn, will affect the overall performance of the wind turbine [2]. Condition monitoring of the drivetrain is therefore essential to explore incipient faults and allow effective maintenance and reliability improvement. Various gearbox failures have been investigated in the literatures [4]. The gearbox may develop hot spots due to the degradation of lubrication oil. This leads to high bearing temperature and accelerates the aging of lubrication oil. Another problem

facing the gearbox is that, when a wind gust hits the rotor blades, blade movement can cause a temporary misalignment between the two shafts connected through the gearbox. This misalignment can produce damage to the bearing loads and reduce the lifetime of the wind turbine [29, 30].

Vibration measurements (of both the gearbox and bearings) return data that enables the calculation of the wind turbine's mechanical characteristics. Sensors attached to the rotational components of the wind turbine can estimate the acceleration level of various rotational spots, which can assist in identifying any incipient mechanical failure [16]. Spectral analysis is a way to analyse the vibration data based on Fourier transform. By analysing the spectrums, the health condition of rotating components can be identified and quantified. According to [31], wavelet and Fourier transformation are the most common signal processing techniques used to analyse vibration and torque signals.

Wang et al. [32] utilises the wavelet method for fault diagnosis of a gearbox under fluctuating loads. Cibulka *et al* [33] investigate the bearing faults in a single stage gearbox, attached to an induction machine, by monitoring the stator current. Yuan and Lilong [34] analyse the vibration signal obtained from both a healthy and a damaged gearbox, using the variable amplitude Fourier series, and compare the outcomes with the wavelet analysis method. In [35], harmonic wavelet-based data filtering is used to enhance time frequency features for multiple sensor signals. Molins *et al* [2] illustrate that by controlling the terminal voltage of an induction generator, through the compensation of a reactive current using a static synchronous compensator, the electromagnetic torque stress on the generator rotor shaft will be mitigated.

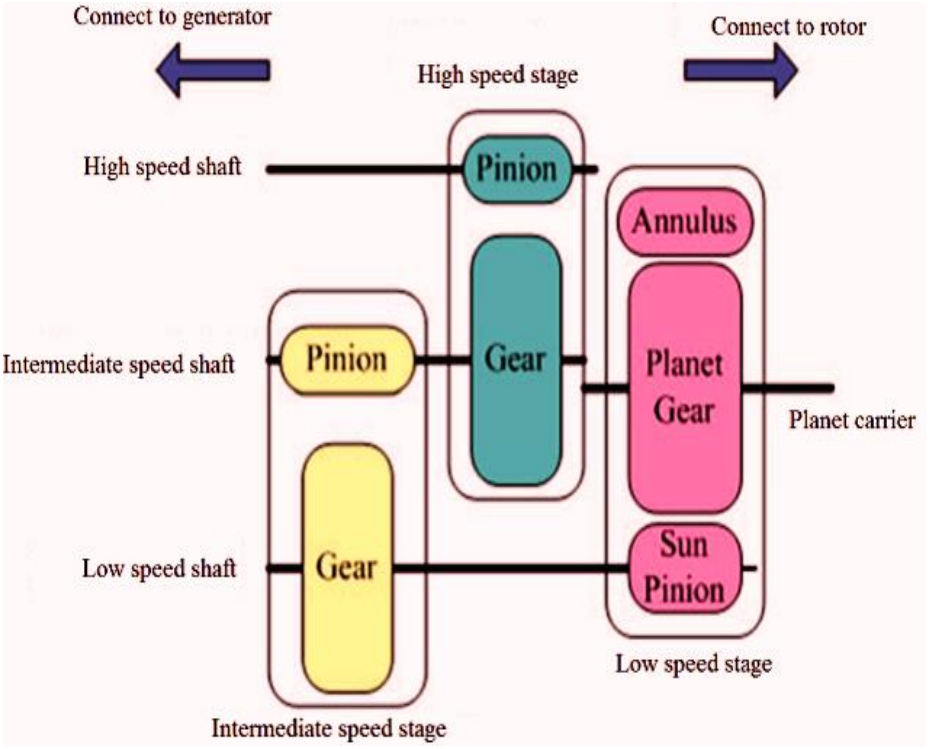

Figure 2.8 Gearbox Structure [31]

Luo et al [21] illustrate that vibration-based condition monitoring is one of the most effective techniques to detect WT gearbox failure, especially in the high speed side (rather than the low speed side). They also report that the digital domain synchronous sampling technique enhances the performance of wind turbine drivetrain fault detection. Zhang *et al* [31] use time domain and frequency domain to analyse the vibration data of an impaired gearbox by connecting the low speed side to the rotor and the high speed side to the generator (as shown in Figure 2.8). Fault detection within the intermediate- and high-speed stages is also successfully achieved.

Watson et al state that spectral analysis of the output power signal is an effective way to monitor the rotor asymmetry as well as the gearbox bearing faults [36]. Wavelet has been validated to detect shaft misalignment and bearing troubles by analysing the output power signal of the variable speed wind turbine [37].

2.8.1 Impact of Varying Load Conditions on WT Gearboxes

Condition monitoring of wind turbine gearboxes is complicated and faces major challenges due to the very complicated structure of the gearbox and the type of signals that can be observed from its rotating components. Signal processing techniques under load variations require advanced features in order to analyse such signals. A number of studies focus on the effect of load variations on condition monitoring techniques. For example, in [38], the Instantaneous Power Spectrum (IPS) is used to detect gear damage under load variations conditions. In [39] investigates the planetary gearbox under non-stationary operating conditions. Acceleration signal harmonics of gear mesh frequency are analysed using the FFT spectrum after applying a band-pass filter to the signal under varying loads [40].

A test rig experimental set-up was used in [14, 32] to highlight the impact of the load variations when carrying out the condition monitoring procedure. The Wavelet technique, based on Morlet continuous wavelet and parametrical modelling analysis approaches, was used to analyse the measured signals[41, 42].

Discrete Wavelet Transform (DWT) is known by its ability to extract most of the signal's features in both time and frequency domains [43]. The exceptional advantage of the wavelet application is that its frequency bandwidths vary in time, making it an appropriate method to study non-stationary signals [44, 45]. Harmonic wavelet-based data filtering is used for enhanced time frequency features, allowing analysis of multiple sensor signals when identifying and quantifying wind turbine gearbox faults [35]. As mentioned earlier in this thesis, 59% of wind turbine failures are attributed to the gearbox. Consequently, industrial gear failure and fault diagnosis is often addressed by researchers [46, 47]. Authors of [48, 49] categorise the common gear failures into two main types of stresses: 1) contact stress and 2) root bending stress. The first type causes gear pitting, and the second type causes tooth crack or tooth damage. Both types can lead to premature gear

wear and failure. In [50], a method for gearbox fault detection through the analysis of the sideband frequency without a tachometer signal is introduced. Tang and Luo [35] demonstrate that vibration-based condition monitoring is an effective technique in recognising gearbox faults, particularly in the high speed stage (compared to the low speed stage), and this is ascribed to the potential ''sensitivity of the accelerometers to high frequency vibration''. Many authors confirm that the ''digital domain synchronous sampling'' procedure improves monitoring of the wind turbine drivetrain.

Authors in [51] introduce a method for wind turbine mechanical stress reduction. Gearbox bearings along with oil quality and the lubrication system – are recognised as a crucial part of the gearbox with the highest link to gearbox failure [30]. Combet and Gelman [52] investigate the sideband ratio features. These features are less affected by a load variation that may result in a passive effect on the gearbox. Instead they produce a non-linear transmission path, as well as disturbance to the vibration signal, to identify the health condition of the gearbox [53].

Figure 2.11 shows a typical vibration signature for a WT gearbox with and without a bearing fault [54]. As can be seen in Figure 2.9 (a), the amplitude of the vibration signal has substantially decreased after the replacement of the faulty bearings, and as a result, the performance of the WT is improved. Figure 2.9 (b) shows increased power generation after attending to this fault.

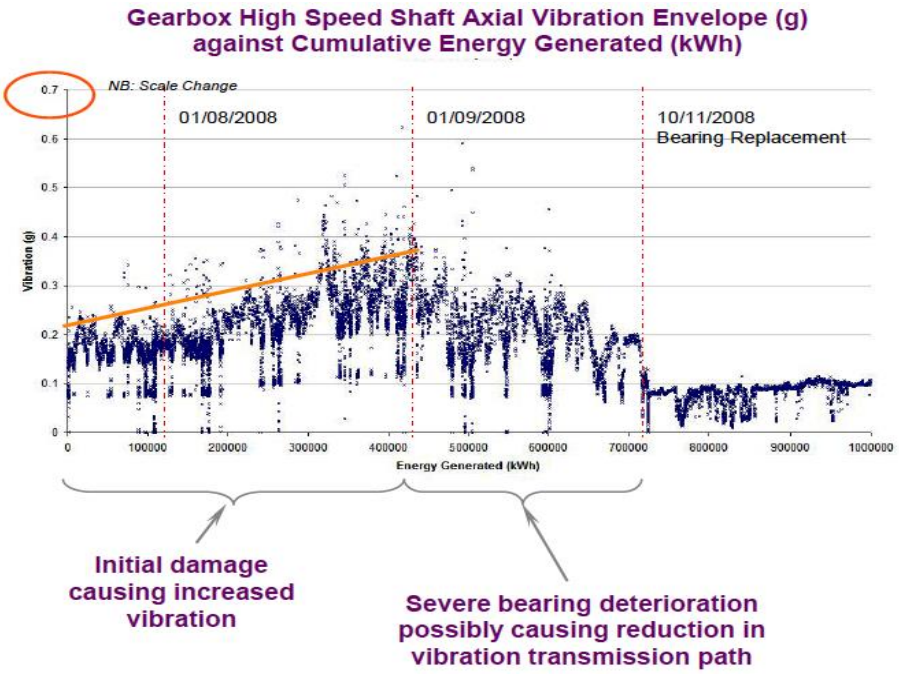

(a)

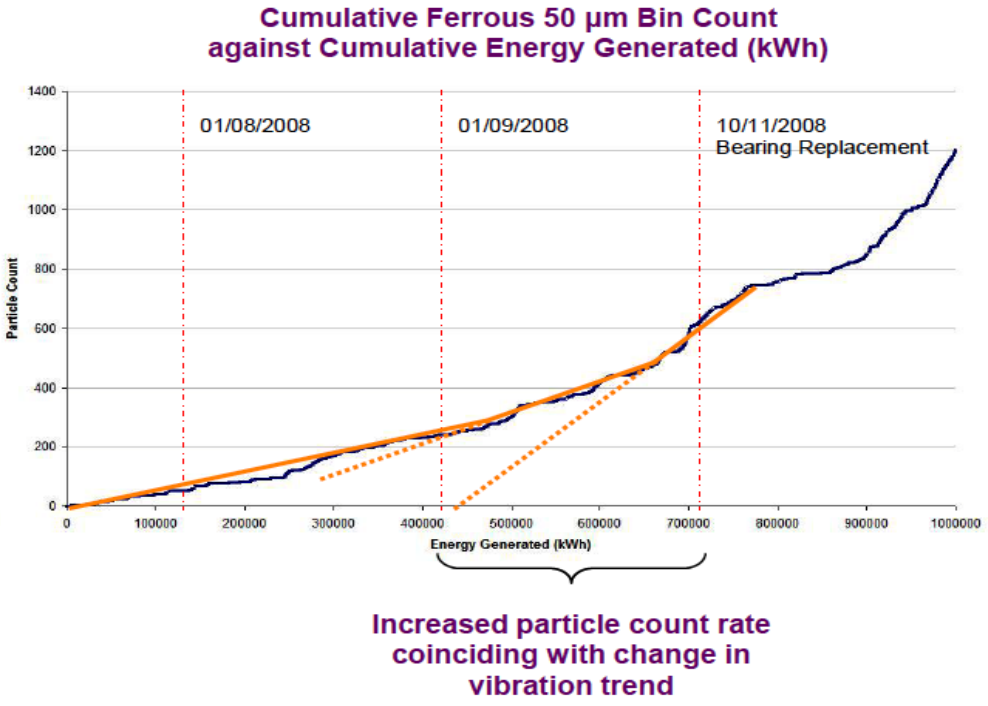

(b)

Figure 2.9 (a) Gearbox fault detection using: vibration analysis and (b) oil debris [54].

2.8.2 Diagnose Fatigues within the Wind Turbine Gearbox and Rotor (Blades)

Nonlinear loads result in a passive effect on the wind turbine gearbox and may lead to disturbances to the gearbox vibration signal [53]. The environment has a significant effect on WTs. For instance, in cold weather and at low wind speed, one of the most common problems facing wind turbine blades is leading edge ice accumulation [55]. Even with the presence of anti-icing systems, ice accumulation can still have a negative impact; not only on the gearbox, but also on the overall performance of the wind turbine [53, 55].

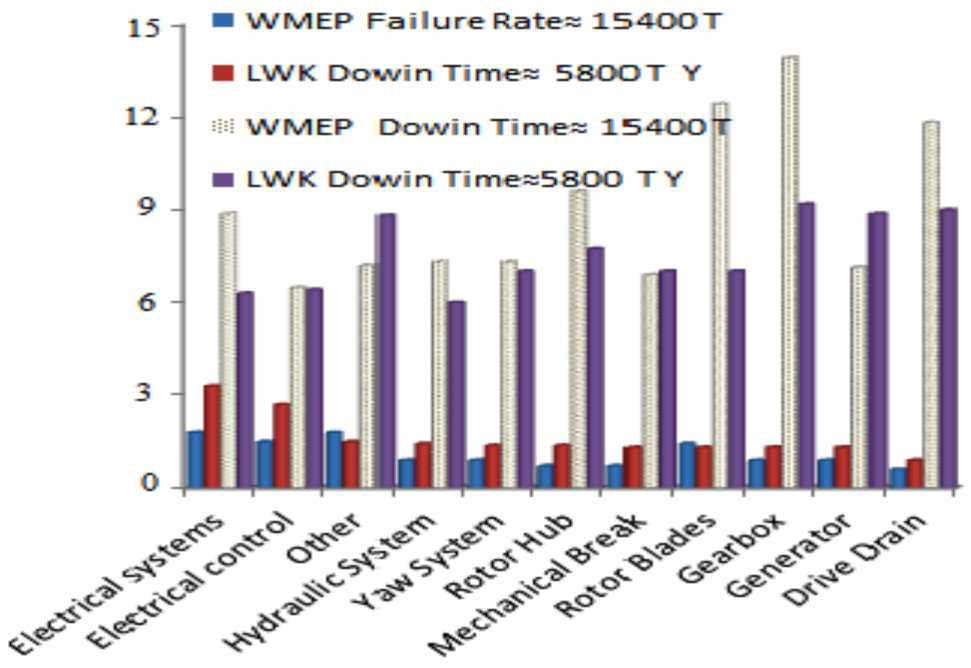

Figure 2.10 Downtime per Failure/year

Ice accumulation on the blades can cause blade fatigue due to ultimate loads [55]. Several countermeasures have been investigated in the

literatures, including the countless shapes of leading edge icing, trailing edge icing and blade surface icing. Paring down blade problems will lead to the reduction of the blade size [55]. Two types of vibration affect the blades: 1) flabwise and 2) edgewise. The last mode has significant negative effect on wind machines as a result of the violent vibrations [56]. Figure 2.10 illustrates the failure modes of WECS according to a statistical survey conducted over 13 years ago [57].

2.8.3 Gearbox Tooth Failure Impact on the Wind Turbine Performance

Condition monitoring (CM) of the rotating machinery, and the vibration analysis technique, have been validated by many researchers, as well as those from within the practical field. Power spectrum, adaptive noise cancellation, time-series analysis, and time-domain averaging have all been used to diagnose failure within rotating machinery. The developed techniques are however not fully matured yet, especially in detecting gear teeth cracking and cylinder wear in reciprocating engines [58, 59].

As we have seen, gearbox failure is a common issue within drive train CM of the WT, and researchers have extensively discussed this [15-19]. Gearbox failure has massive impact on the productivity and availability of the WT and can result in long down time periods [30]. Oil lubrication degradation can also affect the performance of the gearbox and raise its temperature to a critical value [60]. According to a number of studies concerning planetary gearboxes and the damaged gears of wind turbines (based on vibration signals collected from the fitted sensors on the ring gear, and whether a local damage gear goes into mesh), the received signal can be demonstrated as ‘amplitude modulation and frequency modulation (AMFM) with the gear meshing frequency (or its multiples) as the signal carrier frequency and the characteristic frequency of the damaged gear (or its multiples) as the modulating frequency’ [61-66].

Mandic *et al* [67], propose a technique based on load reduction of variable speed WTs to minimise the mechanical stress on the gearbox mechanisms. Another study [68], investigates a way to enhance the detection of a faulty gear tooth (cracked or chipped) by using an autoregressive model and the Minimum Entropy Deconvolution (MED) based filtering technique. Wang et al [69], apply wavelet transform to analyse a helicopter gearbox vibration signal and detect the gear faults.

Tang *et al,* [35] show that non-stationary signals, along with the harmonics generated from WT gearbox operation, are difficult to maintain within a direct harmonic-based method such as Fourier transform. Other studies, [70-73], prove that the harmonic wavelet technique is the most suitable and capable signal processing technique for analysing associated vibration harmonics. This is due to the wavelet's capability to combine the advantages of short-time Fourier transform and also continuous wavelet transform. Wang and McFadden [46] propose a spectrogram application (based on the calculation of the time frequency distribution) in order to achieve an early detection of gear failures. Mallat [74] and Donoho [75] propose and develop a de-noising technique (based on wavelet transform) to eliminate the noise from the signal and achieve an effective fault detection technique.

2.9 Lubrication Oil Monitoring

Lubricant oil monitoring of the wind turbine gearbox is essential when maintaining a high performance gearbox. Different factors can affect lubrication oil and thus the performance of the WT.

Due to high thermal and mechanical stresses, gearbox lubrication oil is subject to degradation including corrosion, and water and particle contamination that affects the performance of the gearbox and hence the overall performance of the WECS [76]. In addition, a deterioration in oil quality can lead to the prediction of gear health condition and misalignments.

A combination of vibration and debris analysis provides an effective condition monitoring technique for the oil [77]. Other studies investigate the capabilities of acoustic emission, vibration, and spectrometric analysis of lubrication oil when detecting the gearbox aging life cycle. Impulse vibration signals and acoustic emission techniques have been successfully used to monitor the condition of the gearbox oil [69, 78-83].

Power spectral analysis using, Fast Fourier Transform (FFT), is used in [84-86] to extract the features of the measured gearbox vibration signal. Oil degradation leads to high thermal stress, within the WT gearbox, that increases bearing temperature and accelerates oil aging [3]. Peng *et al* [87], investigate the effect of contaminated lubricant using wear debris and vibration techniques to extend the life cycle of the wind turbine. Authors of [88, 89] show that oil quality can be assessed through the measurement of parameters such as its level of oxidation, acidity, viscosity, water content, temperature and dissolved particles.

Figure 2.11 demonstrates the aging life cycle of the wind turbine's gearbox teeth and how different factors (e.g. viscosity, water, oxidation and temperature) can cause scuffing and tooth thickness damage. Top quality oil will improve gearbox defence, extend oil life, increase efficiency, and improve seal capability as well as the output efficiency of the wind turbine.

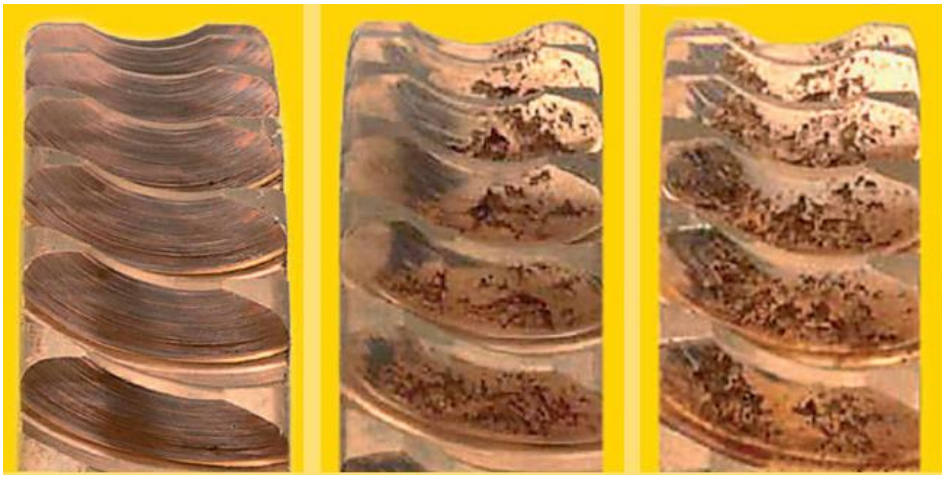

Figure 2.11 Aging sequence of the gearbox teeth under incorrect lubricant[90].

Table 2.1 summarises the advantages and limitations of some of the most effective CM techniques used when monitoring the wind turbine gearbox.

Table 2.1 Typical condition monitoring techniques for the wind turbine gearbox [21].

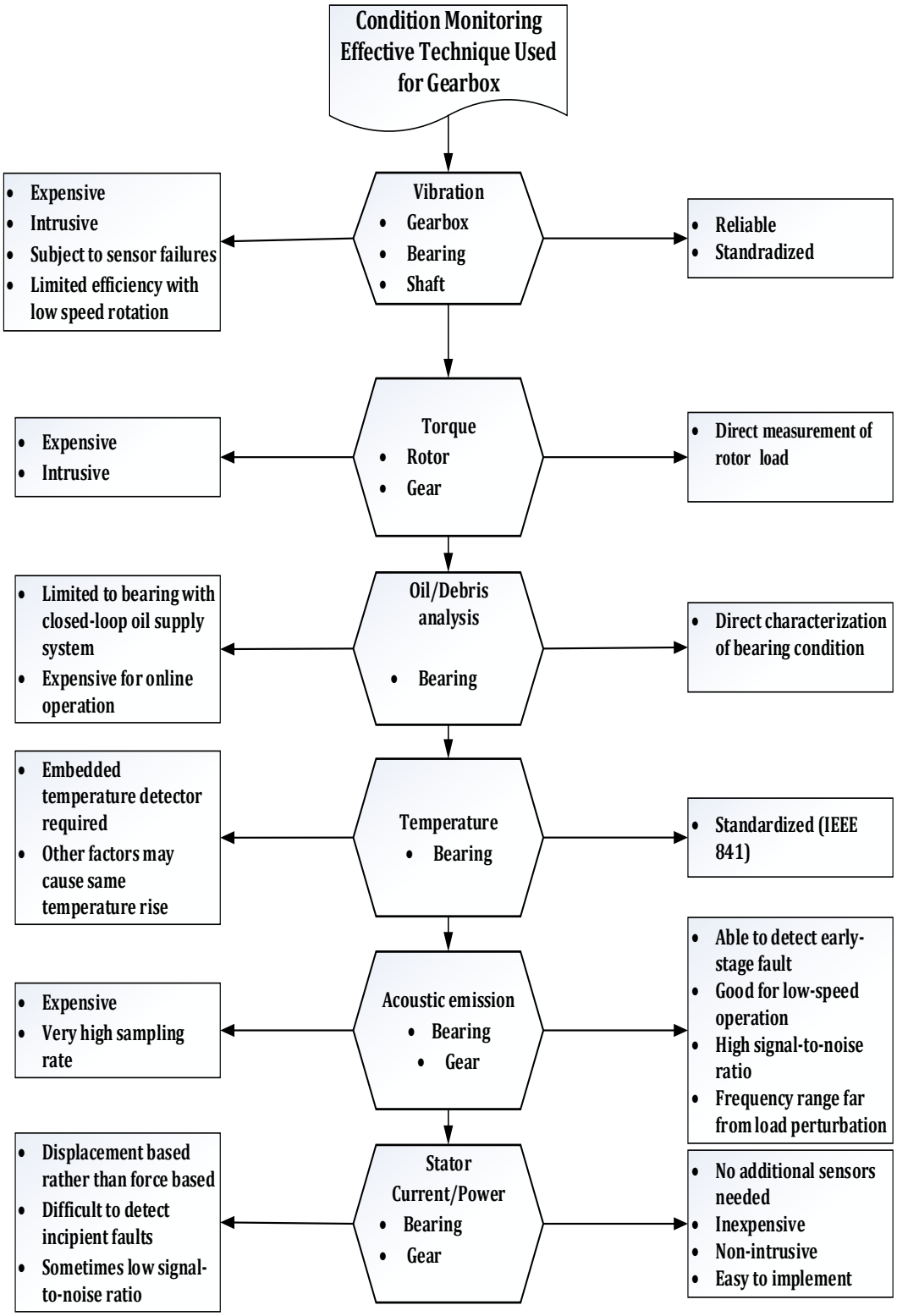

2.10 Wind Turbine Blades

Turbine blades are the most visible part of the wind turbine. This component plays a vital role in producing energy by transferring the wind's kinetic energy to a rotating mechanical energy [8]. Ciang *et al* illustrate that the turbine blades are subject to mechanical faults with a probability of about 70% [91].

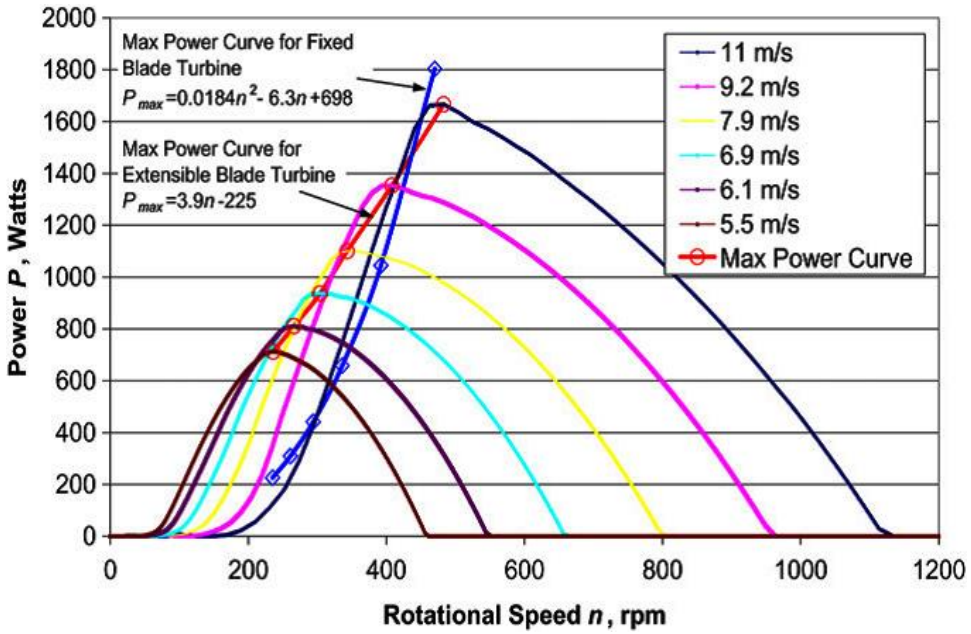

Figure 2.12 Power curves for turbines with variable blade lengths [36].

Wind power can be harvested by the blades, in order to achieve mechanical power, and can be calculated as:

$$P_m = \frac{1}{2}\rho A v_w^3 C_p \qquad 2.1$$

Where,

ρ: air density (kg/m^3),

A: sweep area (m^2),

C_p: power coefficient of the blade, and

v_w: wind speed (m/s).

The maximum theoretical value for C_p is 0.6, while the practical value is between 0.4 to 0.5 (based on tip loss, profile loss and loss due to slow rotation). The tip speed ratio (λ), is given by:

$$\lambda = \frac{u}{v_w} = \frac{D}{2}.\frac{\Omega}{v_w} \qquad 2.2$$

Where,

D : outer diameter of the rotor (m), and

Ω: angular velocity of the rotor (rad/s).

As a result of the rotational speed of the rotor, the torque (T) can be obtained according to the equation below:

$$T = \frac{C_p(\lambda)}{\lambda}.\frac{D}{2}.\frac{\rho}{2}Av_w^2 \qquad 2.3$$

Modern wind turbine blades are generally made from fibre reinforced plastics mixed with other materials such as plastic foam and wood. These materials have the advantages of low cost and high mechanical strength [33, 34]. The wind turbine rotor should withstand a 10^8 stress cycle in 20 years of its estimated life, taking into account both creep and corrosion [15]. Rotor imbalance, which produces large stress and operational instability, affects the blade performance.

If moisture attacks the blade's surface, cyclical freezing may increase the growth of any existing cracks. Icing, surface roughness and other faults may also occur, while transportation has a negative effect on the blade's performance [15]. Maki *et al* illustrate that taller towers enhance the output power by increasing the amount of wind captured by the swept area of the rotor and as per the equation below:

$$v = v_{ref}\left(\frac{Hub_{Ht}}{H_{ref}}\right)^{0.34} \qquad (2.4)$$

Where,

v: wind speed at the hub (m/s),

v_{ref} : reference wind speed at the reference hub height, and

H_{ref}: reference hub height (m).

A power coefficient of 0.34 is suitable for neutrally stable air above human inhabited areas [6]. Sharma *et al* [92] investigate the impact of a variable blade's length on wind turbine performance. Results show that variable-length blades can capture almost twice that of the fixed-length blades (as shown in Figure 2.12). Besnard and Lina [93] report on different condition monitoring strategies for wind turbine blades, which include visual inspection, ultrasonic or thermography techniques, and online condition monitoring using fibre optic. Figure 2.13 compares expected maintenance costs for different maintenance strategies in a practical case study reported in [37]. The figure reveals that the online condition monitoring technique offers the lowest maintenance cost for the investigated case study.

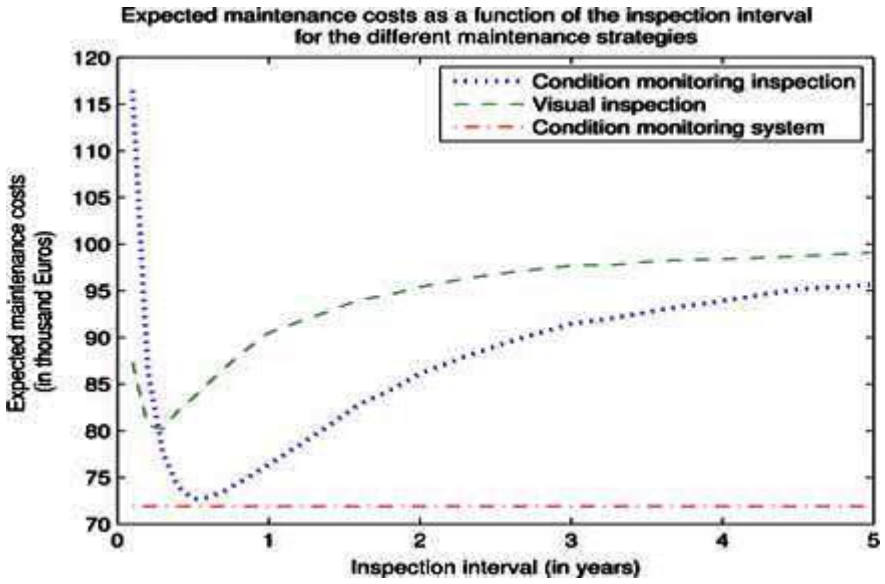

Figure 2.13 Expected maintenance costs for the different maintenance strategies as a function of the inspection in the case study (one blade) [15].

Schubel *et al* [94] compares different methods of monitoring large wind turbine blades, including the dielectric, acoustic, ultrasonic, and fibre optic methods. The implementation of these methods face some difficulties. This is especially true for the dielectric sensor method, as the sensor's size may affect the resin mechanical performance [95-98].

Factors that influence the output power of the wind turbine [23] are the condition of the blades, dust accumulation, wind share and wind shadowing. Thiringer and Linders examine a wind turbine with a fixed pitch angle by controlling rotor progress [99]. Wu and Lai [100] estimate the fatigue life for a small composite sandwich wind turbine blade by calculating the stress limits beneath fatigue loading. Figure 2.14 shows typical damage that the wind turbine blade faces during its lifetime. Figure 2.15 shows two different faults: ''(1) fibre failure in tension and (2) fracture of separate fibres in laminates of the skin.'' Figures 2.16 and 2.17 however show adhesive joint skin failure and adhesive layer debonding respectively.

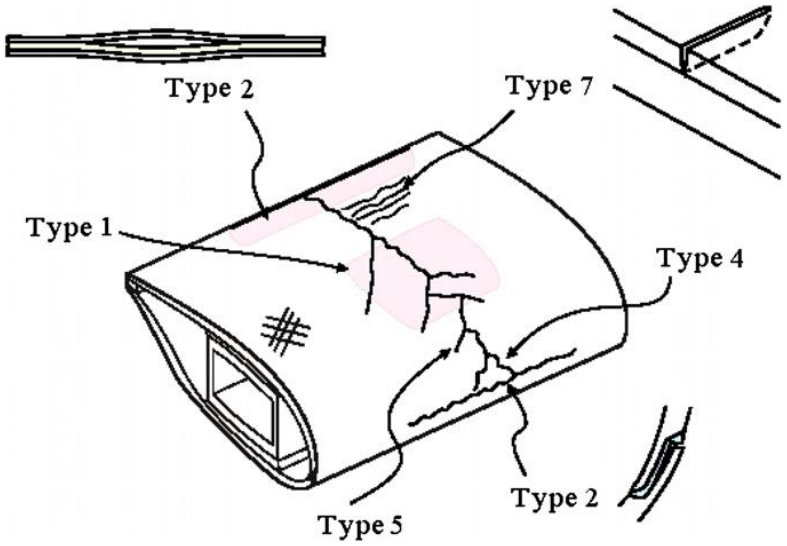

Figure 2.14 A sketch illustrating some of the common damage types found on a wind turbine blade [101].

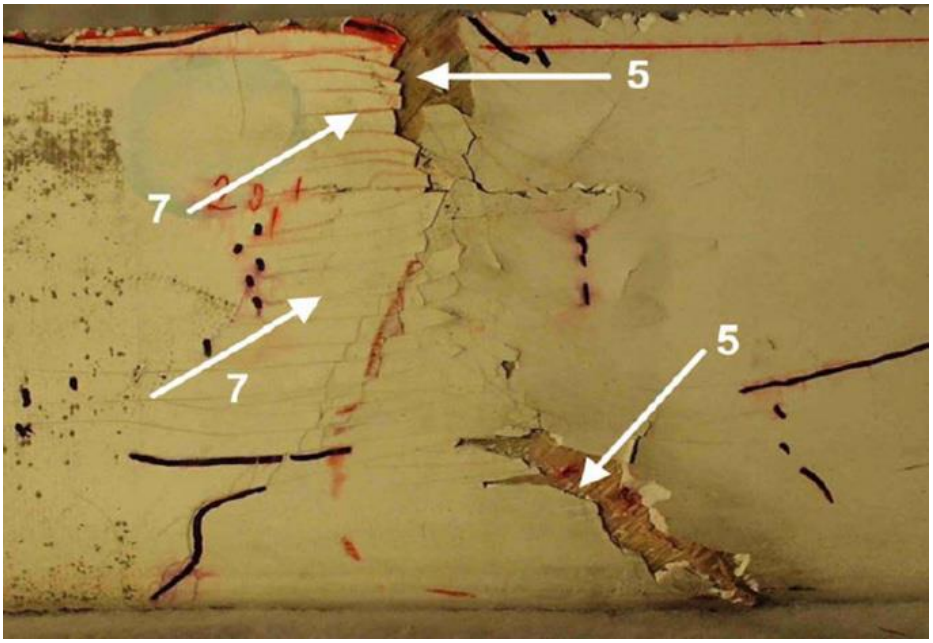

Figure 2.15 Damage type 5 (laminate failure in compression) & type 7 (gel-coat cracking) at the bottom of the leading edge [101].

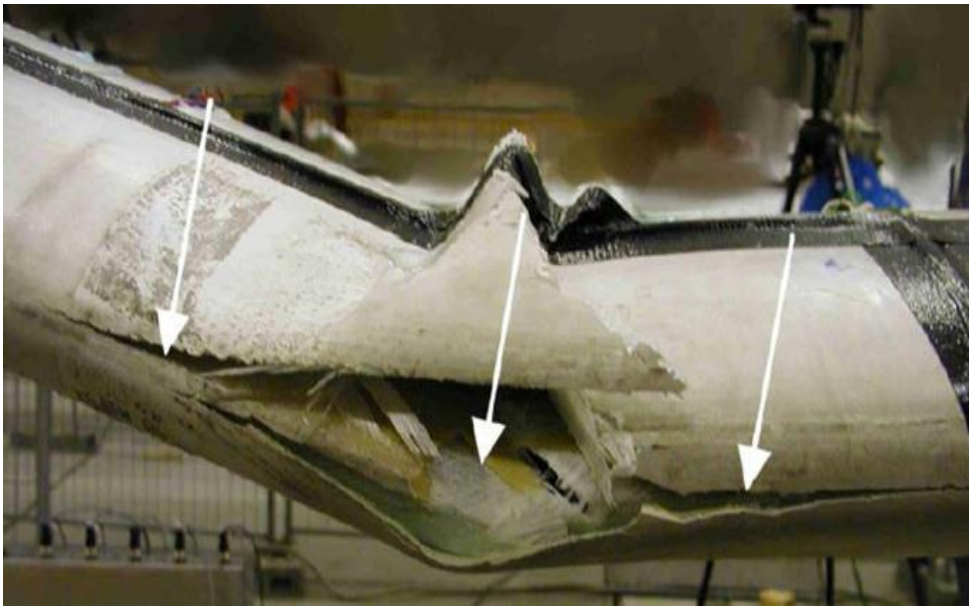

Figure 2.16 Damage type 2 (adhesive joint failure between skins) at the leading edge [101].

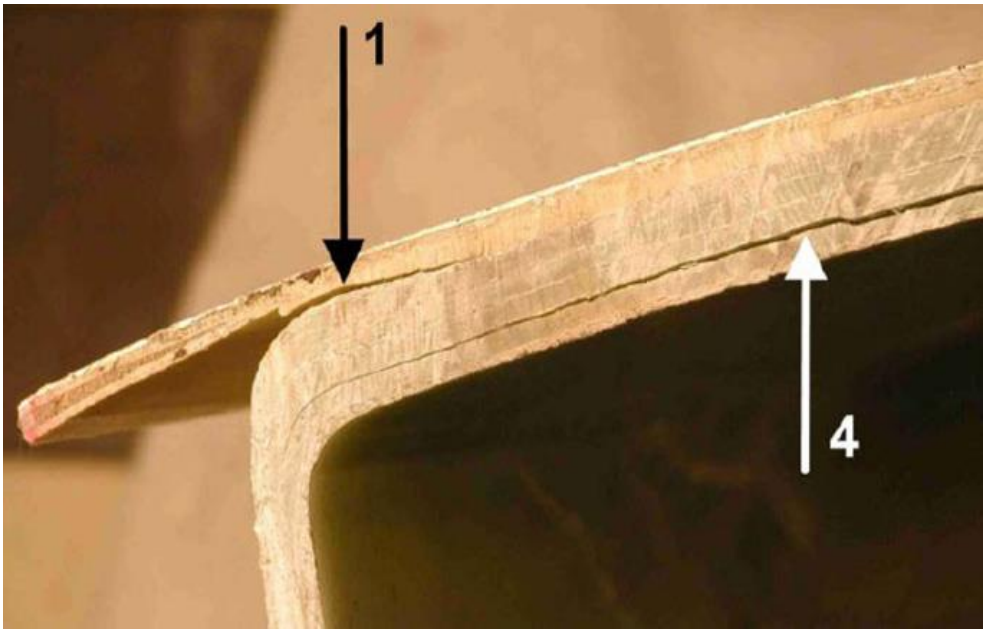

Figure 2.17 Damage type 1 (main spar flange/adhesive layer debonding) and type 4 (delamination by buckling load) [101].

2.10.1 Surface Roughness

When a surface is smooth it means air will flow much easier than over a rough surface. A rough surface slows down the wind speed as a result of friction stress.

Dust and pollution can affect the output efficiency of wind power, reducing it to about 40% below its normal output in a clean environment. Surface roughness has significant impact on the efficiency of the blade's leading edge and may cause trailing edge turbulence [101].

Wind turbines operate for most of their lifetime in unstable weather conditions. As a result, forces on the blades vary, causing constructional responses, blade flapping, wind shear and twisted flow. A variation in blade flapping is the most common reason behind changes to the angle of attack on WT blades [102]. According to [103], and based on various measurements, the output efficiency of wind turbine blades is affected by the airfoil thickness. A thickness of 25%, with less roughness sensitivity, is the best specification for the blades. This is because a thicker airfoil has a high ''lift-to-

drag'' ratio. Table 2 demonstrates different airfoil thicknesses and the effect of roughness on the performance of the WT blades.

Table 2.2 Effect of roughness on performance for (about) 25% thick airfoils [111].

Configuration	**clean**		**"rough"**	
airfoil	L/D-max	cl-max	L/D-max	cl-max
Re= 3.0e6				
DU 91-W2-250 (1)	127.6	1.37	61.8	1.16
NACA 63421-425 (1)	120	1.277	39	0.803*
AH 93-W-257 (2)	120.7	1.41	55	1.04
S 814(1)	114.1	1.408	61.4	1.357**
Re= 1.6e6				
FFA-W3-241 (3)	81	1.37	48.5	1.16***
Ris0-A1-24 (3)	89	1.36	57	1.17***
(1) Delft (2) Stuttgart (3) Ris0				
* at kink in lift curve				
** grit roughness at upper surface x/c=0.02 and lower				
*** ZZ-tape at x/c= 0.05 upper surface and at x/c= 0.10 on lower surface.				

In [104], authors discuss the impact of clean and roughness conditions on the airfoil blades using a numerical simulation method. They find that both the drag coefficient and lift coefficient of an airfoil are affected by roughness and thickness. Further studies concerning the accumulation of dust on wind turbine blades also show the poor performance of the wind turbine under such conditions. For example, in a 300 kW wind turbine that was left 9 months without a clean of the rotor blades, power loss consistently increased due to dust accumulation on the blades (as can be seen in Figure 2.18) [105].

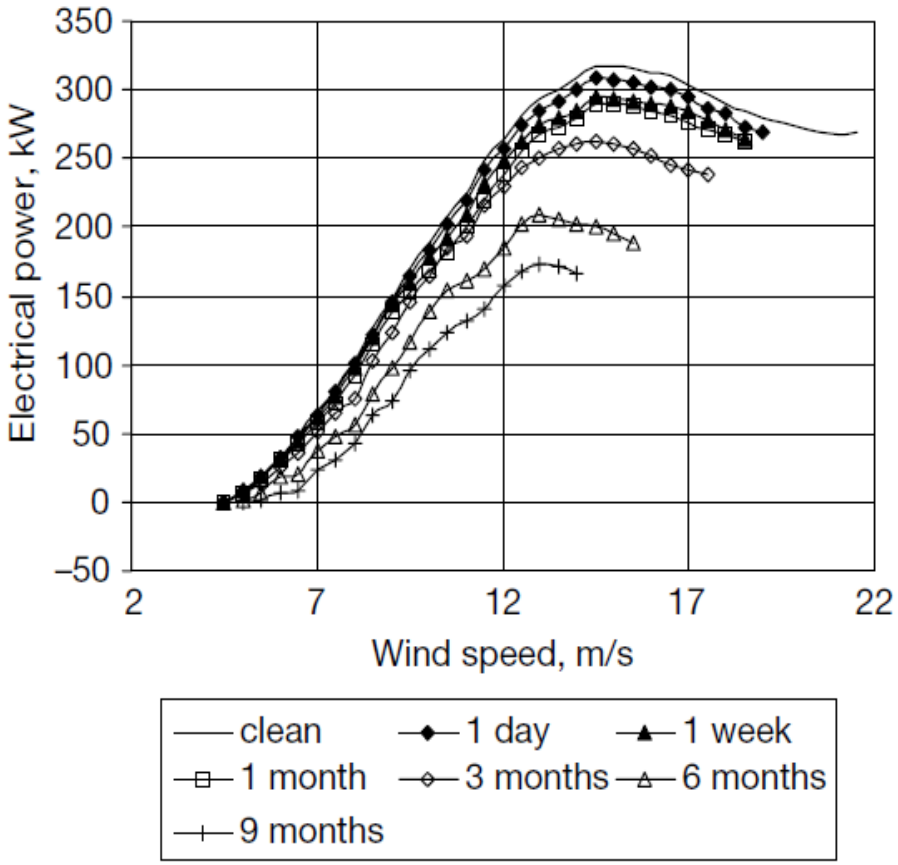

Figure 2.18 Effect of dust for various operation periods on the power curve of turbine.

2.10.2 Lightning Protection

Lightning, which usually hits the blade tip area, is one of the most common problems facing WT rotor blades. In the past, it was thought that fibre glass blades would not be affected by lightning, but this has been found to be false in real life operation.

A lightning system is essential for protection of the rotor blades, especially as WT sizes become larger. Nowadays, this kind of protection has become a standard design feature of wind turbine blades. The main component of this lightning system is the receptor at the blade tip (as can be seen in Figure 2.19). This receptor is made from metal material and screwed to the blades. It can also be easily changed. Inside the blade, a solid wire runs through the whole blade, from tip to base. This wire acts as a lightning conductor and meets the flexible metallic strips at the base of the blade and, from there, the earthing system of the WT.

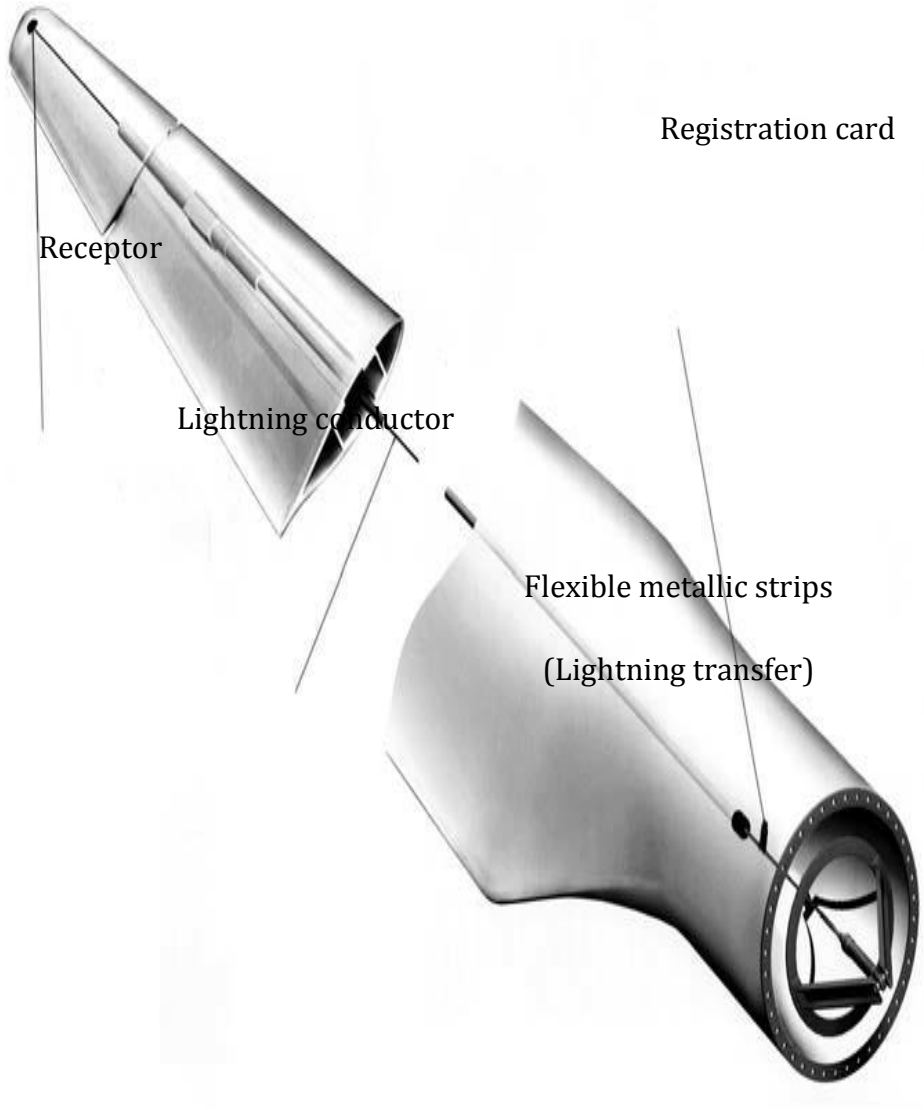

Figure 2.19 Lightning protection of a rotor blade [12].

2.10.3 Ice Accumulations and De-icing

In some countries, due to an extreme weather conditions, WT rotor blades suffer from ice accumulation. Baled rotor designers have therefore come up with a number of techniques to protect and avoid this dilemma. These include an ice warning system, which can be switched on/off, depending on weather conditions. However, this task is still too complicated to provide the WT blades with an effective de-icing technique. In Figure 2.20,

another de-icing technique is shown, whereby heat resistance passes through the rotor blades. However, the material and bending moment of the rotor blades mean this heating system is under high amounts of stress. Recently, it has been reported that coating the rotor blades with a special surface coat can prevent ice accumulation. Nevertheless, a fully matured and widely accepted de-icing system does not yet exist [12].

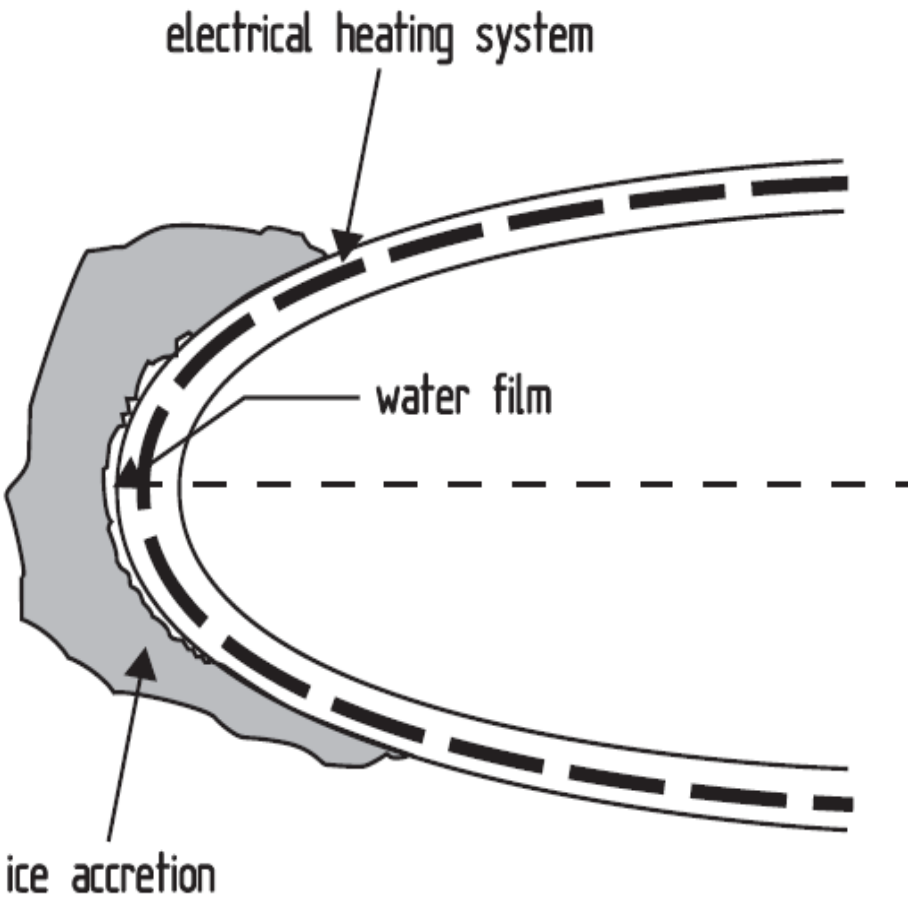

Figure 2.20 Electrical heating system for rotor blade de-icing [12].

2.10.4 Heavy rain

The performance of the WT will not change dramatically with a minor rain. However, immense rain with heavy drops will result in a serious impact on the WT blades. Practical measurements show that the power losses will reach 30% depending on the rain strength [106]. Other studies [107-110], estimated the energy loss of a WT due to severe icing to be 20% raising to 50% on harsh sites on a yearly basis.

Figure 2.21 [111] shows the impact of heavy rain on the power curve of a wind turbine. The curve illustrates a comparison between dry rotor blades, heavy rains and light rains under the same loading conditions. Massive damage can occur to the leading edge of the WT blade when speed exceeds 100 m/s.

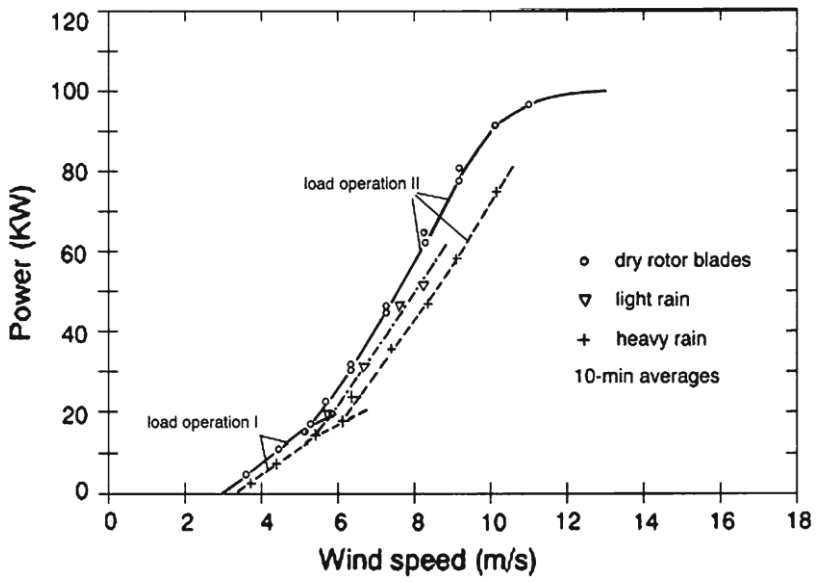

Figure 2.21 Effect of heavy rain on WT power curve (Energiewerkstatt 19950 [111].

Chapter 3 Signal Processing Techniques for Condition Monitoring

3. 1 Introduction

This chapter presents the main and most effective signal processing techniques used in wind turbine condition monitoring, including Fourier transform, order analysis and wavelet transform.

3.2 Fourier Transform (FT)

"An arbitrary function, continuous or with discontinuities, defined in a finite interval by an arbitrarily capricious graph can always be expressed as a sum of sinusoids"

J.B.J. Fourier
Jean B. Joseph Fourier (1768–1830) [112].

Fourier's famous equation for a periodic a signal (e.g. $x(t)$, with periodic time T) can be presented as an infinite trigonometric series (Fourier series) based on [113]. A graphical representation of the Fourier series is shown in figures 3.1 and 3.2.

$$x(t) = a_0 + \sum_{k=1}^{\infty} \left(a_k \cos\frac{2\pi kt}{T} + b_k \sin\frac{2\pi kt}{T} \right) \qquad 3.1$$

Where

a_0, a_k, b_k are Fourier coefficients given by:

$$a_0 = \frac{1}{T}\int_{-\frac{T}{2}}^{\frac{T}{2}} x(t)dt \qquad 3.2$$

$$a_k = \frac{2}{T}\int_{-\frac{T}{2}}^{\frac{T}{2}} x(t)cos\frac{2\pi kt}{T}dt \qquad 3.3$$

$$b_k = \frac{2}{T}\int_{-\frac{T}{2}}^{\frac{T}{2}} x(t)sin\frac{2\pi kt}{T}dt \qquad 3.4$$

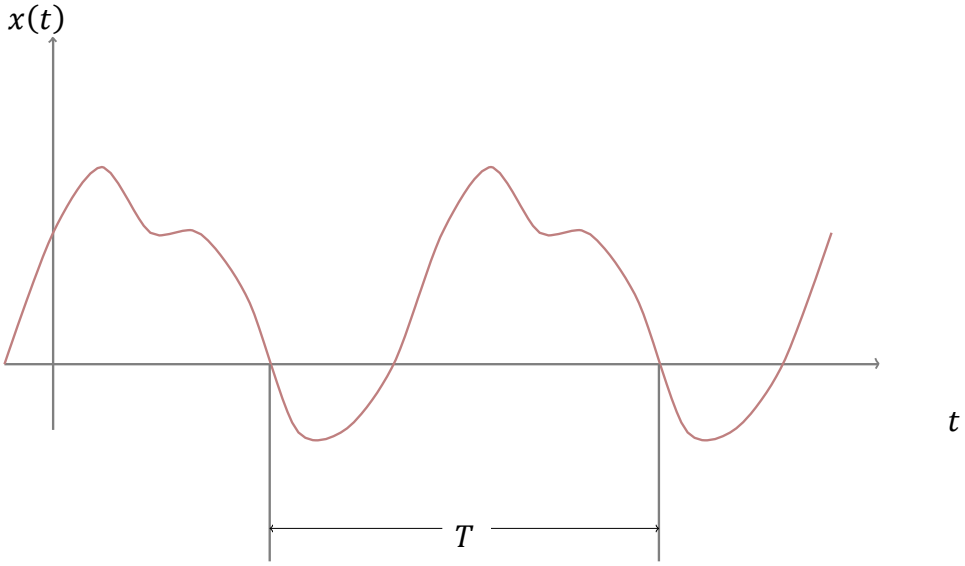

Figure 3.1 A periodic signal

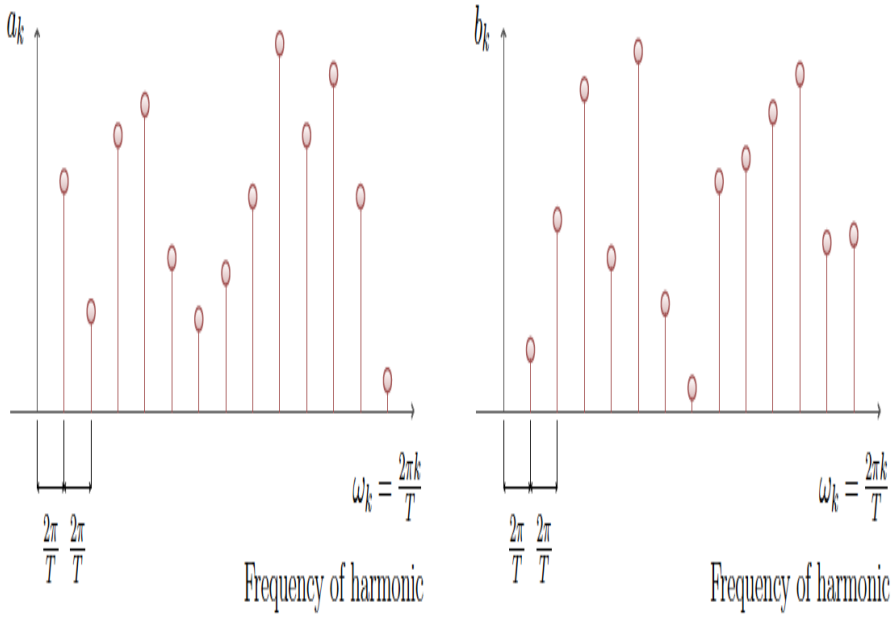

Figure 3.2 Fourier coefficients [113].

3.2.1 Spectral Averaging-based FT

Spectral averaging-based FT is one of the techniques used to prevent the corruption of weak frequency components mixed with unwanted noise, which is one of the limitations of FT. A previous study by Combet *at al* [52] shows that sideband ratio features are also effective in detecting the health condition of a rotating machine because they are less affected by load variations. A more traditional technique is Time Domain Averaging (TDA), which is used to detect faulty signals in rotating machine industries, and achieved by extracting the periodic component from a raw signal. A TDA pattern has been proposed by [114] to diagnose gearbox failures. [115]. In [116], the oscillation of electric power is used by means of an angular data clustering technique, and by doing so, the oscillation of the electric power in the time domain becomes mapped into a discrete waveform in an angular domain.

3.2.2 Discreet Fourier Transform (DFT)

DFT is a discreet version of a continuous time signal. FT of a signal $f(t)$ can be expressed as:

$$F(w) = \frac{1}{\sqrt{2\pi}} \int_{\infty}^{\infty} f(t)\, e^{-jwt} dt \qquad 3.5$$

Where,

w is the angular frequency, and the invers FT of the same signal can be written as:

$$f(t) = \frac{1}{\sqrt{2\pi}} \int_{\infty}^{\infty} F(w)\, e^{jwt} dw \qquad 3.6$$

Both Eq. (3.5 and 3.6) confirm that FT for a signal is a superposition of sinusoidal components of all probable amplitudes and frequencies of the signal. Consequently, FT has the ability to extract the frequency statistics of a time signal and obtain the "strength/energy of a particular frequency component".

In real application, the signal data is not continuous but instead sampled at a specific frequency $f(s)$. Discrete Fourier Transform of the sampled data in Eq. 3.5 (and its invers 3.6) is shown in 3.7 and 3.8 respectively:

$$F(k) = \frac{1}{N}\sum_{n=0}^{N-1} f[n]e^{-j\frac{2\pi kn}{N}} \qquad 3.7$$

$$f(n) = \frac{1}{N}\sum_{n=0}^{N-1} F(k)e^{j\frac{2\pi kn}{N}} \qquad 3.8$$

Where N represents the sample number of $f(n)$ and $k = 0, 1, 2$ N-1

The sampled data shows one to one mapping (a distinctive representation), but this is not always the case. This is proved in [117], where further details can be found.

Discrete Fourier Transform has limitations, such as aliasing phenomena and leakage. Aliasing is when the initial samples are not suitably narrow-spaced to characterise the high frequency orders that appear in the underlying function. DFT data becomes inaccurate and aliasing will take place. However, to minimise these high frequencies, a pre-filter should be used. Leakage, a second limitation of DFT, is when a finite amount of data and a finite size of frequencies, when combined, result in frequency energy that is performed over a range of frequency intervals (-∞ to + ∞).

3.2.3 Order Analysis-based FFT

Order tracking analysis is one of the vibration analysis techniques suitable for tracking the machine's health condition [118]. Fluctuating load conditions and deformity in the rotating machines cause constrained vibrations. By involving spectra and time histories, with the speed of the moving parts, order analysis can detect the vibration of fluctuating loads, critical speeds, and unstable actions [118]. Order tracking of the spectrum is a method used to analyse the vibration signal, based on related spectral components, rising with the instantaneous rotating speed. When the collected vibration data comprises of numerous spectral components with significant rotational speed variations during measurement time, the processed signal is unclear and challenging to analyse. This then leads to misinterpretation [119]. A comprehensive discussion and further detail, including the strengths and limitations of the order analysis technique, are presented in [120, 121]. Eggers at al [122] prove that Computed Order Tracking (COT) can effectively identify and detect faults within the pinion gear in the gearbox. However, order tracking requires the collected vibration signal from the machine to be sampled at fixed angular increments, which means the shaft speed should be proportional to the sampling rate. Without extra specified equipment, such as a ratio synthesiser and an anti-aliasing tracking filter, the measured signal will not be accurate [118]. Figure 3.3 explains the stages of the order tracking system for the vibration signal based on different models.

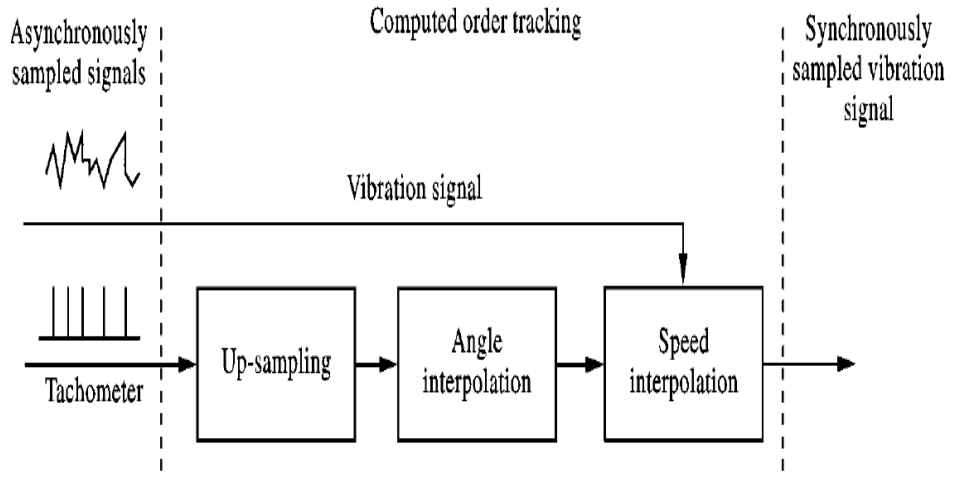

Figure 3.3 An example of a synthesised synchronous system [119].

3.3 Wavelet Analysis Technique

Wavelet analysis is considered a very effective tool for analysing vibration signals [123]. By using a single function, called a mother wavelet, all wavelets can be generated by translation and dilation. Many research fields have shown interest in this theory, and it has been developed with many different applications [123]. Wavelets are a systematic way to represent functions on unbounded domains. This is achieved by the use of linear combinations of orthogonal basis functions that are compactly supported and overlapped. These basis functions are potentially realisable by physical devices [124] [125]. Table (3.1) summarises a few of the wavelet transform applications within various disciplines.

Table 3.1. Prominent areas of application of the wavelet transform.

Discipline	Applications
Maths	Harmonic analysis
Physics	Phase space analysis
Digital signal processing	Multi-rate filtering, quadrature mirror filters, and sub-band coding
Image processing	Pyramidal image representation and compression
Speech processing	Efficient representation and equalization

According to [126] ,the formal definition of wavelet transform is "a tool that cuts up data, functions or operators into different frequency components, and then studies each component with a resolution matched to its scale".

Wavelet effectiveness, and its accuracy when analysing complicated signals, has been proven by many researchers [126-132]. The wavelet technique has been used to detect shaft misalignment and bearing troubles by analysing the output power signal of variable speed wind turbines [37]. Figure 3.4 shows the approximation and detail coefficients frequency range of a wavelet function that can be expressed as [30]:

$$X[n] = \sum_{j} a_{i_{0,j}} \varphi_{i_{0,j}}[n] + \sum_{i=i_0}^{j-1} \sum_{j} d_{i,j}\, \psi_{i,j}[n] \qquad 3.9$$

$$a_{i_{0,j}}(n) = \int_{-\infty}^{\infty} x[n]\, \varphi_{i_{0,j}}[n] dn \qquad 3.9.1$$

$$d_{i,j}(n) = \int_{-\infty}^{\infty} x[n]\, \psi_{i,j} dn \qquad 3.9.2$$

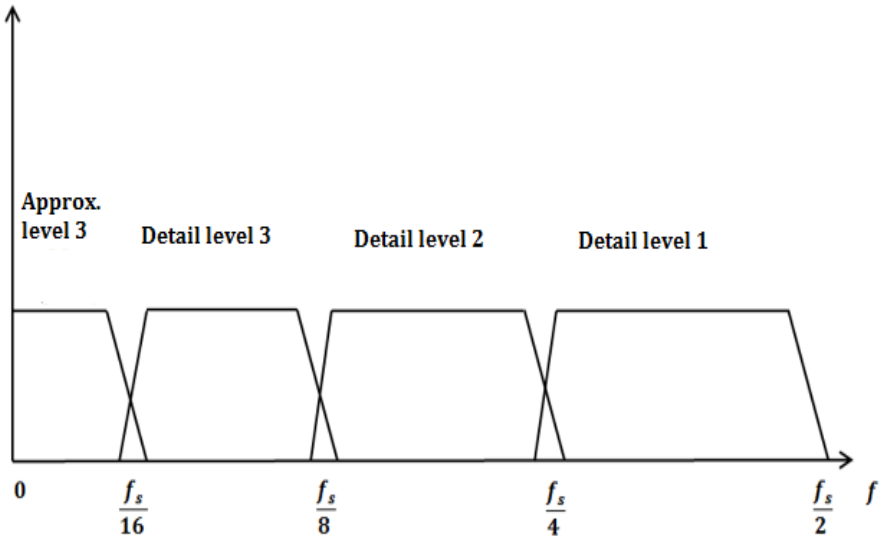

Figure 3.4 Frequency range includes the details and approximation coefficients

Where,

ψ [n]: the mother wavelet, and

$\varphi_{i,j}[n] = 2^{\frac{i_0}{2}} \varphi(2^{i_0} n - j)$: scaling functions at a scale of

$s = 2^{i_0}$ shifted by j.

Similarly,

$\psi_{i,j}[n] = 2^{\frac{i}{2}} \psi(2^{i} n - j)$: the mother wavelet at a scale of

$s = 2^{i_0}$ shifted by j $a_{i_0,j}$: approximation coefficients at a scale of

$s = 2^{i_0}$, and

$d_{i,j}$: detail coefficients at a scale of $s = 2^{i}$

There are two techniques used in wavelet transform: 1) Discrete Wavelet Transform (DWT) and 2) Continuous Wavelet Transform (CWT). DWT reduces noise in speed signals and highly variable shaft torque, because the method can correctly extract time-frequency features from the highly variable wind turbine signals [6]. CWT (DWT for a signal $x\ (t)$ as shown in Figure 3.5) can be represented by:

$$CWT_{a,b}(t) = \int_{-\infty}^{\infty} x(t)\Psi_{a,b}(t)dt \qquad 3.10$$

The DWT and CWT both are related by [74]:

$$DWT_{j,n}(t) = CWT_{2j,2jn}(t) =$$

$$\frac{1}{\sqrt{2j}}\int_{-\infty}^{\infty} x(t)\Psi\left(\frac{t}{2j} - n\right)dt, \qquad (j, n \in Z) \qquad 3.11$$

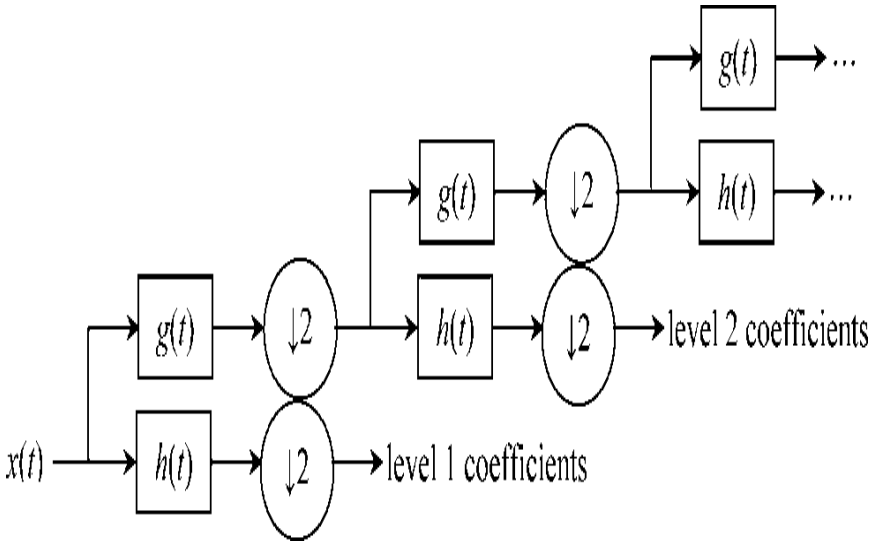

Figure 3.5 Discreet wavelet transform of x(t) signal [133].

References [133] and [75] present the noise reduction approach of the signal thresholding wavelet coefficients, given by:

-First Hard Thresholding

$$\hat{d}_{j,n}(t) = \begin{cases} d_{j,n}(t) & if \quad |d_{j,n}(t)| > \theta \\ 0 & if \quad |d_{j,n}(t)| \leq \theta \end{cases} \qquad 3.12$$

-Second Soft Thresholding

$$\hat{d}_{j,n}(t) = \begin{cases} \hat{d}_{j,n}(t) - \theta & \text{if} \quad |d_{j,n}(t)| > \theta \\ 0 & \text{if} \quad |d_{j,n}(t)| \leq \theta \\ d_{j,n}(t) + \theta & \text{if} \quad |d_{j,n}(t)| < \theta \end{cases} \qquad 3.13$$

Where

$\hat{d}_{j,n}(t)$ are the thresholded values of $d_{j,n}(t)$.

θ Can be calculated as

$$\theta = \sigma\sqrt{2\log(L)}$$

Where

σ : t estimated noise level, and

L : number of coefficients in the same level.

Thus, the main de-noised signal can be built using the following equation:

$$\hat{x}(t) = \sum_{n=-\infty}^{\infty} \hat{a}_{0,n}(t) g_{0,n}(t) + \sum_{j=0}^{\infty} \sum_{n=-\infty}^{\infty} \hat{d}_{j,n}(t) h_{j,n}(t) \qquad 3.14$$

Calculation of $\hat{a}_{0,n}(t)$ is similar to $\hat{d}_{j,n}(t)$. Investigative work has found that the hard thresholding approach is easier to calculate, and using a fixed threshold amount will result in cut-offs in the de-noised signal.

For example, a high-order wavelet (Daubechies 14) is capable of minimising the overlap between frequency bands. Due to the ability of discrete wavelet transform to correctly localise frequencies with accurate time locations, any unforeseen transient variations that could take place within any steady-state regime can be detected by this application [134]. The harmonic wavelet transform offers many advantages at reduced complexity. The use of orthogonal wavelet families result in no redundancy, which means N data points produce N wavelet amplitudes [113]. Wavelet common function families — Daubechies family, Coiflets family and the Symlet family are illustrated in Figure 3.7 [135].

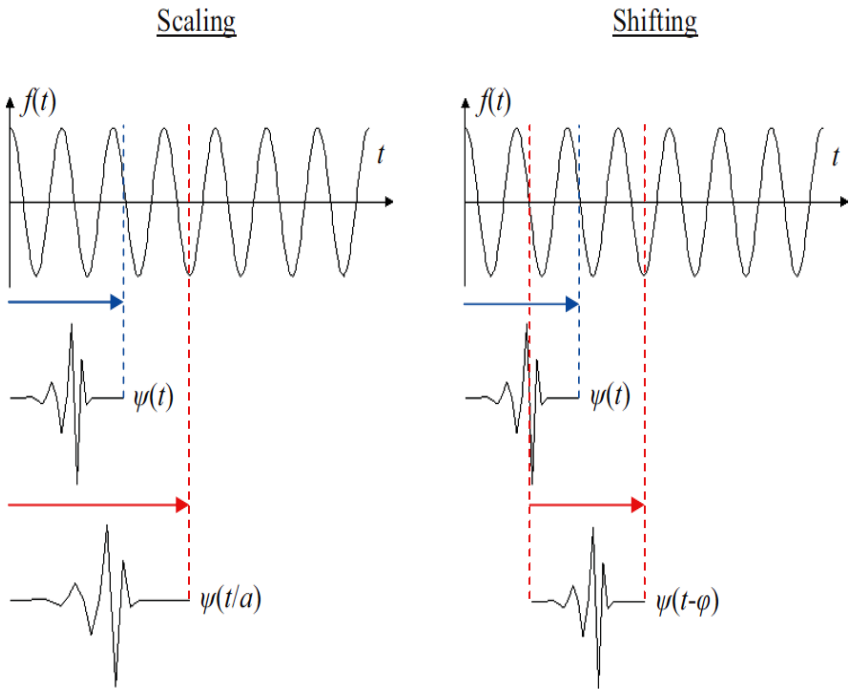

Figure 3.6 Wavelet transform mother function principle.

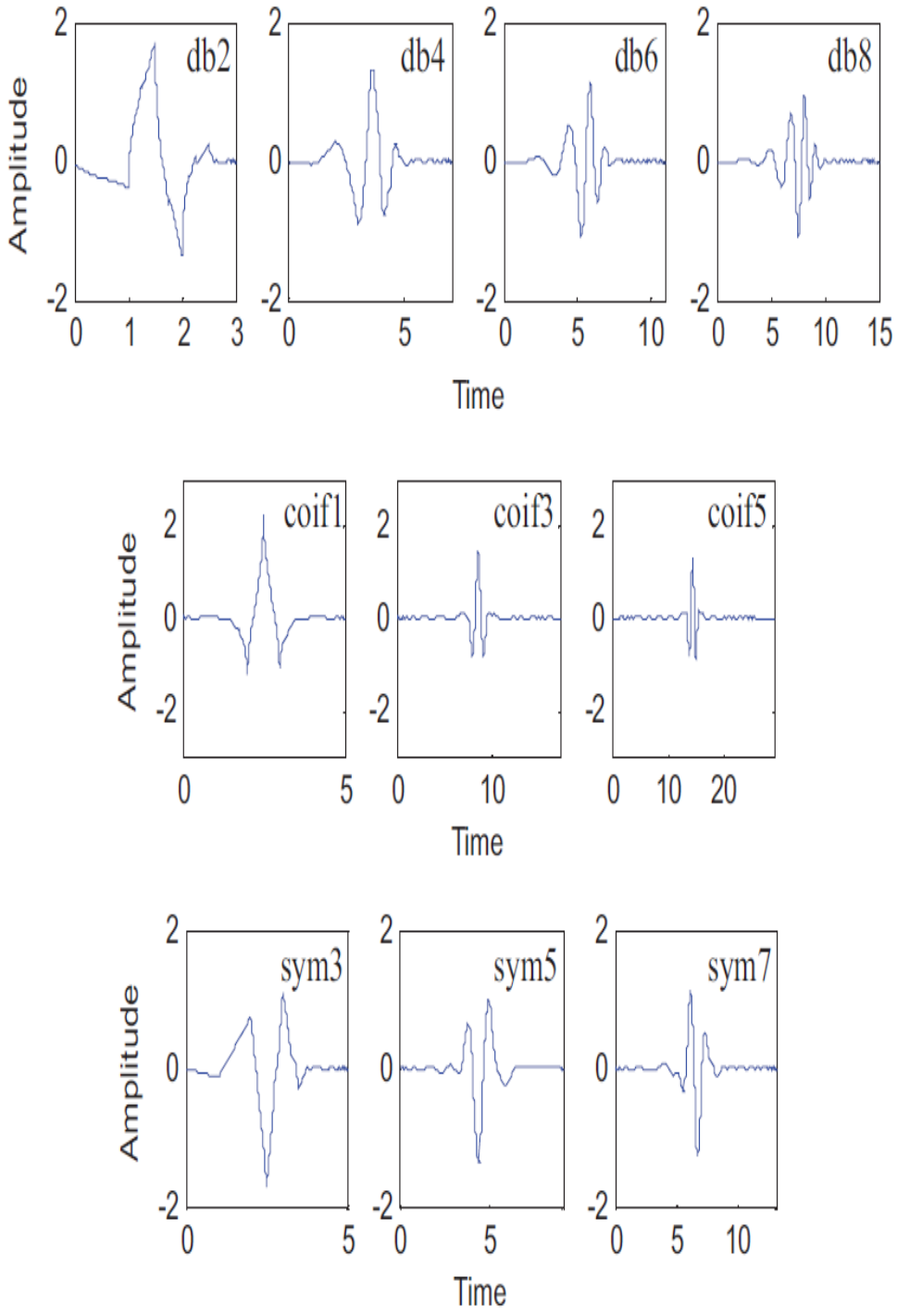

Figure 3.7 Wavelet transform functions: Daubechies family (db), the Coiflets family (coif) and the Symlet family (sym).

Discrete wavelet transform has been applied to different signal classifications and power quality applications in [124] and [136-139]. Mallat [140] developed a new technique, in wavelet transform, to detect multi-resolution signal decomposition, which helps when analysing the information content of images. Daubechies [141] provides a full description of different wavelet transform applications, focusing on time-frequency localisation and signal analysis.

According to [142], the decomposition levels can be tested and calculated based on the following formula:

$$n_d > \frac{\mathrm{Log}(f_s/f)}{\mathrm{Log}(2)} + 1 \qquad 3.15$$

Where

f_s: sampling frequencies, and

f : supply frequencies

3.3.1 Wavelet and Fourier Transform Correlation

Based on [123]:

$$\mathcal{F}\left[\Psi_{b,a}(x)\right] = \frac{1}{\sqrt{|a|}}\int_{-\infty}^{\infty} e^{-ixy}\,\Psi\left(\frac{x-b}{a}\right)dx$$

$$= \int_{-\infty}^{\infty} e^{-i(b+az)y}\,\Psi(z)\frac{a}{\sqrt{|a|}}dz; \qquad 3.16$$

So that:

$$\mathcal{F}\left[\Psi_{b,a}(x)\right] = \frac{a}{\sqrt{|a|}}e^{-iby}\widehat{\Psi}(ay) \qquad 3.16.1$$

By using the Parseval formula below (3.17) and substituting n=1:

$$(f,g) = \left(\frac{1}{2\pi}\right)^n (\hat{f},\hat{g}) \qquad 3.17$$

$$(W_\Psi f)(b,a) = \left(f,\Psi_{b,a}\right) = \frac{1}{2\pi}\left(\hat{f},\hat{\Psi}_{b,a}\right) \qquad 3.18$$

$$= \frac{a|a|^{-\frac{1}{2}}}{2\pi}\int_{-\infty}^{\infty} \hat{f}\ (\omega) e^{ib\omega}\overline{\hat{\Psi}(a\omega)}d\omega$$

$$= a|a|^{-\frac{1}{2}}\mathcal{F}^{-1}\left[\hat{f}\ (\omega)\overline{\hat{\Psi}(a\omega)}\ \right](b,a) \qquad 3.19$$

Hence:

$$\mathcal{F}[(W_\Psi f)(b,a)](\omega) = a|a|^{-\frac{1}{2}}\widehat{f}\ (\omega)\overline{\hat{\Psi}(a\omega)}. \qquad 3.20$$

The relation shown in 3.16 holds in general, for $f \in L^p(\mathbb{R})\ and\ \Psi \in L^q(\mathbb{R})$

Where $1+1/r = 1/p + 1/q$ and $1 \leq p,q,r \leq 2$

Some other special techniques used in WT condition monitoring are summarised in Table 3.2.

Table 3.2 Special applications in fault detection and analysis of the wind turbine gearbox.

Technique	Advantage	Disadvantage
Frequency Domain	Costs avoided by analysis of the sideband frequency and extraction of gearbox conditions without a tachometer signal [50].	Noises in signals can be affected by other sources, such as the shaft and other gear mechanisms.
Cepstrum	More suitable for a group of harmonics, and ideal for checking the gearbox condition by comparing sidebands with amplitude modulation [143].	Group of harmonics may occur due to shaft or misalignment issue which is not a gear fault. Also requires a baseline to which to compare the cepstrum and investigate the changes.
Bearing Envelope Analysis	Recent technique under development, and more suitable for detecting early bearing spalls [144].	Requires a high sampling rate, depending on the motivated vibration.
Spectral Kurtosis Filtering	Employs a suitable filter in its envelope technique and calculates the features from filtered signals [145].	Faults and spalls are not impulsive, which means this technique will overlook these types of fault.

Time Synchronous Averaging	Effective for vibrations synchronous with shaft. Comparing the amplitude with phase modulation will result in identification of a soft tooth, and residual signals may follow the irregularities in normal meshing [146].	Specific tachometer required for carrying out the synchronous averaging. Takes a long time to read the samples for averaging, due to low shaft speed.
Planet Separation Method	Particular algorithm considered for carrying out synchronous averaging for planetary gearboxes [147], which allows the gearbox condition to be analysed in detail.	Long acquisition time, and requires a specific tachometer for arranging the data (taking into account the rotations process, which has to be collected for averaging).

Chpater 4 Experim-ental Test Rig Setup

4.1 Introduction

In this chapter, the hardware set-up used to conduct the experimental measurements is presented. Figure 4.1 demonstrates the test rig components used in investigating various failure modes of real wind turbines. Components of the developed test rig are briefly presented below:

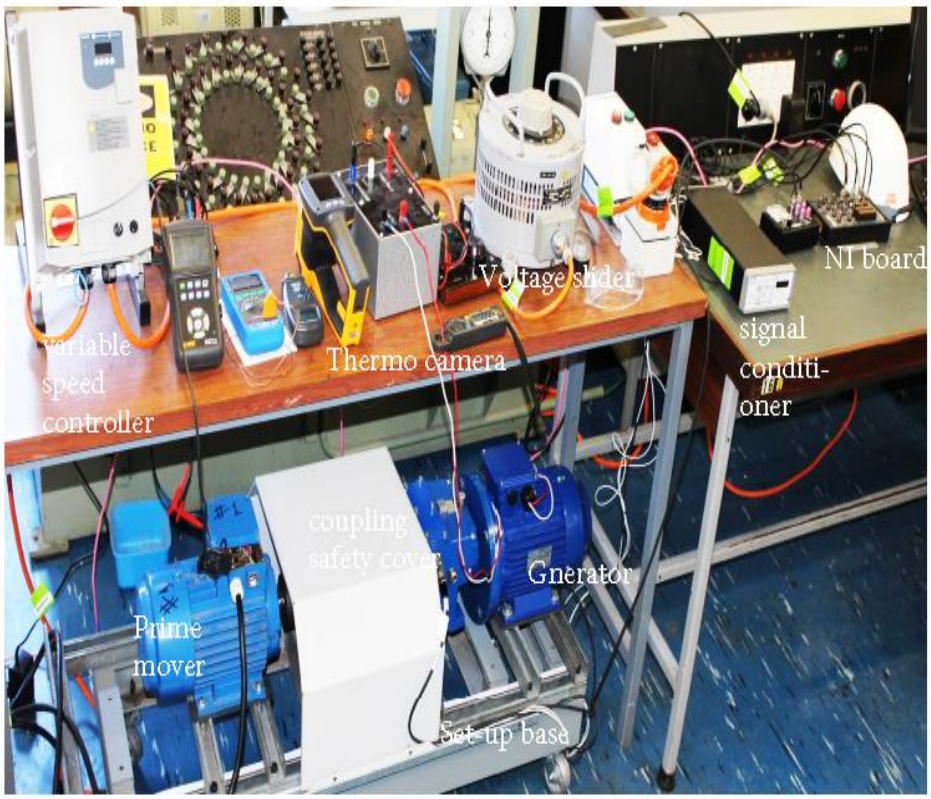

Figure 4.1 Test rig configuration

4.2 Wind Turbine Test Rig Components

4.2.1 The Drivetrain

The drivetrain of the wind turbine includes the hub, gear box, shafts and the generator (as shown in figure 4.2) [148]. The drivetrain also involves other sub-systems, such as bearings, coupling and mechanical breaks.

The dynamic forces generated by wind gust will not only affect the turbine blades but will also have a direct impact on the internal drivetrain components.

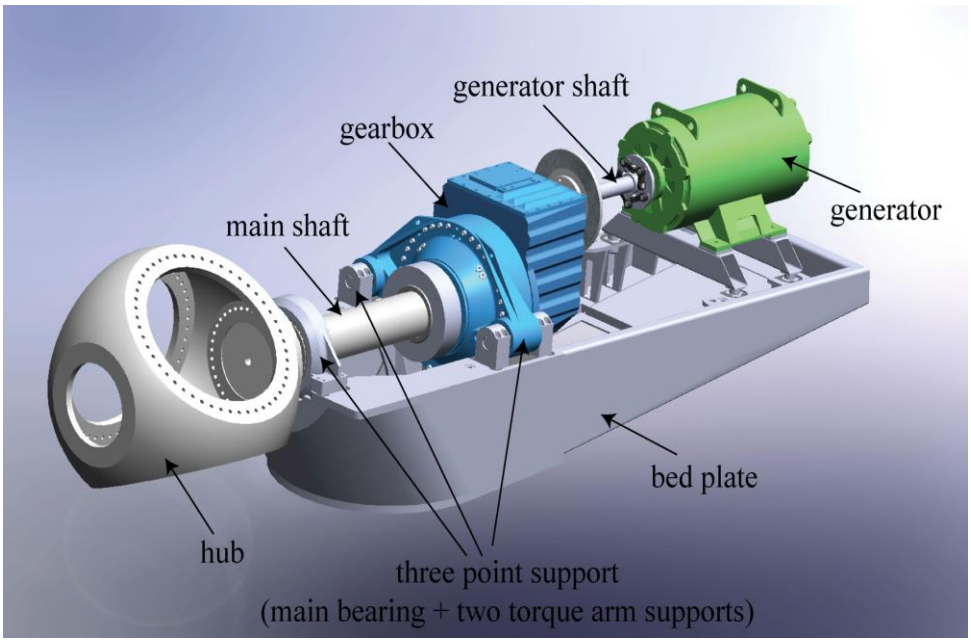

Figure 4.2 Wind turbine drive train arrangements [149].

In the developed test rig, a synchronous generator shaft is coupled with the shaft of an induction motor through a gearbox.

4.2.2 Coupling and Gearbox

A coupling is the way to connect two shafts together and allows rotational torque between these shafts. In wind turbines, the coupling is used to connect the high speed shaft of the gearbox and the generator. In order to protect the gearbox and for safety reasons, some manufactures design the coupling with an internal clutch, which avoids any torque transient transfer in case of generator failure (e.g. short circuit).

A two stage gearbox with a ratio of 1: 4.34, manufacturer SITI, type NHL25 was in the hardware setup. The gearbox was lubricated with mineral oil SOVG 220. Figure 4.3 shows the dynamic model of the drivetrain.

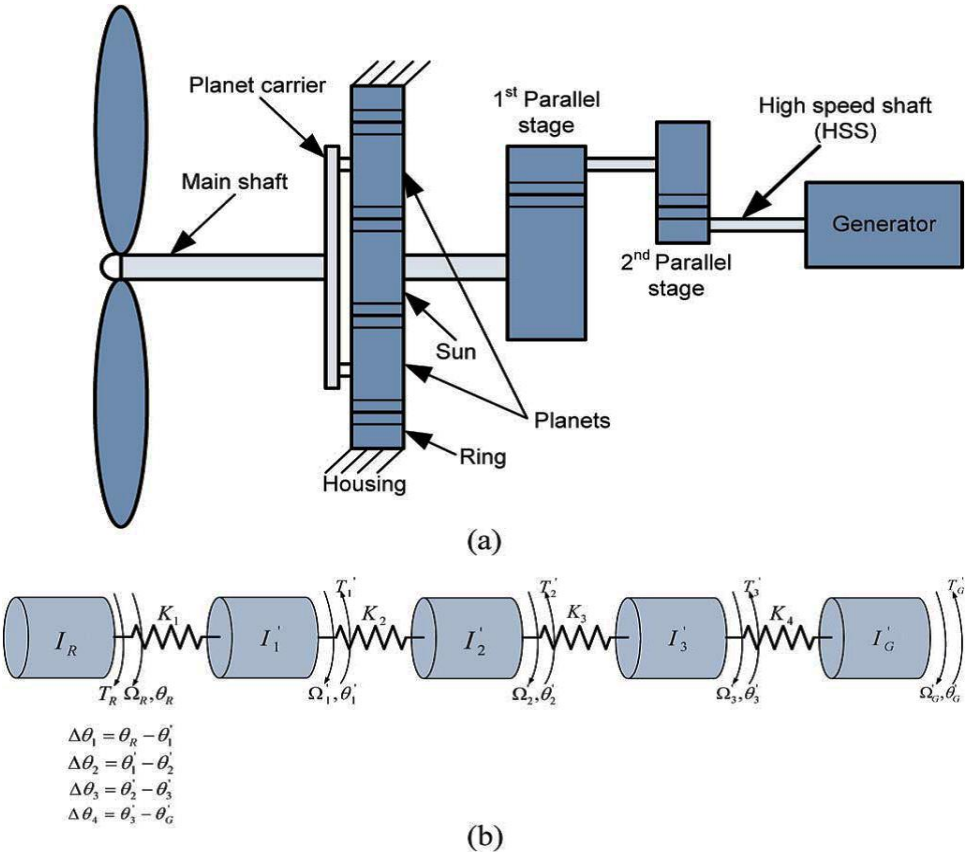

Figure 4.3 (a) Multi-stage representation of the gearbox. (b) Equivalent dynamic model [67].

The homogenous motion equation of the torsional model of this 5-mass drivetrain is given by:''

$$I\ddot{\theta} + K\theta = 0$$

Where

$\theta = [\theta_h \theta_{s_1} \theta_{s_2} \theta_{s_3} \theta_{Gen}]^T$: displacement vector,

K: stiffness matrix, and

I: diagonal inertia matrix.

$$I = \begin{bmatrix} I_h & 0 & 0 & 0 & 0 \\ 0 & I_{S1} & 0 & 0 & 0 \\ 0 & 0 & I_{S2} & 0 & 0 \\ 0 & 0 & 0 & I_{S3} & 0 \\ 0 & 0 & 0 & 0 & I_{Gen} \end{bmatrix}$$

$$I_{S1} = I_{PC} + N_1^2 I_S$$

$$I_{S_2} = N_1{}^2 I_{G_1} + (N_1 N_2)^2 I_{P_1}$$

$$I_{S_3} = (N_1 N_2)^2 I_{G_2} + (N_1 N_2 N_3)^2 I_{P_2}$$

$$I_{Gen} = (N_1 N_2 N_3)^2 I_{Gen}$$

Where

I_h : mass inertia for the rotor (blades);

I_G : planetary carrier inertia;

I_S : sun inertia;

I_{S1} : effective inertia of stage I;

I_{G_1}: gear inertia of stage II;

I_{P_1} : pinion inertia of stage II;

I_{S_2} : effective inertia of stage II;

I_{G_2}: gear inertia of stage III;

$I_{P_{12}}$: stage III pinion inertia; and

I_{S_3} : effective inertia of stage III.

The stiffness matrix can be written as:

$$K = \begin{bmatrix} K_1 & -K_1 & 0 & 0 & 0 \\ -K_1 & K_1 + K_{e2} & -K_{e2} & 0 & 0 \\ 0 & -K_{e2} & K_{e2} + -K_{e3} & -K_{e3} & 0 \\ 0 & 0 & -K_{e3} & K_{e3} + -K_{e4} & -K_{e4} \\ 0 & 0 & 0 & -K_{e4} & K_{e4} + -K_{e5} \end{bmatrix}$$

Where

$$K_{e2} = N_1^2 K_2$$

$$K_{e3=}(N_1 N_2)^2 K_3$$

$$K_{e4=} (N_1 N_2 N_3)^2 K_4$$

$$K_{e5=} (N_1 N_2 N_3)^2 K_5$$

Individual shaft stiffness can be expressed as:

$$K_{Shaft} = \frac{I.G}{L}$$

Where

I : polar moment of inertia,

L : length of the shaft, and

G: shear modulus.''

These equations help to understand how the mechanism of the gearbox works based on every stage, depending on the gearbox type and the number of stages.

4.2.3 Bearings

The main purpose of a bearing is to smooth the frictional resistance between two surfaces within proportional motion, either linear or rotational. Two types of bearings are employed in the WT drivetrain: 1) linear/axial, and 2) rotational/radial. The first type is usually fitted in the main shaft, while rotational bearings are commonly used for gears. Many studies have reported that the bearing is one of the main causes of gearbox failure [150, 151].

4.2.4 Shaft

The shaft is designed to rotate based on the transmitting torque function. A shaft can be fitted within the WT drivetrain in several different ways, depending on the speed stage. At a high speed stage (HSS), the shaft is connected to the rotor side (WT blades, main shaft), and at a low speed stage (LSS), the shaft is fitted to the generator side (generator shaft).

4.2.5 The hub

The hub is located where the blades join together and is connected to the main shaft. The hub also carries the electrical and mechanical control systems, which improve the position of the blades. There are different hub structure designs available in the industry, but they are predominantly made from cast iron. This is due to cast iron's solid nature and low cost.

4.2.6 Mechanical Brakes

One of the methods to control the over speed of a wind turbine is the use of mechanical brakes. A mechanical brake is a steel disc, typically fitted on the high speed shaft and combined with a calliper to accomplish braking. The braking procedure involves extreme heat and stress, especially to the disc. Temperature can reach up to 700 degrees Celsius [152], and for this reason, special disc materials are used. The braking practice is called "a fail-safe system," because when power fails, the mechanical braking system is engaged. It is compulsory in most countries for a wind turbine to be equipped with two fail-safe systems. This is so that the the turbine can always be stopped in the case of an emergency and so that any further consequences can be avoided [153].

4.2.7 Signal Conditioning and Transducers

A signal conditioner was part of the test setup that was required for low noisy signals and data acquisition purposes. Signal filtration cuts out any noisy signals or irrelevant information, which can lead to large amounts of data that may affect the analysis process and lead to speculation on the real condition of the equipment. A real photo of the signal conditioner used in the experimental setup is shown in Figure 4.1.

4.2.8 Accelerometers

Figure 4.4 shows a number of accelerometers that have been fitted to the experimental setup test rig. The ISOTRON (ENDEVCO model 2258A-10) accelerometer has excellent output sensitivity (10-100 mV/g), is of a small size and light in weight (15 gm). This accelerometer is mounted on the gearbox towards the low speed stage shaft. The other high performance and low frequency accelerometer (model AC133-1D), with a sensitivity of 500 mV/g, is mounted at the top side of the gearbox casing. Figures showing the

two accelerometers, including their specifications, are provided in appendix (A), tables A.1 and A.2.

(A)

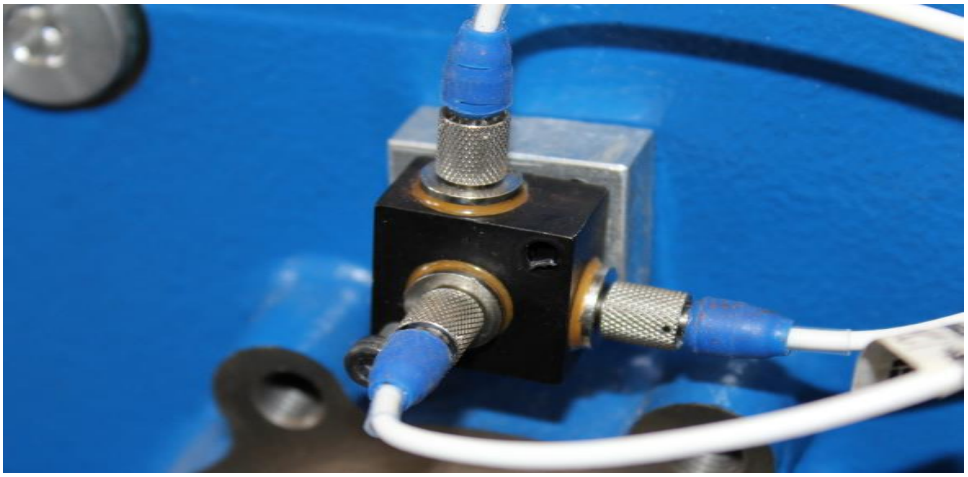

(B)

Figure 4.4 Accelerometer model AC133 (A). ISOTRON (ENDEVCO model 2258A-10) accelerometer (B).

4.2.9 Torque Transducer

A torque transducer (FUTEK model TRS605) was fitted between the prime mover and the low speed shaft of the gearbox to measure the shaft torque (rated torque is 100 Nm). Figure 4.5 shows the torque transducer and the IN board with the signal conditioner. The technical specifications along with electrical block diagram for the torque transducer are given in appendix (A), figure A.2 and A.3.

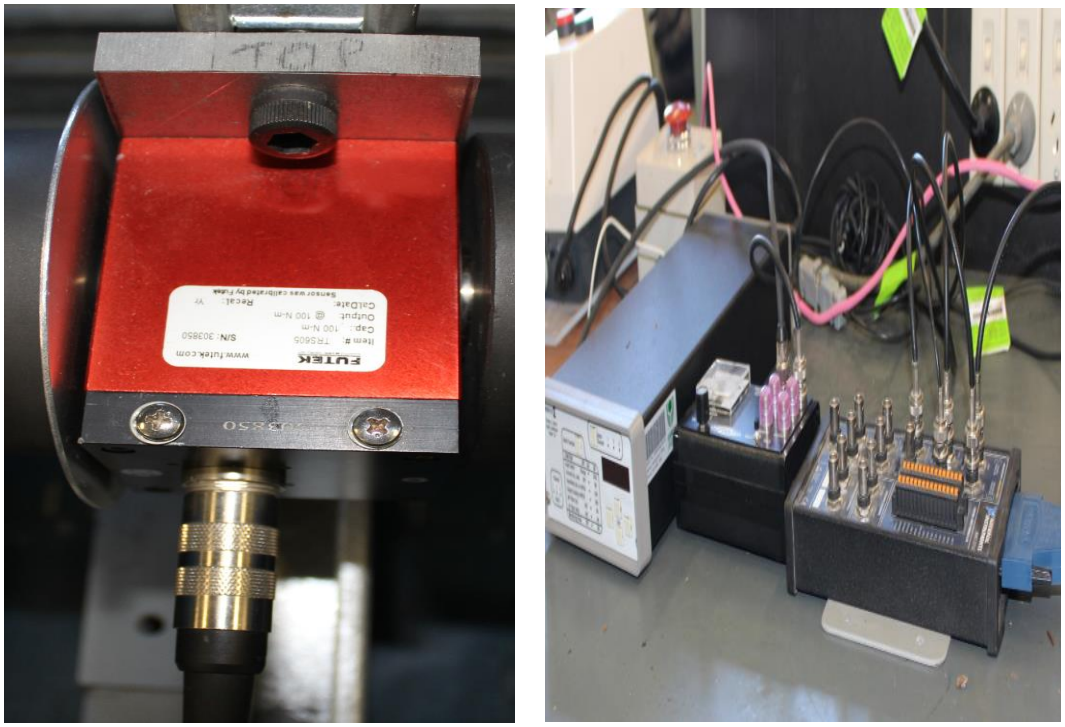

Figure 4.5 Torque transducer (FUTEK model TRS605) -left. Signal conditioner and IN board -right.

Figure 4.6 shows a schematic diagram of the experimental setup and illustrates the flow of the data collected through the control interface based on the sensor, transducers and signal conditioner and the data acquisition (using LabVIEW software).

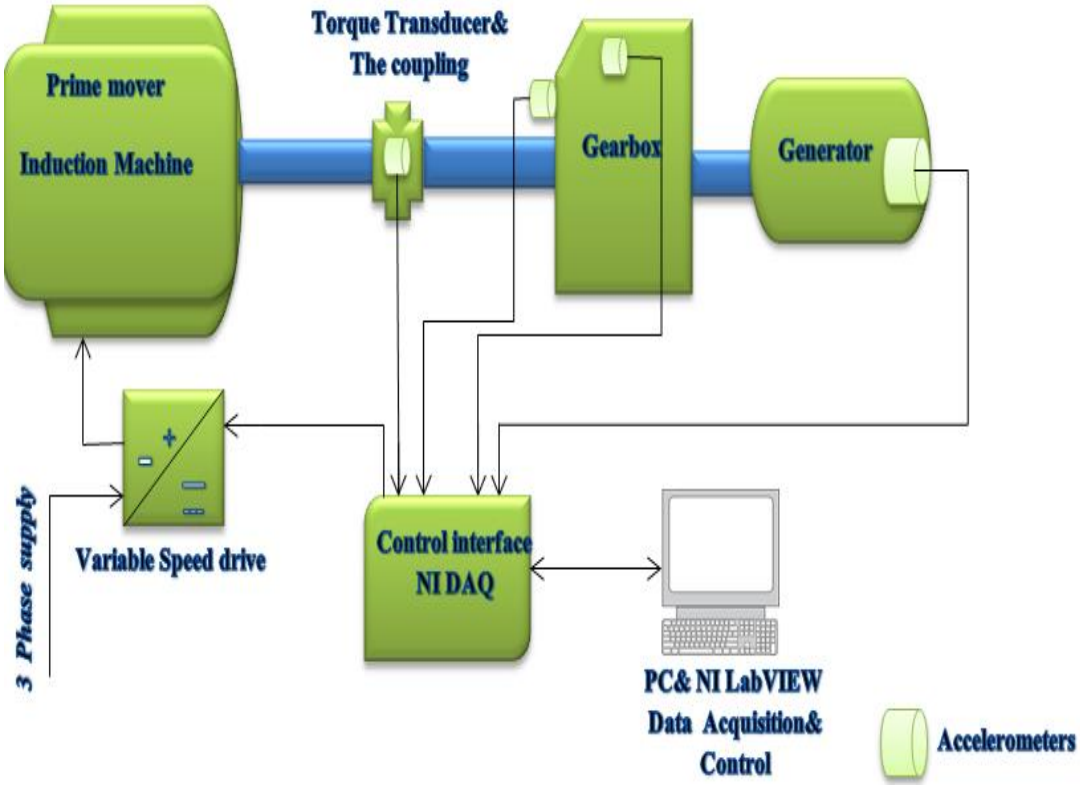

Figure 4.6 Schematic diagram of the test rig setup for wind turbine.

Chpater 5 Results and Discussion

5.1 Case Study: Wind Turbine Drivetrain Stresses Based on Narrow Band Wavelets

5.1.1 Introduction

This section introduces an improved technique to monitor the condition of the wind turbine gearbox based on gearbox vibration and shaft torque signatures analyses. In this context, shaft torque and mechanical vibration signals are detected using high resolution sensors and are analysed using two signal processing techniques: 1) wavelet and 2) fast Fourier transform (order analyses). This is in order to investigate the impact of investigated fault levels on the wind turbine drivetrain. Both signal processing techniques are compared, based on their sensitivity to detect incipient fault conditions.

5.1.2 Results and Discussion

Figure 5.1 (a) shows the torque signal during normal operating conditions. The torque signal was measured by the torque transducer, which was fitted between the prime mover and the low speed stage of the gearbox. When there is no mechanical stress applied to the drive train, the torque amplitude is measured at a rotor speed of 200 rpm. The results of the wavelet technique have been calculated up to level 7.

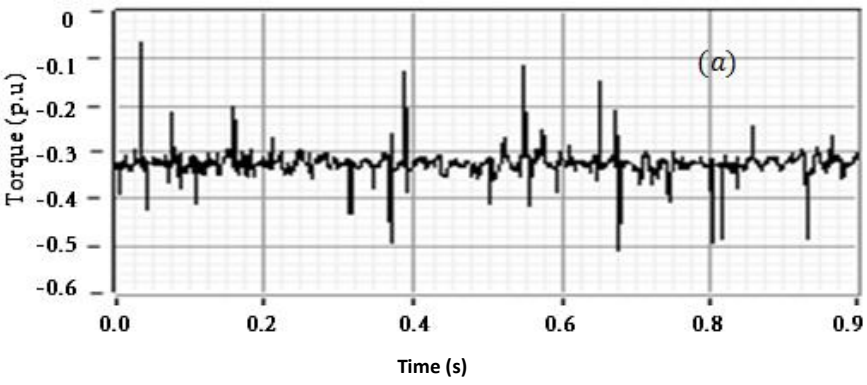

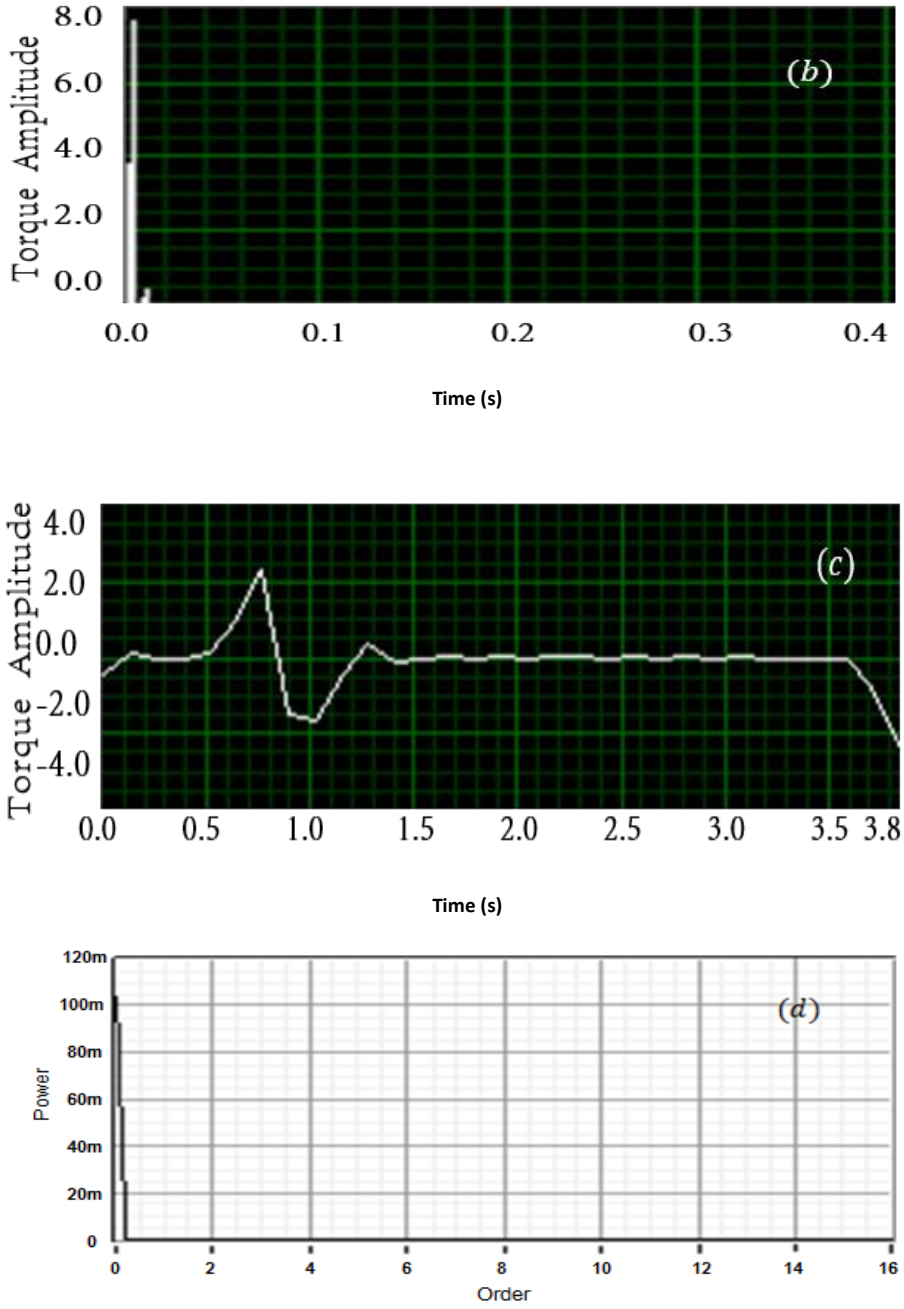

Figure 5.1 Torque signal under normal operating conditions (healthy conditions)

Figure 5.1 (b) shows approximated coefficients of the healthy torque signal using wavelet db14 (Daubechies 14), while figure 5.1 (c) shows the detail coefficients of the signal. Figure 5.1 (d) uses order analysis to show the signal in a frequency domain representation. The healthy signature signals presented in figure 3.7 are used as a reference, against which future

measured signatures signals are compared. Any variation can be assessed as a possible fault.

A stressed shaft is simulated by injecting a current of 85% of the generator's rated current (9.39 A) through the generator stator terminals. This also emulates real fault conditions on the wind turbine blades, such as icing accumulation, wind shear, and gust wind. The 85% is the pulse current represents the maximum value of the full load that can be injected, this has been done to emulate the stress on the WT drivetrain when the rotor (blades are in full capacity operation). This current was injected for short time due to the load capacity otherwise if the injected current continue longer then the whole drivetrain will over heated which may cause catastrophic failure to the WT.

As can be seen in figure 5.2 (a), there is a significant increase in the torque amplitude when compared with the healthy condition shown in figure 5.1 (a). Most of the rolling elements, such as the bearings, are designed to operate with a relatively smooth transition between loaded and unloaded modes. The rapid and significant amplitude change, shown in the torque signal of figure 5.2 (a), is attributed to the machine delivering more mechanical power to overcome the stress on its shaft. This can have a significant impact on the surface durability of the rolling elements.

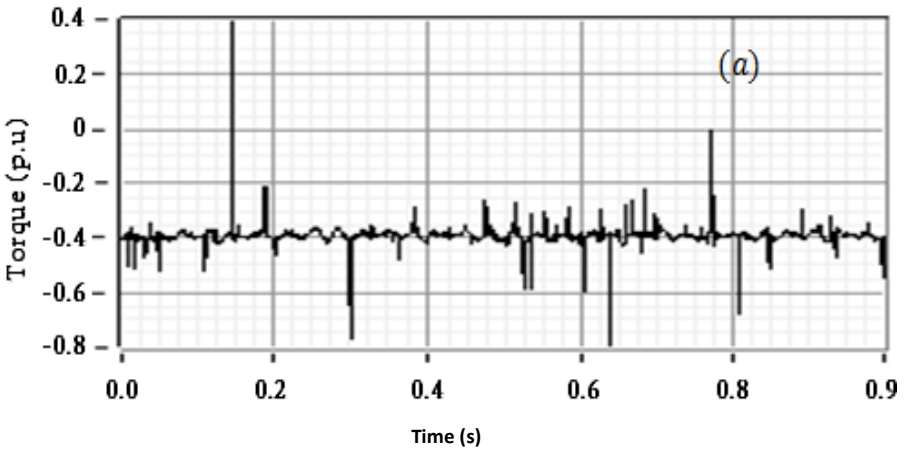

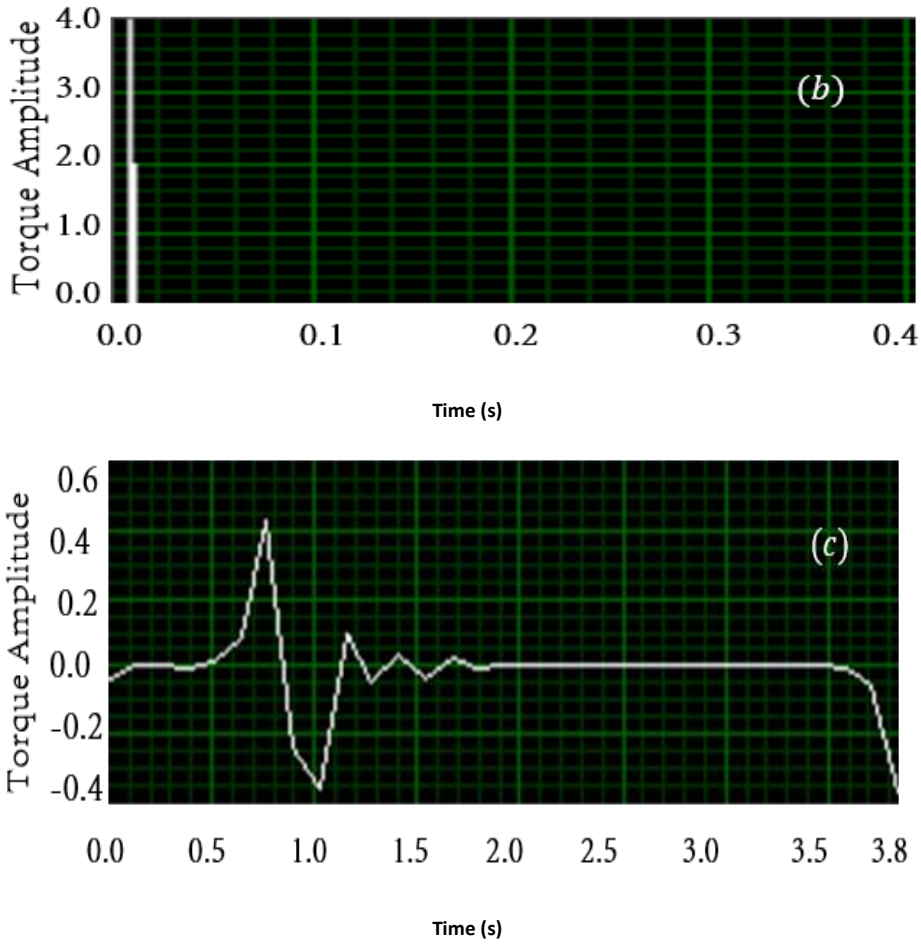

Figure 5.2 Torque signal under stressed shaft

The wavelet approximation coefficient shown in figure 5.2 (b) exhibits a significant drop in amplitude when compared with the normal operating condition signal shown in figure 5.1 (b). Consequently, the detail coefficient of the wavelet signal significantly decreases (as can be seen in figure 5.2 (c)). The power spectrum of the order analysis technique could not be captured in this instance. This may be attributed to the high stator injected current, which can cause stress on the rotor of the generator and force the whole drive train to stop when the shaft speed reaches critical speed.

The vibration signal during normal operating conditions (shown in figure 5.3 (a)) is measured using a sensor, which is located on the low speed stage of the gearbox towards the main shaft. As shown in figure 5.3 (a), the vibration signal oscillates between maximum and minimum limits with some

spikes. When analysed using the wavelet technique, we can gain a better understanding of the healthy vibration signal can be gained and store for future comparison. This is shown in the approximate and detail coefficients presented in figures 5.3 (b) and (c). Figure 5.3 (d) shows the harmonic contents in the order power spectrum of the vibration signal during healthy operating conditions.

When 85% of the full load current is injected to the generator stator terminals, while maintaining the shaft speed (200 rpm) and the sensor locations, the vibration signal was recorded as shown in figure 5.4. To show the impact of rotor speed on the measured vibration signature, figure 5.5 shows the vibration signature for a normal operating condition with a rotor speed of 650 rpm, while figure 5.6 shows the vibration signal of a stressed shaft (through the injection of 85% of the generator's rating current through the stator terminal) conducted at a higher speed.

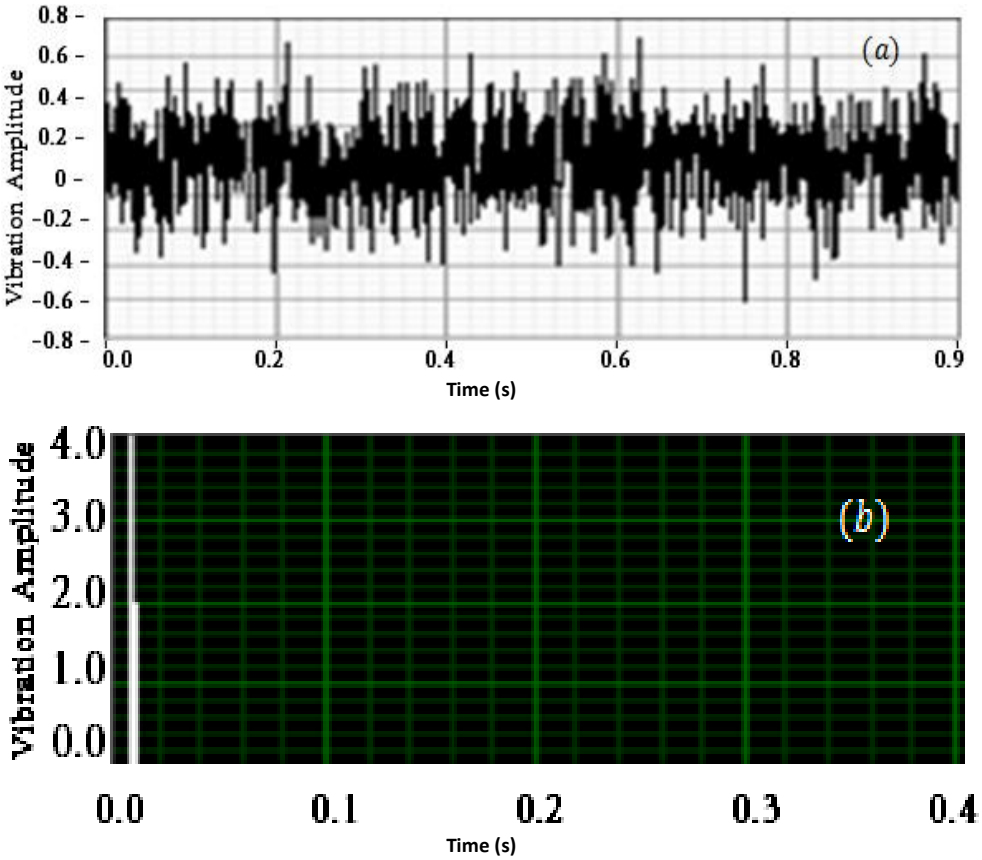

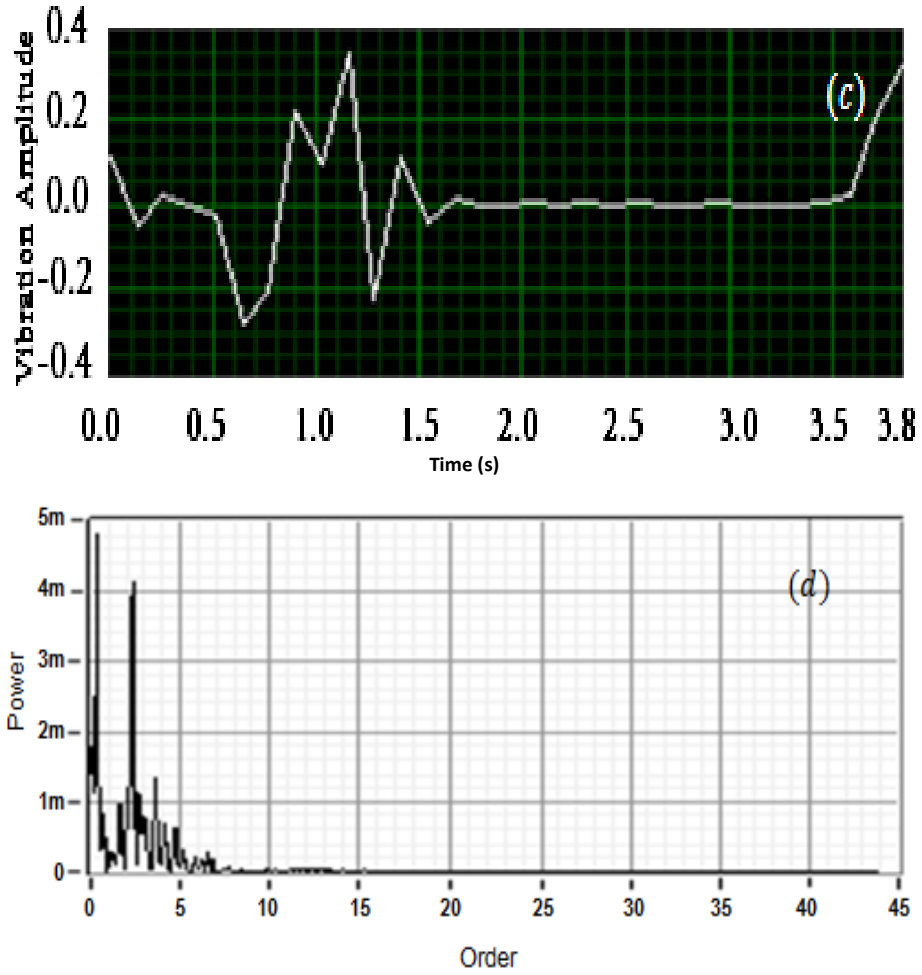

Figure 5.3 Vibration signal under normal operating conditions.

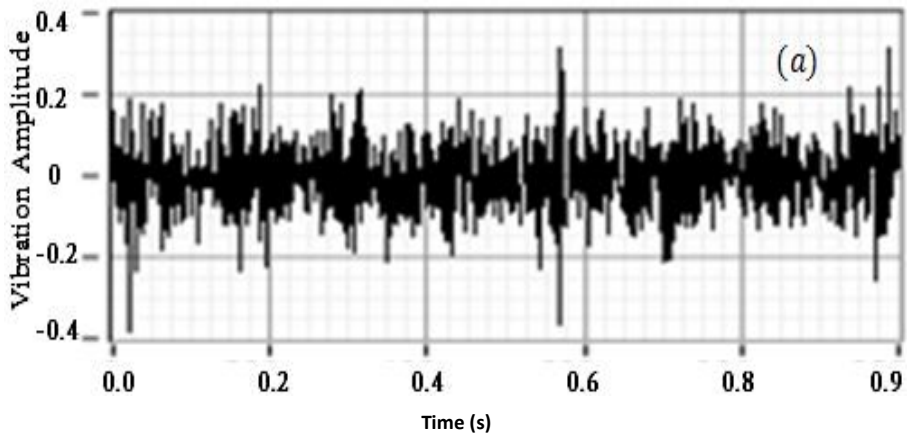

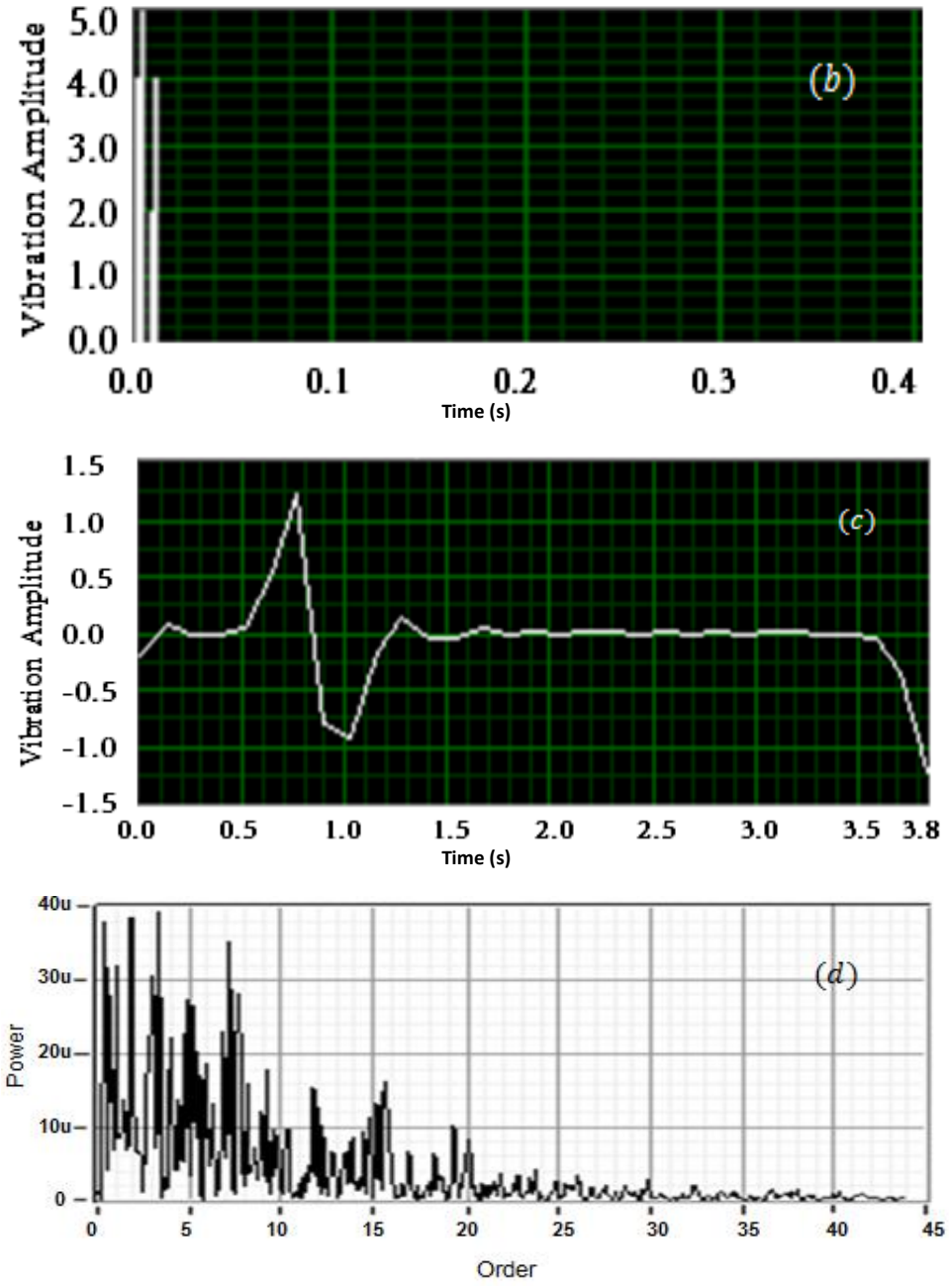

Figure 5.4 Sensors signals under critical faulty operating conditions.

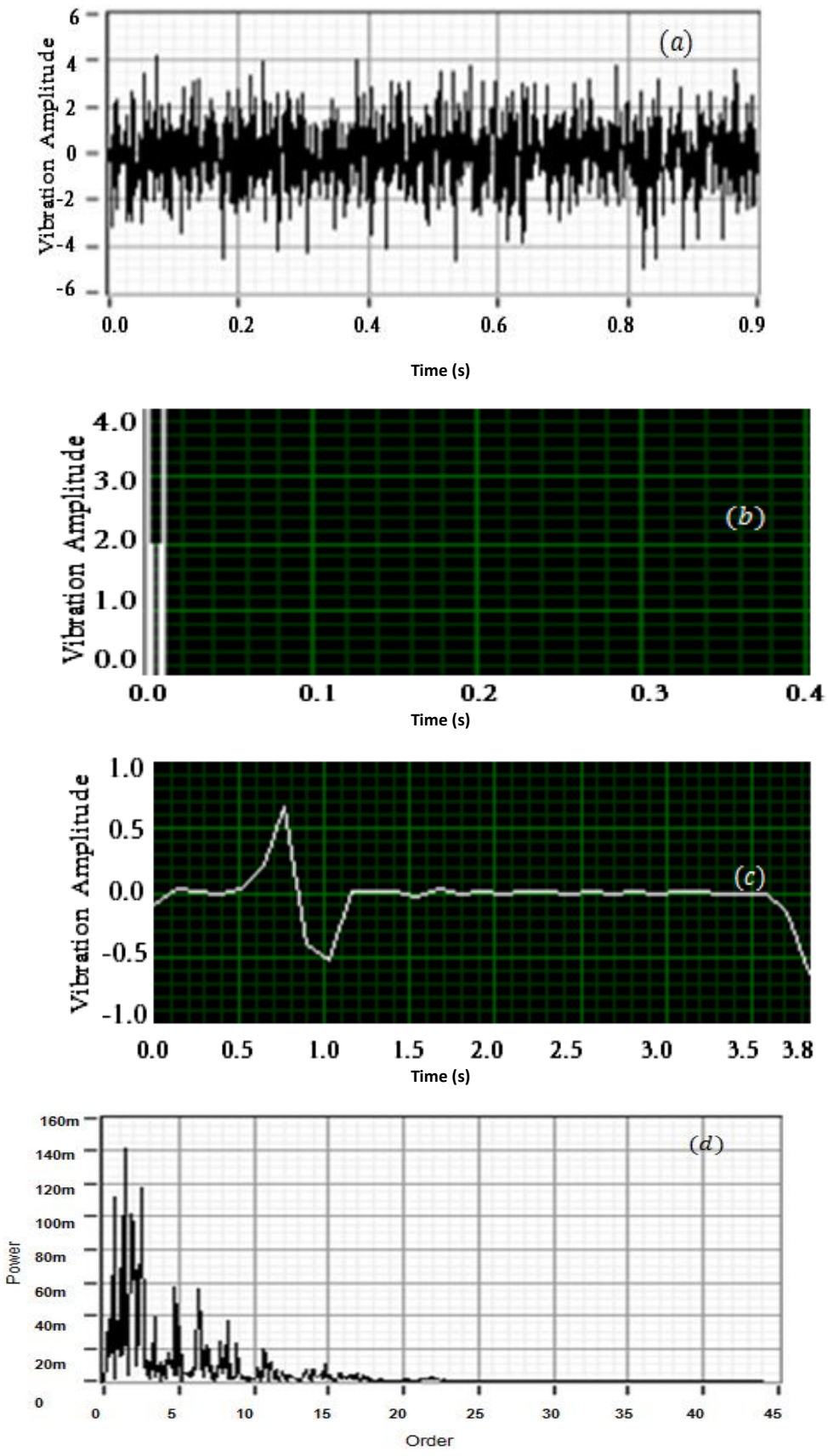

Figure 5.5 Signals conducted with extra speed under normal operating conditions.

The results of figures 5.5 and 5.6 show that rotor speed greatly influences the measured vibration signature. A higher rotational speed corresponds to a higher vibration amplitude, and vice versa. It can also be observed that the faulty signal (shown in figure 5.6 (b)) exhibits a crest value of 80, which is 20 times the amplitude of the normal signal (shown in figure 5.5 (b)).

We can also see that the detail coefficients of the measured signal increase from 0.65, in normal operating conditions, to 12, in a stressed shaft condition. This can can be seen in figures 5.5 (c) and 5.6 (c) respectively. On the other hand, the power spectrum for the faulty signal (shown in figure 5.6 (d)) exhibits more harmonics with less amplitude when compared with the healthy signature power spectrum (shown in figure 5.5 (d)).

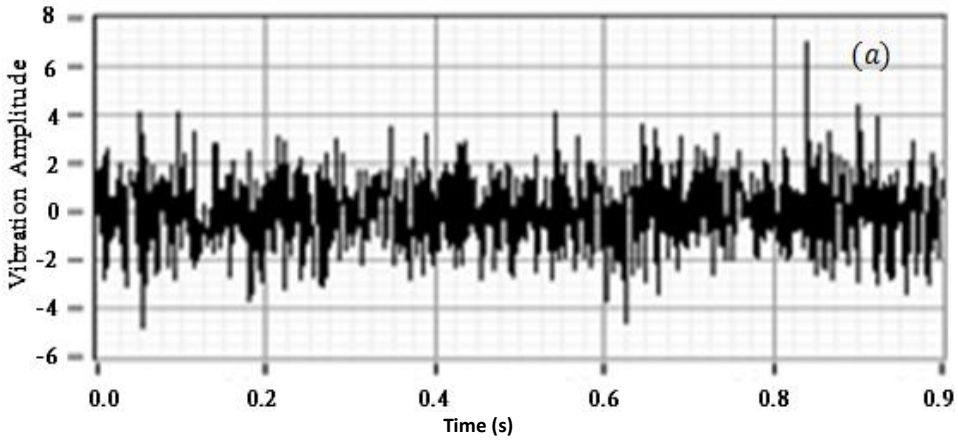

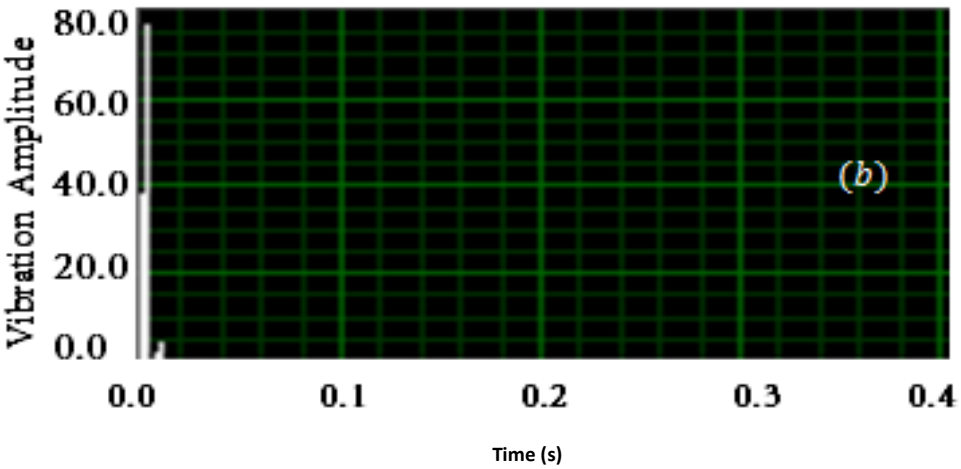

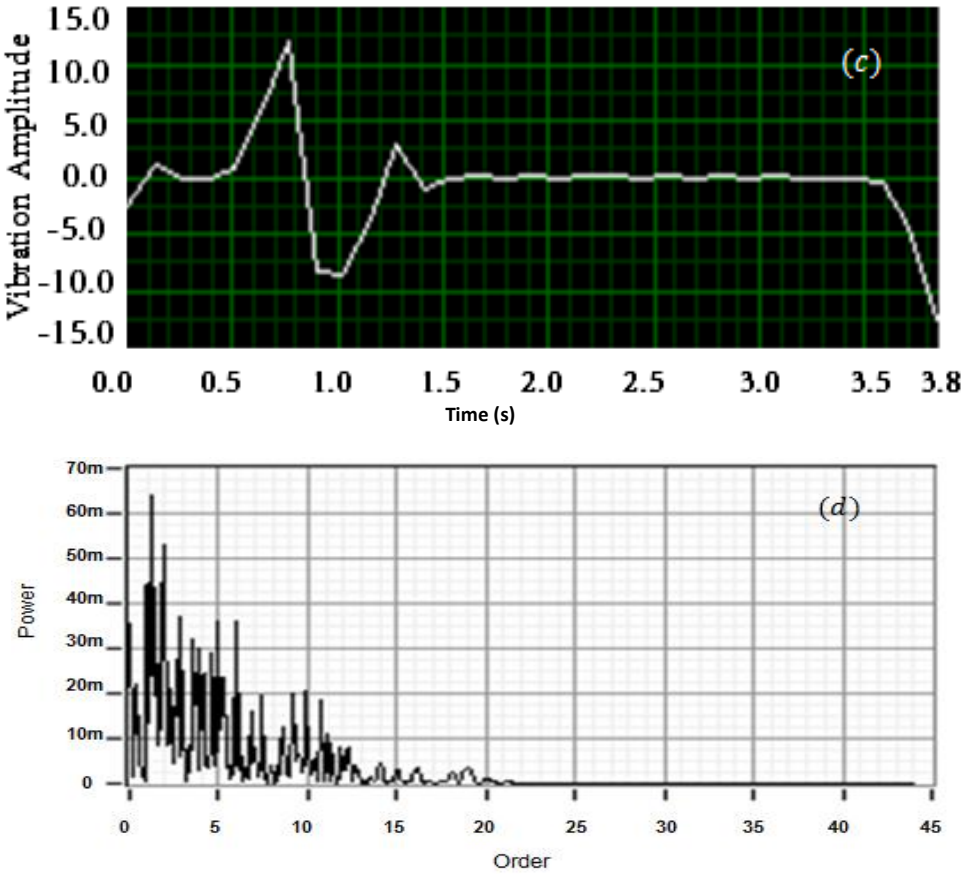

Figure 5.6 Signals conducted with extra speed under faulty operating conditions.

5.1.3 Conclusion

In this case study, different scenarios have been applied to the test rig, including changes in rotor speed, which show WT blades are affected by fluctuating loads. The shaft torque and gearbox vibration signals were measured using highly sensitive sensors, during both normal operating conditions and when the drivetrain shaft is stressed (implemented by injecting an electric current into the generator stator winding to create an opposite torsional torque on the main shaft).

The healthy and faulty signals were then processed and analysed using wavelet and order analyses techniques. Experimental results show that the wavelet analysis technique has the ability to localise the frequencies with

accurate time locations, as well as detect unforseen transient variations based on different faulty and healthy scenarios applied to the test rig. On the other hand, order analysis shows more harmonics in the analysed faulty signal, however it is hard to diagnose the cause of the root failures.

5.2 Case Study 2: Impact of Gearbox Oil Contamination on the Performance of the Wind Turbine Drivetrain

5.2.1 Introduction

This case study investigates the impact of gearbox lubrication oil contamination on the performance of the wind turbine drivetrain. In this context, the vibration signal of the gearbox is measured and analysed under various contamination levels of gearbox oil. A thermal camera is used to identify the hot spot location within the gearbox during the investigated case studies. Results show that quality of gearbox oil has a significant impact on the overall performance of the wind energy conversion system.

Table 5.1 shows the characteristics of the mineral lubricants used within the gearbox, along with ISOVG (International Standards Organisation Viscosity Grade). Typical oil properties can be found on Appendix A, table A.3 and table A.4.

5.2.2 Results and Discussion

Table 5.1 Oil types and specifications

Mineral Oil type	Viscosity (cSt) At 40°C	Density kg/L
ISOVG 220	224	At 20°C 0.861
ATF MHP	37	At 15°C 0.849

Figure 5.7 shows the measured vibration signal of new and contaminated lubrication oil. Oil is contaminated by dissolving 100 grams of fine iron powder into the oil. Figure 5.8 shows the vibration signal of the drivetrain when a current of 8 A is injected, to simulate real stress conditions, into phase A of the generator stator winding. As can be seen in figure 5.8 (a), the magnitude of the vibration signal is increased when compared with the no-stress condition shown in figure 5.7 (a). This is attributed to the high current injected into the generator stator windings, which creates an opposite torque. This then causes high mechanical stress to the generator shaft and, consequently, to the gearbox.

Figure 5.8 (b) shows the power spectrum of the measured vibration signal, using the peak hold technique, where it is easy to identify the maximum peaks. This figure also reveals that the peaks of the measured vibration signal take place at 13.3Hz, 53.3Hz and 130Hz. These frequencies represent zero, first, and second frequency modes.

Figure 5.8 (c) shows the rotor spectral map, from which it can be observed that the speed of the rotor (800 rpm) corresponds to order 1 the first frequency oscillating mode of 53.3 Hz. Figure 5.9 shows that the power spectrum is decreased when compared with that of figure 5.8. This is attributed to the contaminated oil, which leads to a change in oil viscosity and also wear and tear within the gearbox. The time data collection was not detailed enough to observe the real effect of gearbox degradation; in order to have enough data with which to compare, a minimum of six months' solid data is required

In figure 5.9 (c), the spectral map of the new oil, before the contamination process and also under stress conditions, shows the differences in order spectrum between this stage and figure 5.9 (c).

Under normal operating conditions, there is no considerable difference in terms of torque variation between the new oil (type ATF MHP) and the original oil type (VG 220). Figure 5.11 shows the different experiments conducted on the test rig setup: (a) rotor speed 700 rpm

healthy condition, (b) low speed 200 rpm in contaminated lubricant condition, and (c) faulty condition 200 rpm. Comparing the three measured torque signals shows a significant increase in the torque between (b) and (c). This is due to gear tooth surface wear, as a result of a contaminated lubricant.

Figure 5.11 (a) illustrates the effect of wind speed, including the side effect of wind speed on the torque pattern. Higher wind speeds cause mechanical stress and increase fatigue life on the drive train of the wind turbine.

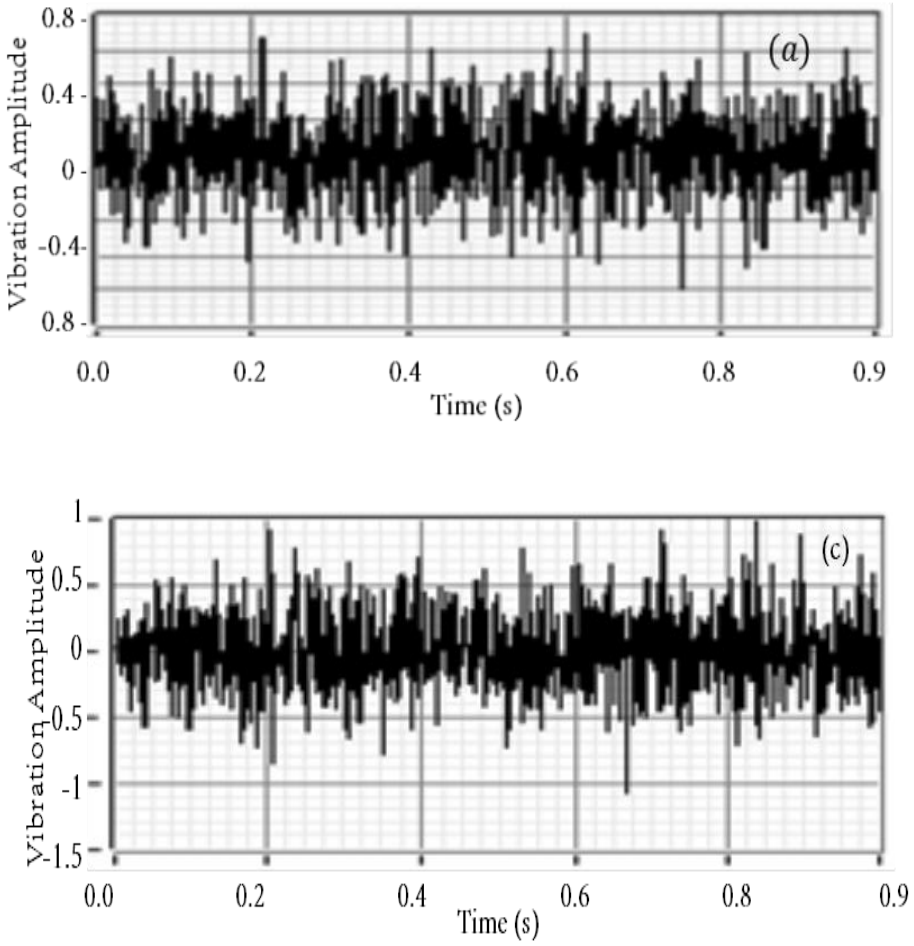

Figure 5.7 (a) New oil ATF MHP, (b) New oil ATF MHP after contamination. All under normal operating conditions.

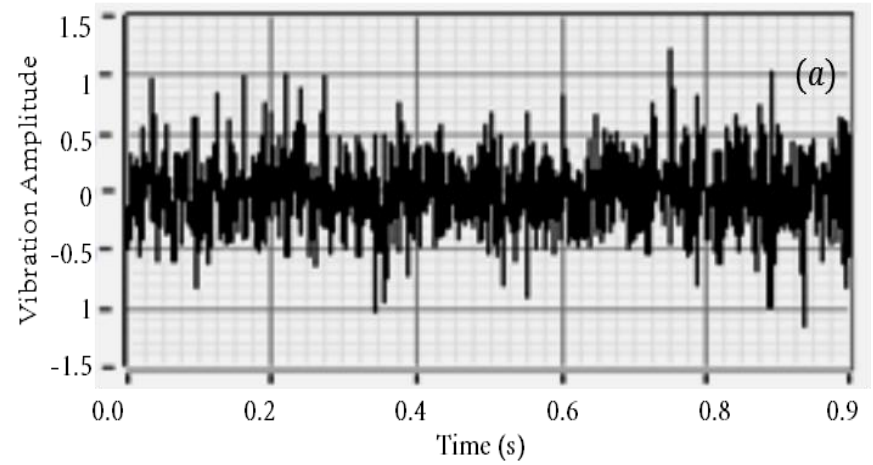

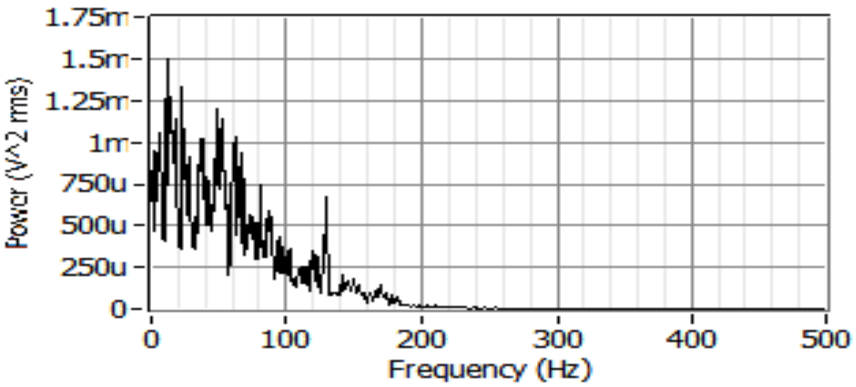

(b)

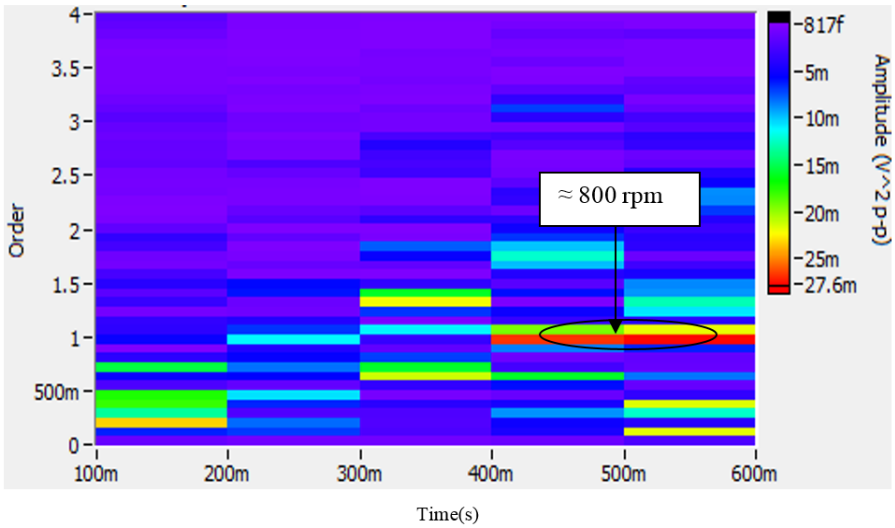

(c)

Figure 5.8 (a) New oil after contamination and under load variations, (b) Power spectrum of the signal (a), (c) Spectral map

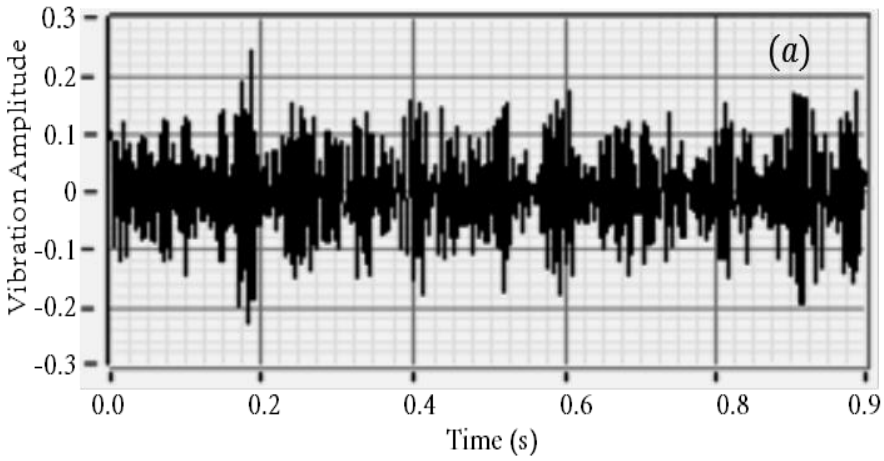

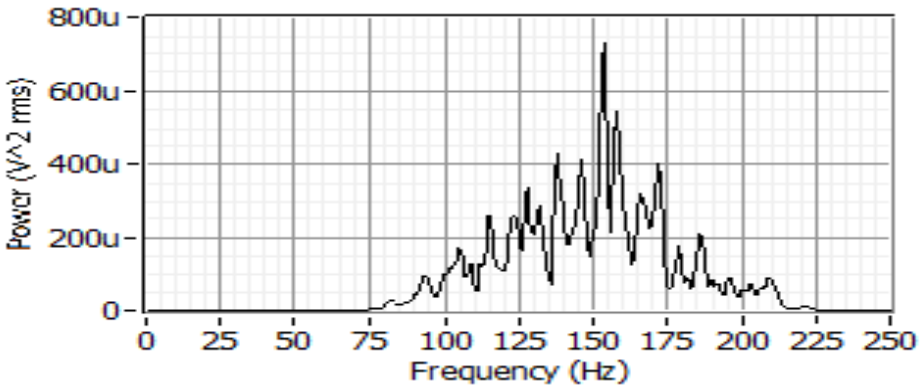

(b)

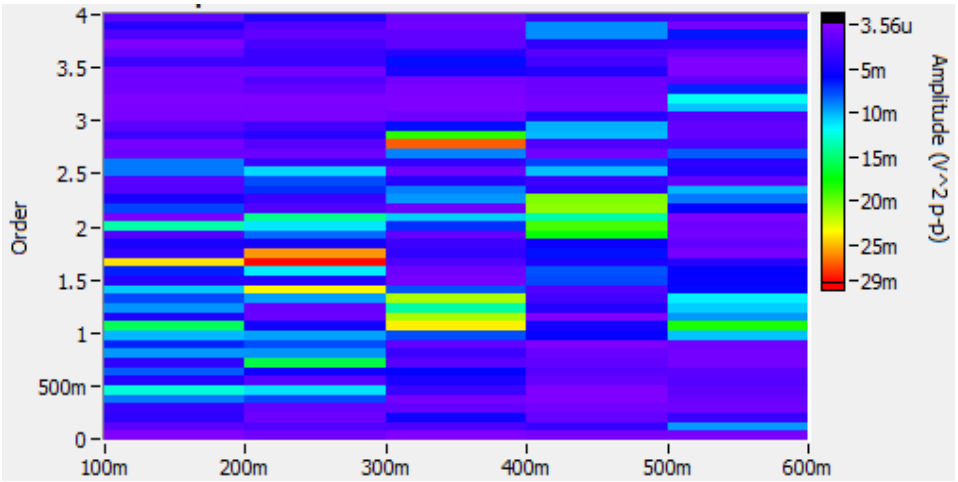

(c)

Figure 5.9 (a) New oil before contamination and under load variations, (b) Power spectrum of the signal (a), (c) Spectral map

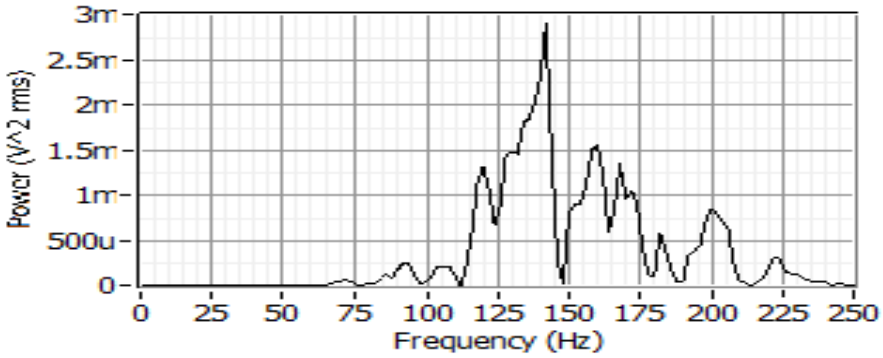

Figure 5.10 Power spectrum of contaminated ATF MHP oil under load variations

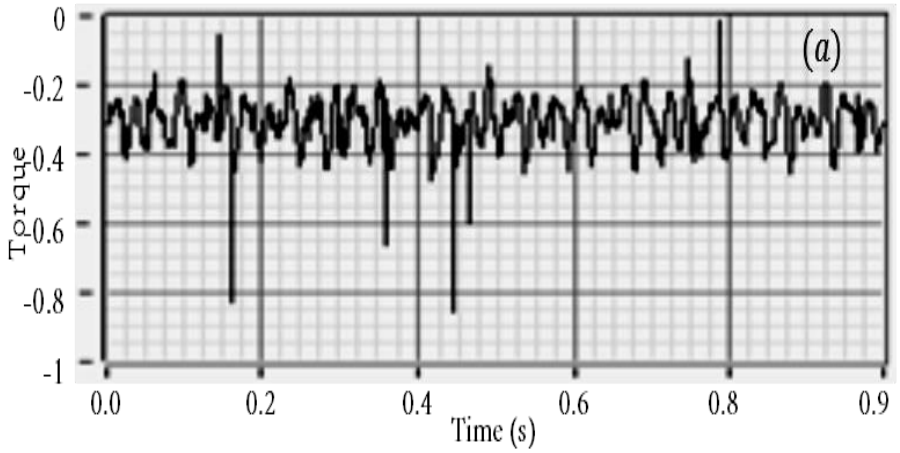

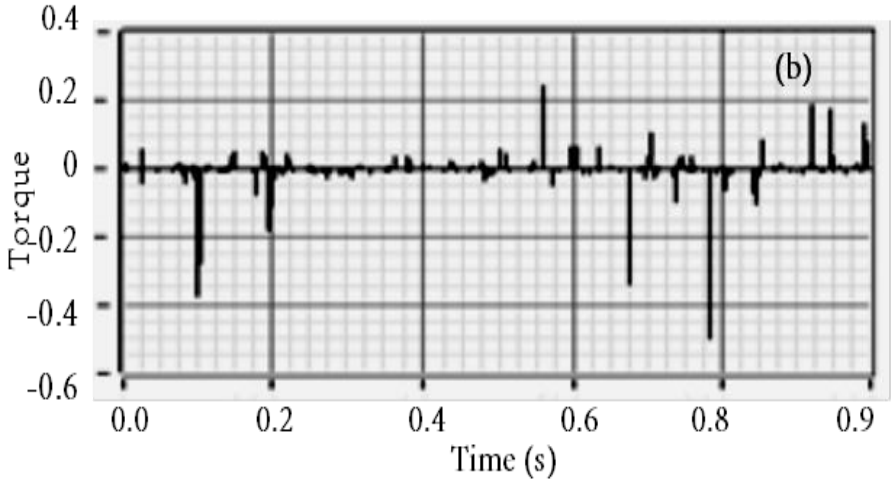

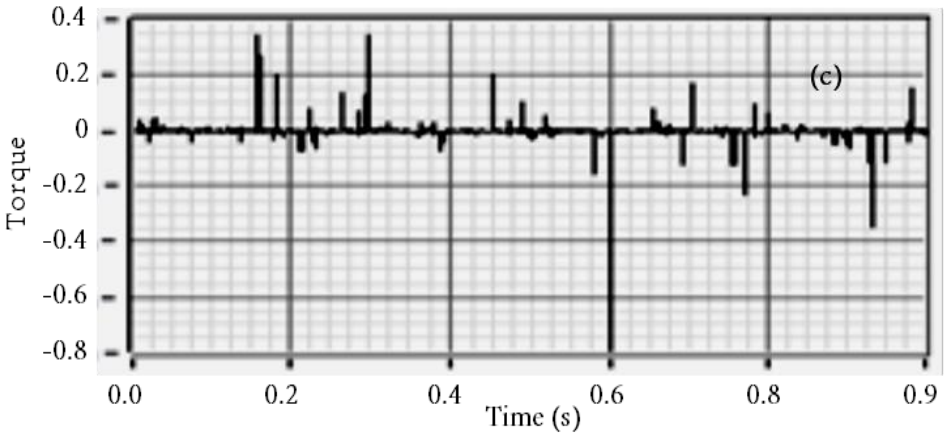

Figure 5.11 (a) Torque signal with contaminated oil at high speed under load variations, (b) Torque signal with contaminated oil at low speed and normal operating conditions, (c) Torque signal with contaminated oil at low speed and under load variations

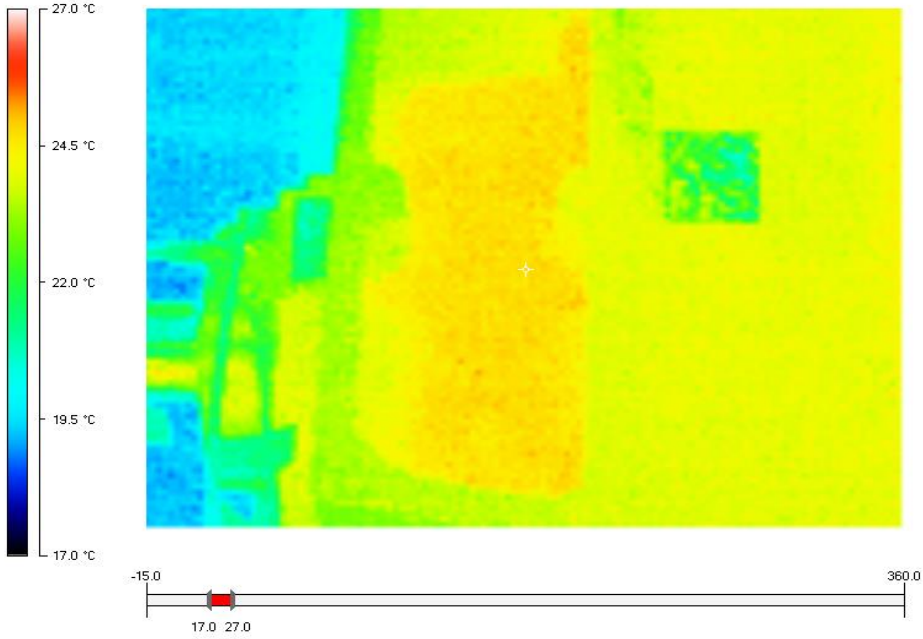

(a) Gearbox running before lubricant contamination

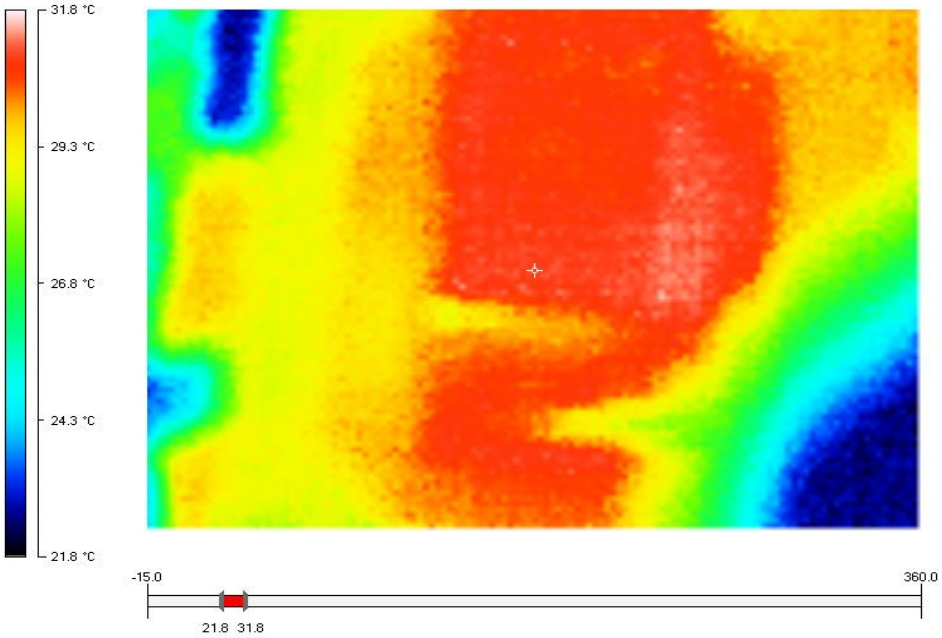

(b) Gearbox running after lubricant contamination

Figure 5.12 Thermal images of the gearbox under different lubricant conditions

A thermal imager Fluke Ti20 (Appendix a figure A.5) is used to record the thermal images of the lubricant before and after contamination at an ambient temperature of 27°C (as shown in figure 5.3). Before oil contamination, there is no sign of overheating within the gearbox (as shown in figure 5.12 (a)). In comparison, figure 5.12 (b) shows an overheating spot within the gearbox due to oil contamination. The overheating spot may lead to an increase in mechanical losses, due to increased gear friction and extreme wear from rubbing.

5.2.3 Conclusion

In this case study, experimental measurements have been collected on a test rig that simulates wind turbine operation. This is in order to study the impact of oil contamination on the overall performance of the drivetrain. Results show that the vibration and torque oscillations depend on the

condition of the oil lubricant. Contaminated oil leads to overheating within the gearbox and generates peaks on the vibration signature at the zero, first, and second frequency modes. The overall performance of the wind turbine is enhanced with contamination-free oil lubricants with high grade viscosity. Better condition monitoring is also achieved through the detection of faults at an early stage. Furthermore, smoothing the drivetrain torque signals results in less mechanical stress and, therefore, decreases the drivetrain component's fatigue life.

5.3 Case Study 3: Monitoring the Impact of Gearbox Teeth Failure on the Performance of the Wind Turbine.

This case study investigates the impact of gear box tooth damage/breakage, and gear eccentricity (misalignment due to a bent shaft), on the investigated torque and vibration signatures.

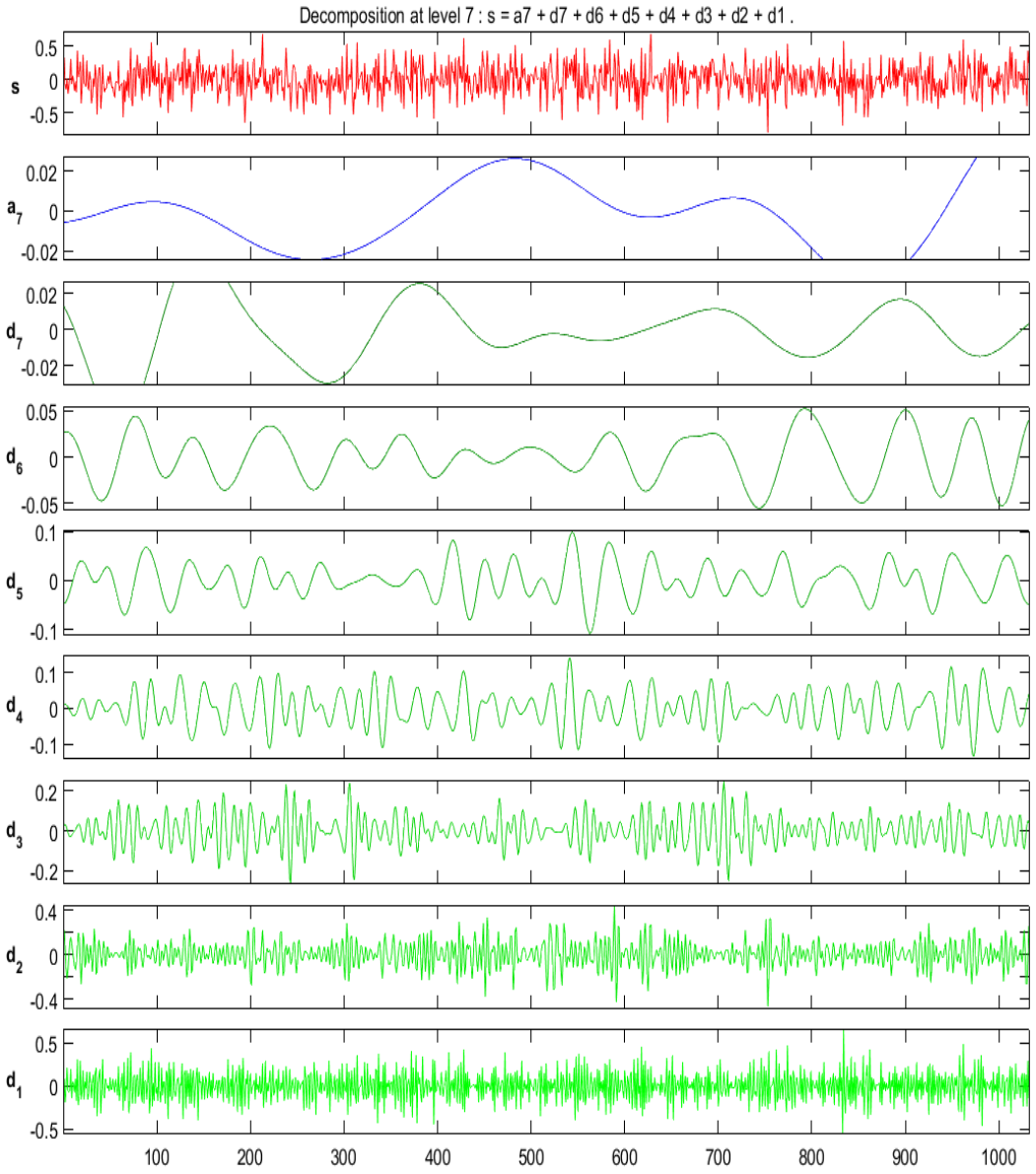

Figure 5.13 Gear in healthy condition before fault is applied

Damage was applied to the gearbox (specifically on the pinion gear as shown in figure 5.14) by taking a chip of the tooth. As discussed in chapter 4, the location of the sensor has a potential effect on the vibration signal. Therefore, mechanical stress, as a result of the broken tooth, will cause unbalanced vibration data that is recorded using the installed accelerometers. Figure 5.14 (a, b, c and d) illustrates (respectively), the conditions of the gear: a) healthy gear, b) teeth wear on the pinion gear as result of gear speed rotation, c) fully removed tooth, and d) chipped tooth.

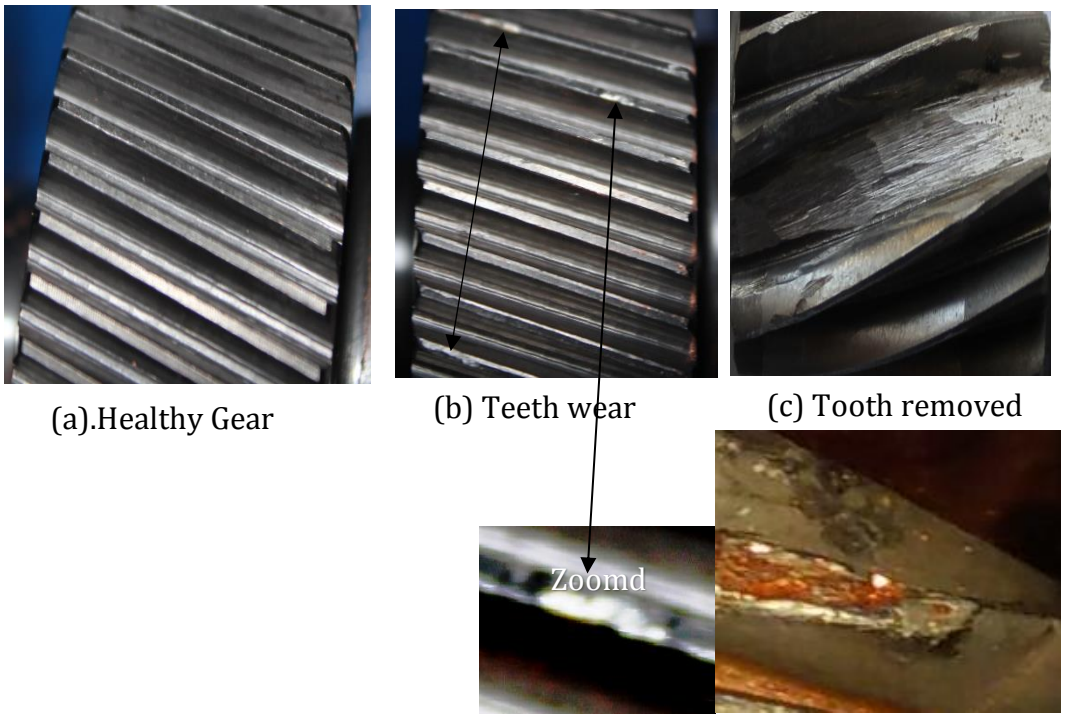

(a).Healthy Gear (b) Teeth wear (c) Tooth removed (d) Tooth chipped

Figure 5.14 Gears conditions, (a). Healthy Gear (b) Teeth wear (c) Tooth removed.

The recorded signals were processed and filtered to avoid any unwanted noise that may have affected the output data.

Figure 5.13 shows the healthy gearbox based on the wavelet analysis technique (Daubechies family) (decomposition up to level 7). The figure reveals a smooth signal, which reflects normal gearbox operation. Figure 5.15 shows the same signals after taking a part of the tooth (tooth chipped). As a WT operator, and based on the CMSs fitted to the wind turbine, it is clear from the signal that the fault is progressively relocated across the gear. As can be seen at decomposition level (d1), the amplitude changes along the entire frequency range of all the levels of the decomposition signal (compared to figure 5.13 (healthy case)). Furthermore, a fault with the vibration monitoring system also occurs when the entire tooth is removed (as shown in figure 5.16). This is shown by the level of the faulty signal.

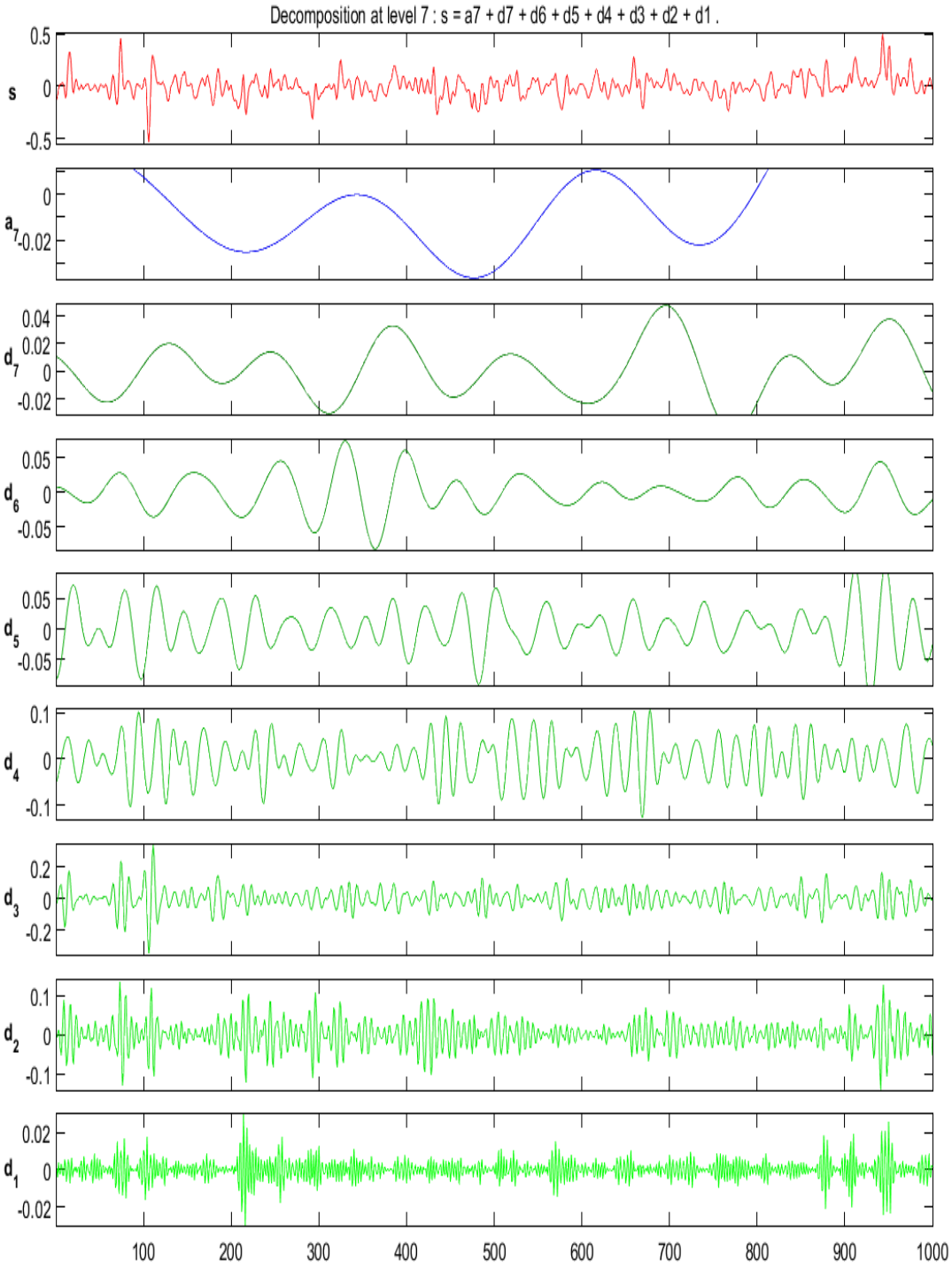

Figure 5.15 Gear in faulty condition after tooth is chipped

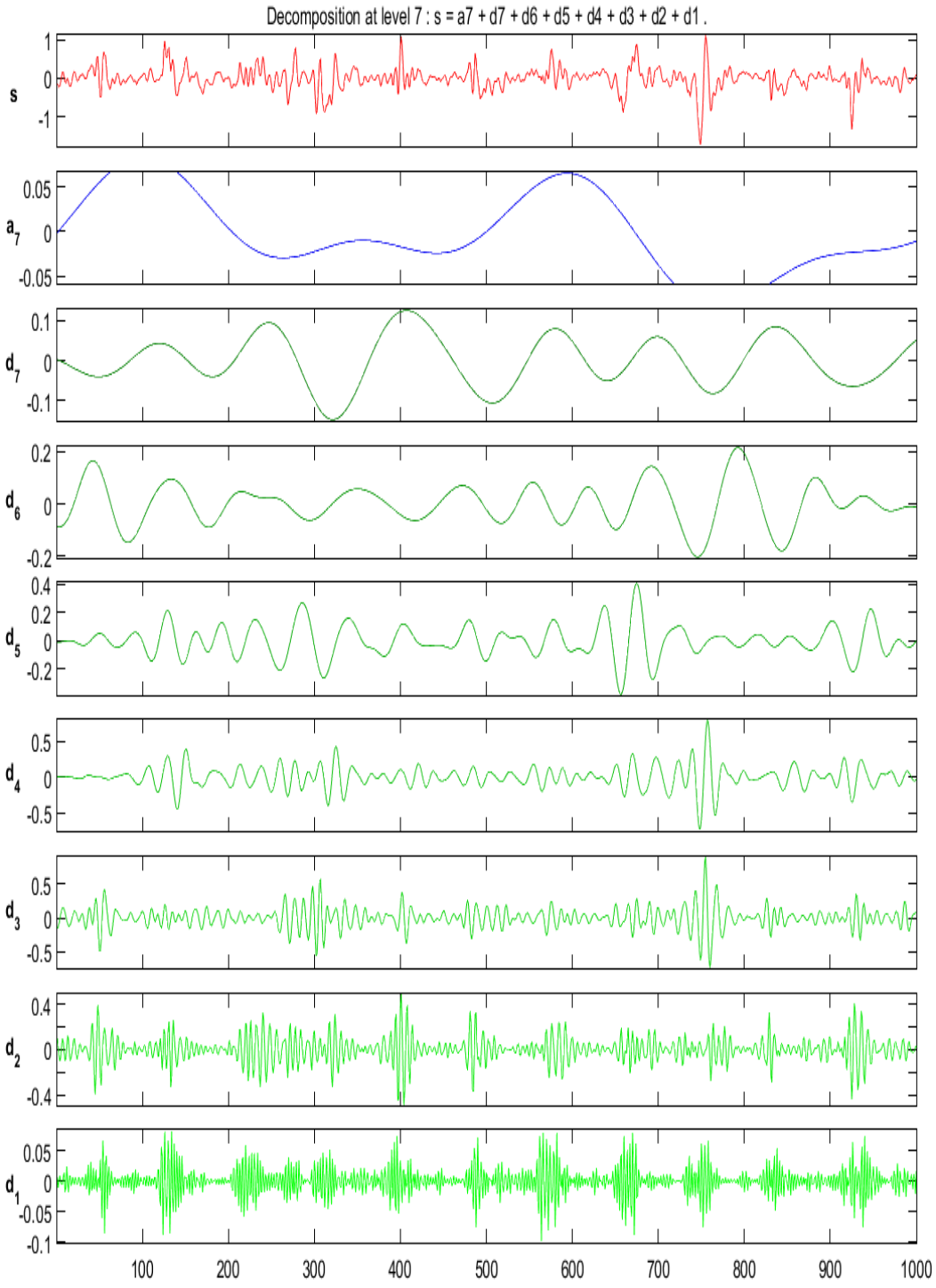

Figure 5.16 Gear in faulty condition after tooth is removed

For further investigation the results obtained were subsequently analysed by FFT to confirm the fault status.

Figure 5.17 (a) represents the time domain vibration signal, recorded during a 10 sec period, when a part of the tooth was removed (tooth chipped). In figure 5.17 (b), the signal was filtered using a low pass filter to block any unwanted noise from other parts of the test rig. The harmonic peaks and the vibration amplitude indicate an increase in wear when compared to the healthy condition shown in figure 5.22 (a, b).

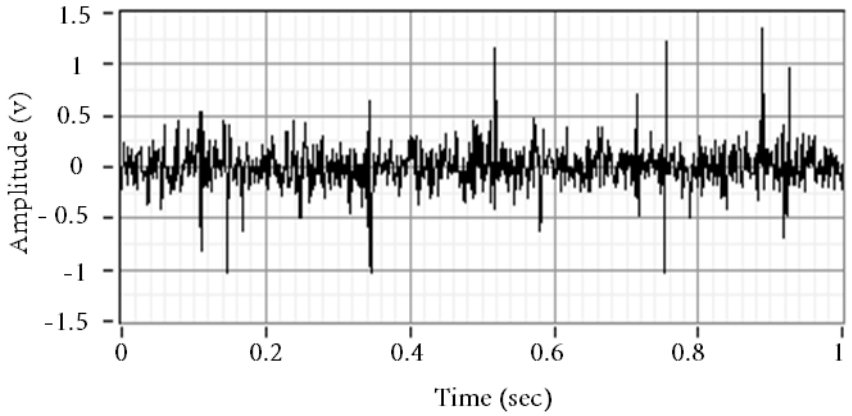

(a) Vibration signal

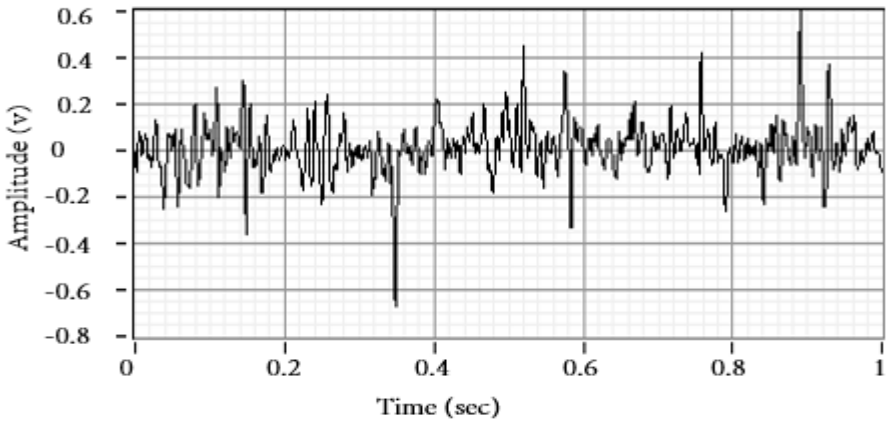

(b) Filtered data

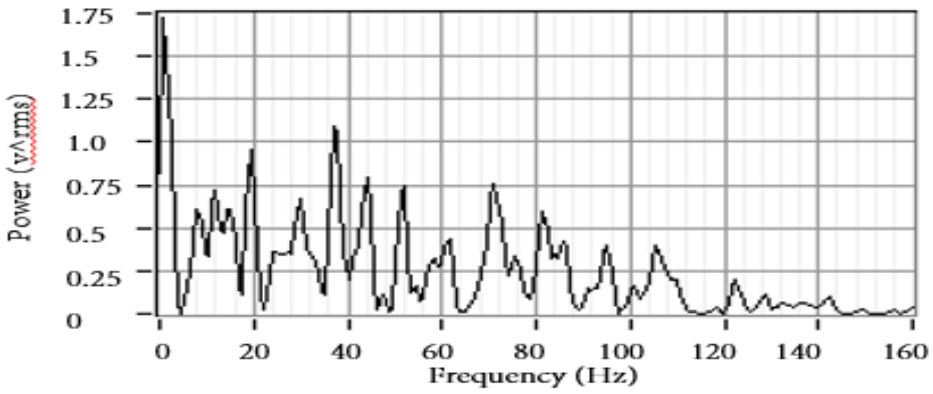

(c) Power spectrum of the filtered signal

Figure 5.17 Broken tooth fault. (a) Vibration signal, (b) Faulty signal filtered, and (c) Power spectrum of the faulty signal

The power spectrum in figure 5.17 (c) shows the gear vibration signal and sideband harmonics that are related to the gear meshing teeth frequency and shaft rotational frequencies. The test was conducted with input shaft speed = 200 RPM, gearbox ratio = 1:4.34, and output shaft speed S_O=200rpm×4.34=868 RPM. Hence, 1st carrier speed can be calculated as:

$$R_1 = \frac{N_1 + N_{21}}{N_{21}} = \frac{13 + 62}{62} = 1.209$$

$$C_s = P_G(RPM) \times R_1 = 200 \times 1.209 = 241.8\ RPM$$

Where

R_1& C_s: 1st gear stage ratio and 1st carrier speed (respectively).

After the gearbox was disassembled at the end of the experiments, the number of gear teeth was counted (as in table 5.2).

Table 5.2 Outline of the gearbox shaft speed (input/output) and number of gear teeth.

Symbol	**Shaft speed/Gears teeth number**	**Calculated**
P_G	Pinion gear RPM	200
S_O	Output gear RPM	868
C_s	1st carrier speed RPM	241.8
N_1	Pinion gear teeth no.	13
N_{21}	2nd gear teeth no.	62
N_{23}	3rd gear teeth no.	40
N_3	4th gear teeth no.	44
Ratio	Gearbox ratio	0.23 (1:4.34)

Figure 5.18 illustrates the gear's dynamic arrangement used in this study. From the outline provided in table 5.2, and based on each gear's number of teeth, the output gear ratio can be calculated as follows:

The output gear ratio N= $(N_1 \times N_3)/(N_{21} \times N_{23}) =$

$$(13 \times 44)/(62 \times 40) = 0.23$$

Which agrees with the gearbox ratio provided by the gear manufacture (1:4.34).

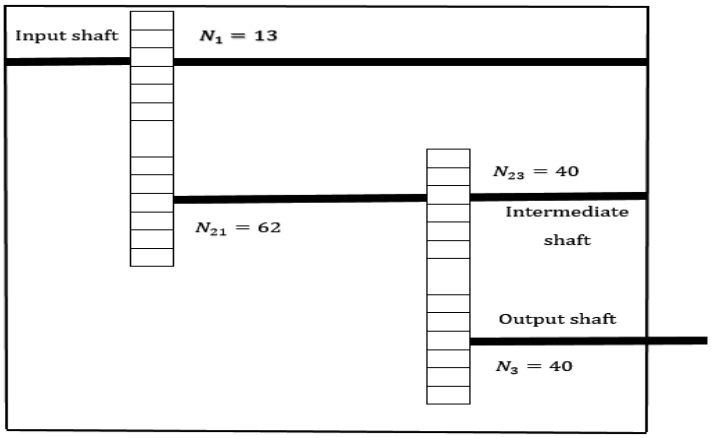

Figure 5.18 Gearbox dynamic arrangements

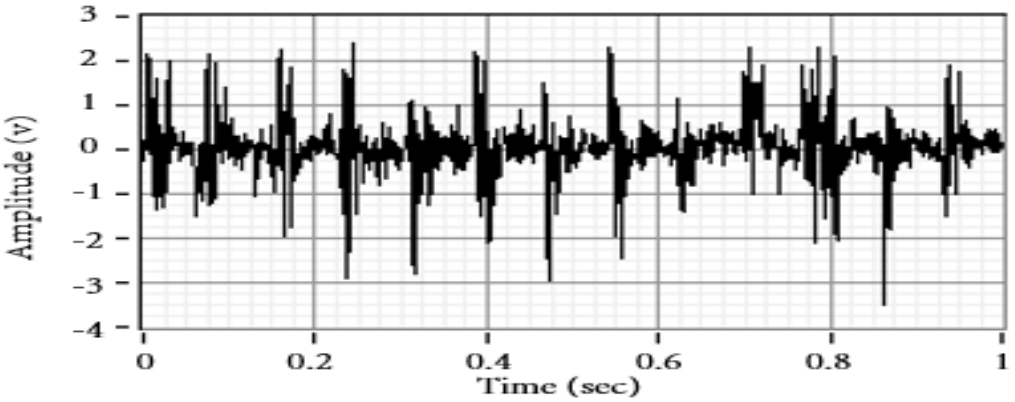

(a) Faulty data

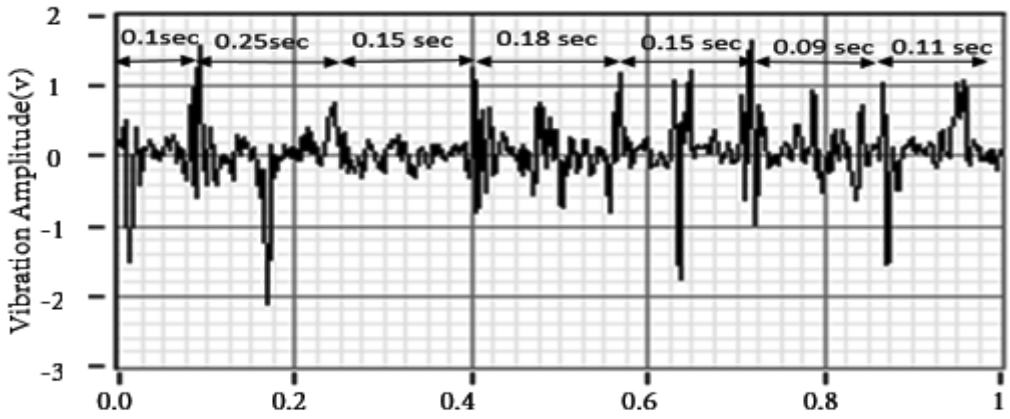

(b) Filtered data

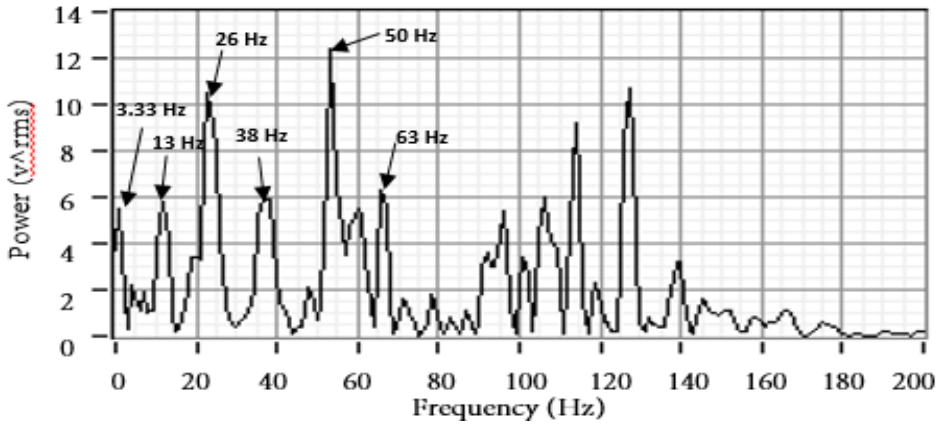

(c) Power spectrum of the removed tooth

Figure 5.19 Data of the removed tooth. (a) Faulty vibration signal, (b) Filtered signal, (c) Power spectrum of the filtered signal

The signal in figure 5.19 (b) was adaptively filtered through the band-pass filter. Peaks duration changes because of changes in the rotational speed. Carrying out pulse position analysis, the time average for the pulse changes can be calculated as follows:

Time duration average = (0.1+0.25+0.15+0.18+0.15+0.09+0.11)/7= 0.147

Relative frequency at 3.33Hz of input shaft = 1/0.147=6.802 Hz

Damaged gear rpm = 6.802×60=408.2

The power spectrum presented in figure 5.19 (c) shows the faulty frequencies that reflect the gearbox condition. As can be seen from the figure, the first harmonic indicates the input shaft running frequency is 3.33 Hz. The remainder of the harmonics (13 Hz, 26 Hz, 38 Hz, 50 Hz and 63) are caused by the rotational speed of the faulty gear tooth, along with gear mesh frequencies. The fault's precise frequencies can however exist under a normal power signal and under normal operating conditions, but those harmonic peaks will be at a lower magnitude when compared to those from a faulty condition.

$$Hunting\ tooth\ frequency = \frac{Gear\ mech\ freuquency\ \times Common\ frequency}{No.teeth\ pinion \times No.Teeth\ bull\ gear}$$

Since the only multiplication of the 13 teeth is 1, then the common frequency in this case would also be 1. Thus the hunting tooth frequency (HTF) is calculated as:

$$HTF = 2600 \times \frac{1}{13} \times 62 = 3.22\ cpm$$

Which explains the peaks in figure 59 (c) at 3.22 Hz ($1 \times 3.22 = 3.22\ Hz$)

As calculated previously, the 1st carrier speed is 241.8 rpm, and the calculation HTF at this speed is as follows:

$$HTF = \frac{14992 \times 2}{13 \times 62} = 37.2\ cpm$$

Which is close to the fourth peak (38 Hz), despite the differences between theoretically calculated and practical measured values.

It is well known that tooth breakage can cause serious damage, not just to the broken section, but also to the rest of the gear. This is due to fleeting through the transmission and explains the sideband harmonics (next to the mentioned faulty frequencies) in the figure.

Furthermore, due to the fact that gearbox teeth are extremely hard to break, the little distortion you can see in figure 5.19 (a, b, and c) may refer to the inflate surface of the removed tooth while removing it.

5.4 Case Study 4: Gear Eccentricity

A bent shaft is the most common reason for gear eccentricity [154, 155]. An unbalanced shaft was applied to the test rig (figure 4.1) by creating a difference in shaft level between the input shaft (from the prime mover side) and the output shaft (from the generator side). The difference between the two levels is then adjusted to 3.5 cm from level zero, which is based on the test bed. A detachable sign of the gear's eccentricity is higher GMF amplitude and high sideband (when compared to normal shaft operation).

A signal was collected for processing from the torque transducer, when the input shaft was at a rotational speed of 200 RPM. When comparing figures 5.21 (healthy condition) and 5.20 (faulty condition), the torque signal shows dramatic changes in amplitude between the healthy and the faulty case, as well as sideband variations. In figure 5.20 (faulty case), the vibration amplitude reaches 0.6 much higher than in figure 5.21 (healthy case). The higher amplitude-based GMFs that pass through the gears can cause excessive backlash and unexplained frequencies (including the gear's resonant frequencies). Furthermore, poor coupling alignment of the input and output shafts, as a result of unbalanced shafts, will have an acute effect on the frequency spectrum amplitudes. This can be seen in figure 5.20 (c) when compared to figure 5.21 (c).

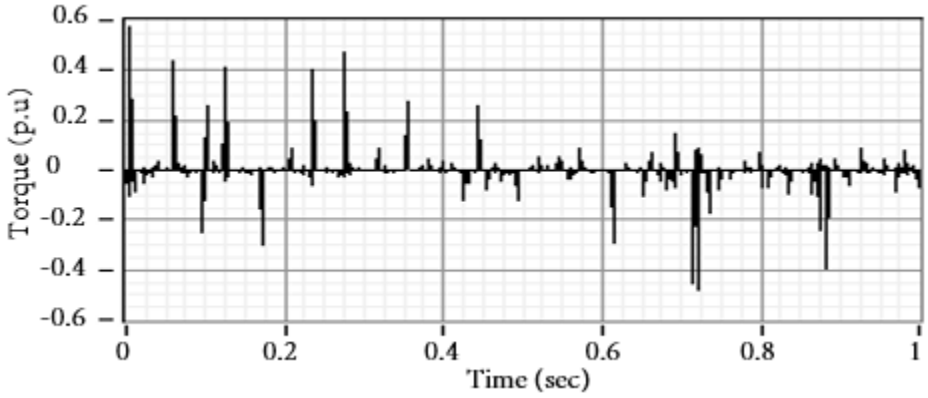

(a) Torque signal

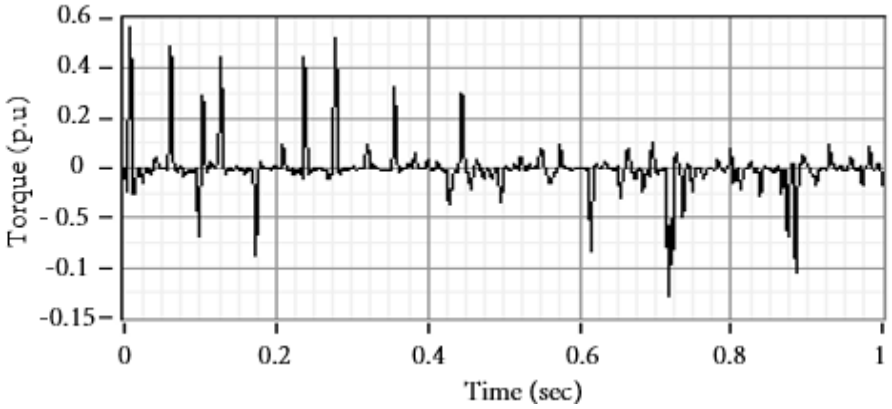

(a) Filtered data

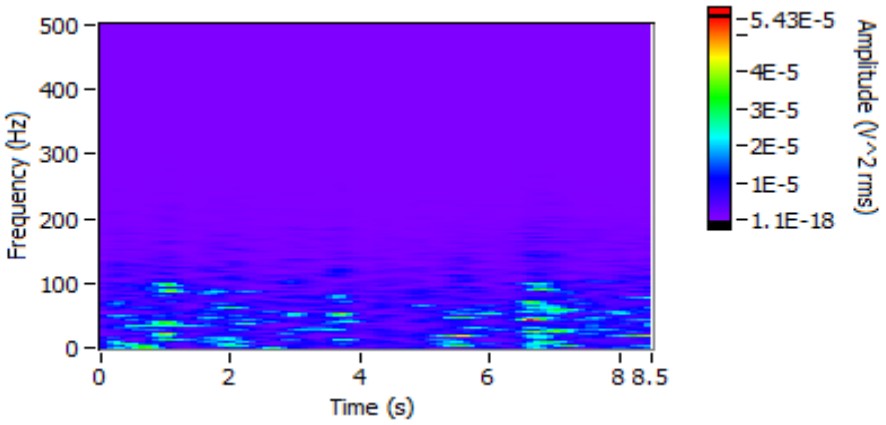

(b) Frequency spectrum of the filtered torque signal

Figure 5.20 Torque signal under faulty conditions

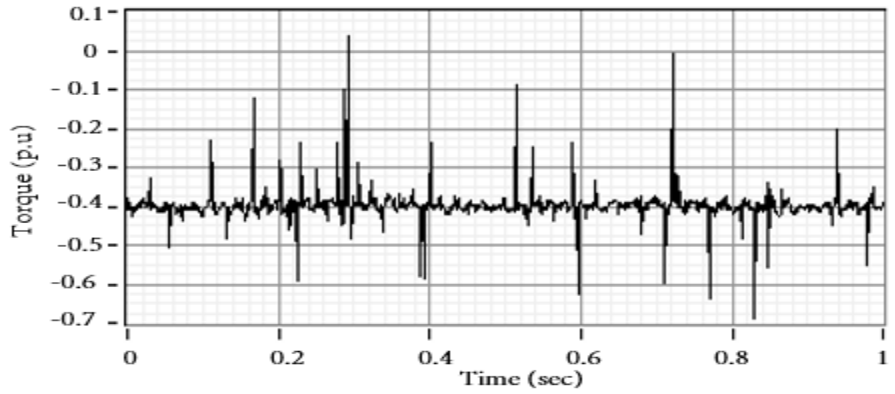

(a) Torque signal

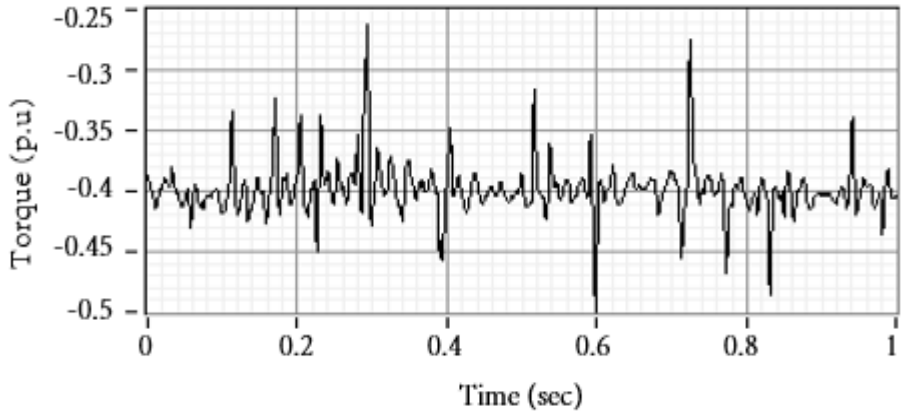

(b) Filtered signal

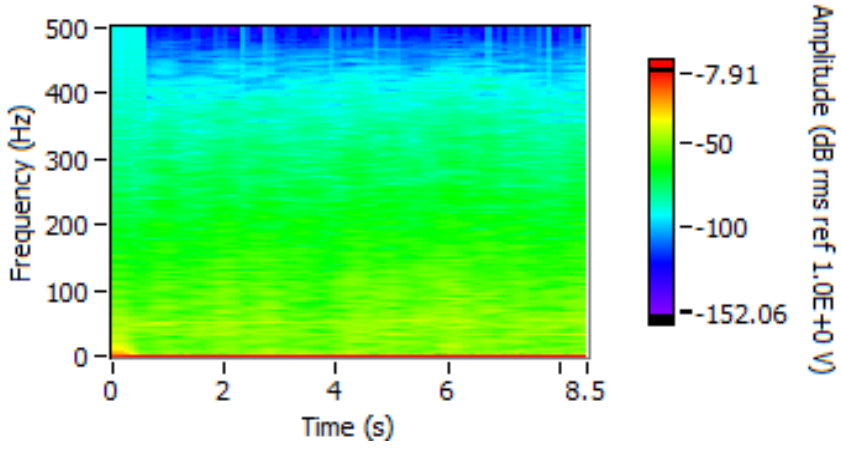

(c) Frequency spectrum of the filtered healthy torque signal

Figure 5.21 Torque signal under healthy conditions

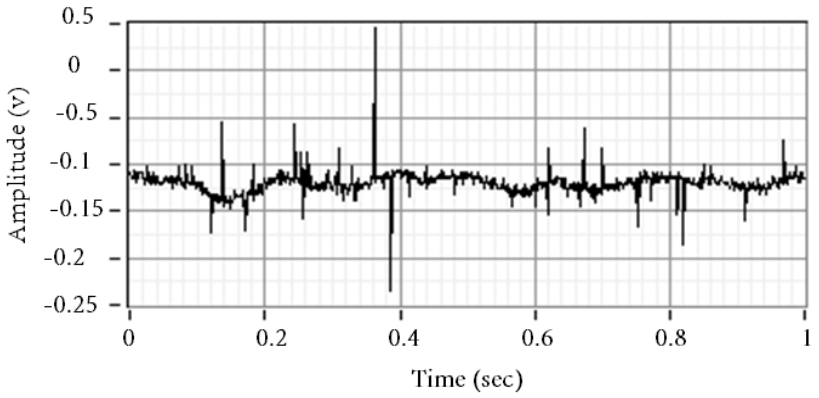

(a)Vibration signal under faulty conditions

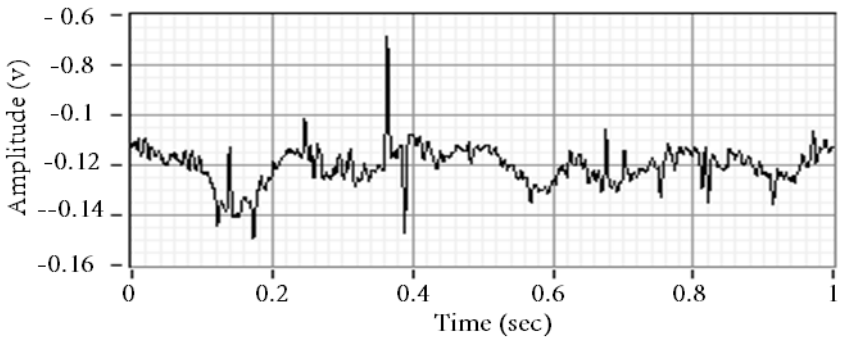

(b) Filtered data

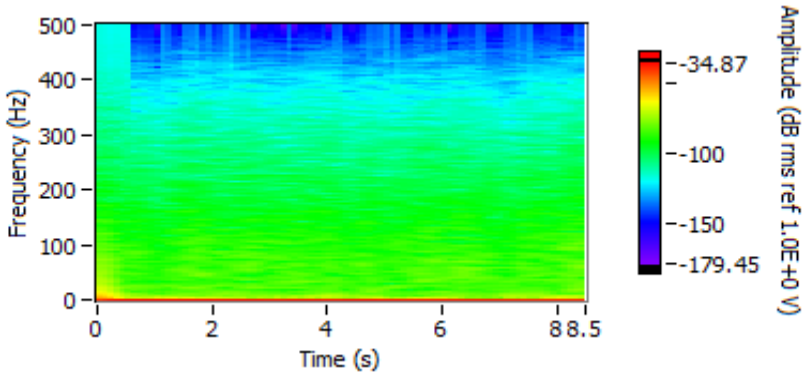

(c) Frequency spectrum of the filtered faulty signal

Figure 5.22 Vibration signal under faulty conditions

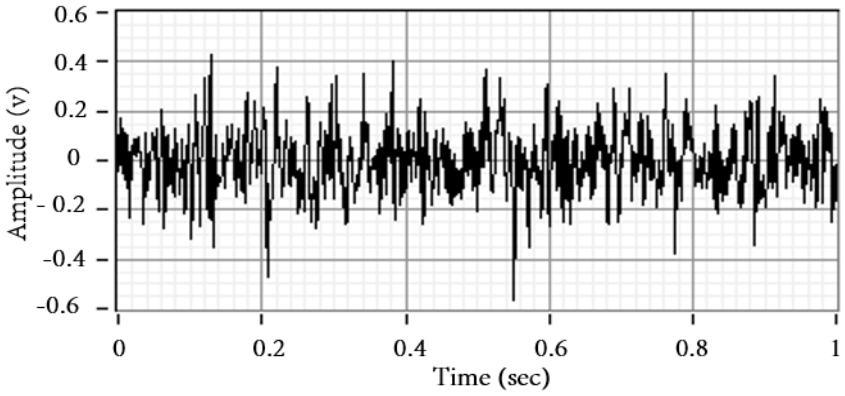

(a) Vibration signal under healthy conditions

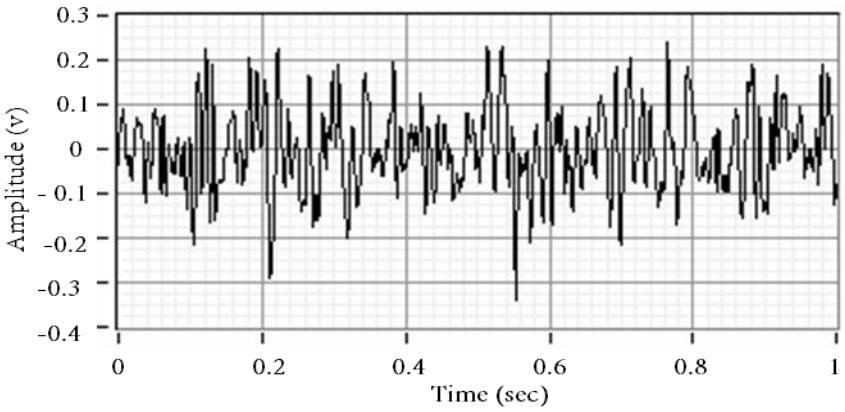

(b) Filtered data of the healthy signal

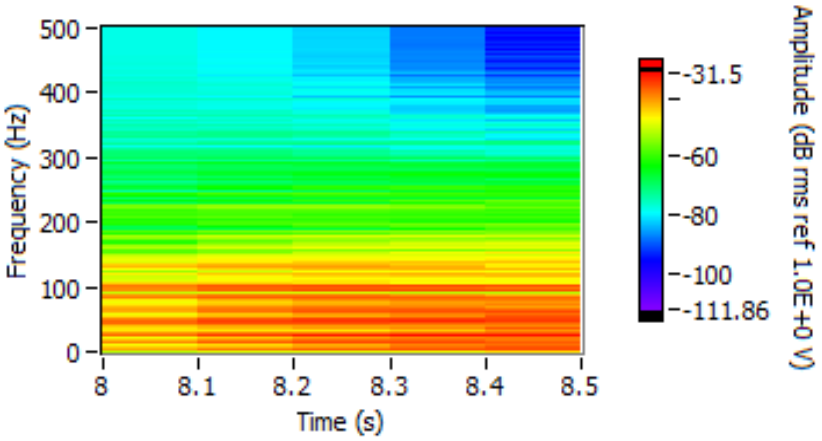

(c) Frequency spectrum of the filtered healthy signal

Figure 5.23 Vibration signal under healthy conditions

Figures 5.22 and 5.23 show the measured vibration signatures during normal and eccentricity fault conditions. Both cases use the same shaft speed of 200 rpm and collect data from sensors positioned in the same place on the gearbox. In fact the reason why this case was chosen to be conducted on a single RPM because this speed is the ideal speed of the test rig setup based on the capacity of the generator side and the rotor side (prime mover which represents the blades of the WT). However, different variable speed was applied on the test rig in other cases in this thesis. This ensures that any differences can only originate from the bent shaft. In figure 5.23 (a, b), the normal and the filtered signals show a smooth vibration signal with normal harmonic sidebands; however, in figure 5.22 (a, b), the signal shows a different starting point, with more fluctuating harmonics, as a result of the abnormal alignment of the shaft sections. This stressed rotation can cause teeth wear patterns and also progress to tooth breakage (due to heat action), inclusions, and grinding burns. In figure (e), the frequency amplitude changes in relation to the amount of stress (due to gear misalignment).

5.5 Fuzzy Logic Model

Fuzzy logic is utilised in a wide range of technologies. For wind energy conversion systems, it is used to control power convertors, for wind assessment and in maximum power search [156]. In this section, a fuzzy logic model is introduced to identify various faults within the drivetrain of a wind turbine. For all case studies, the inputs into the proposed model include the maximum vibration amplitude and the corresponding time. These are considered fuzzy variables.

In the first case study, a fuzzy logic model is developed based on the vibration signature of a stressed drivetrain (shown in figure 5.4 (c)). Inputs to the model are the vibration amplitudes and the time when the fault occurred (as shown in table 5.3), while the output (represented by Gaussian

membership functions (MF)) is assumed to be in the range of 0-1. Membership functions for the input and output variables (lowest to highest) are as shown in figure 5.24 (a, b) and (c) respectively. Based on the results of this case study, a set of rules has been developed to relate the input variables with the output (as shown in figure 5.24 (d, e)). Results were collected from a worst case scenario, where the wind turbine drivetrain is under a high level of stress. This can be seen in figure 5.4 (c). Table 5.3 summarises all faulty conditions, and outlines the recommended asset management decision (based on the condition of the WT, and in order to establish the wind turbine's best availability and grid support).

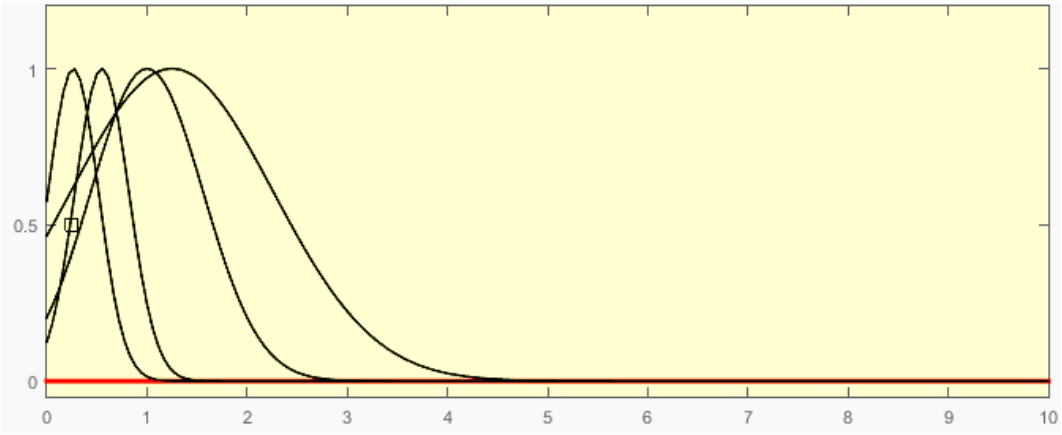

(a)

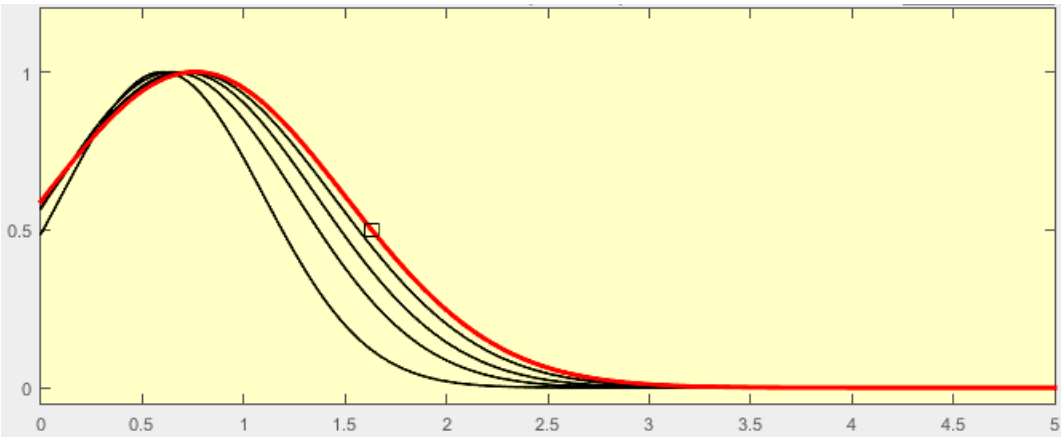

(b)

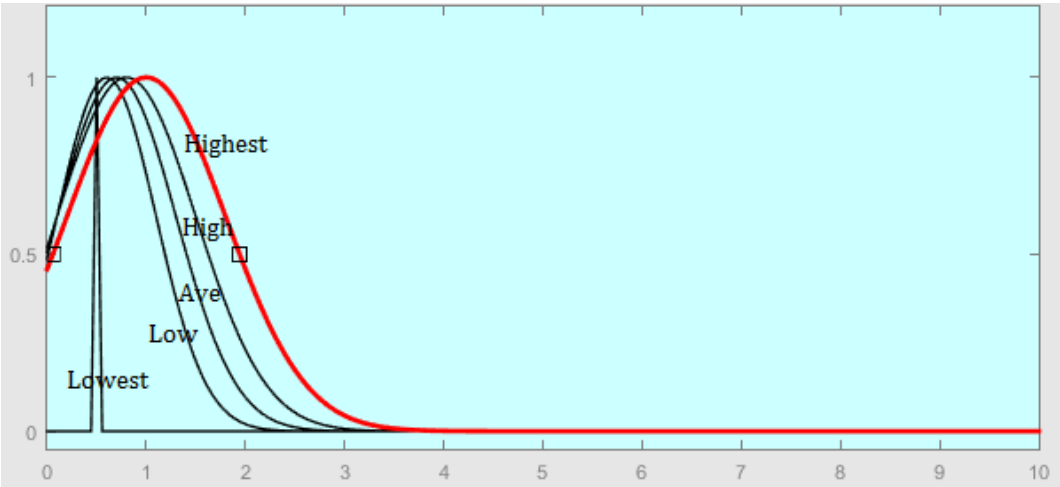
Highest
High
Ave
Low
Lowest
1
0.5
0
0
1
2
3
4
5
6
7
8
9
10

(c)

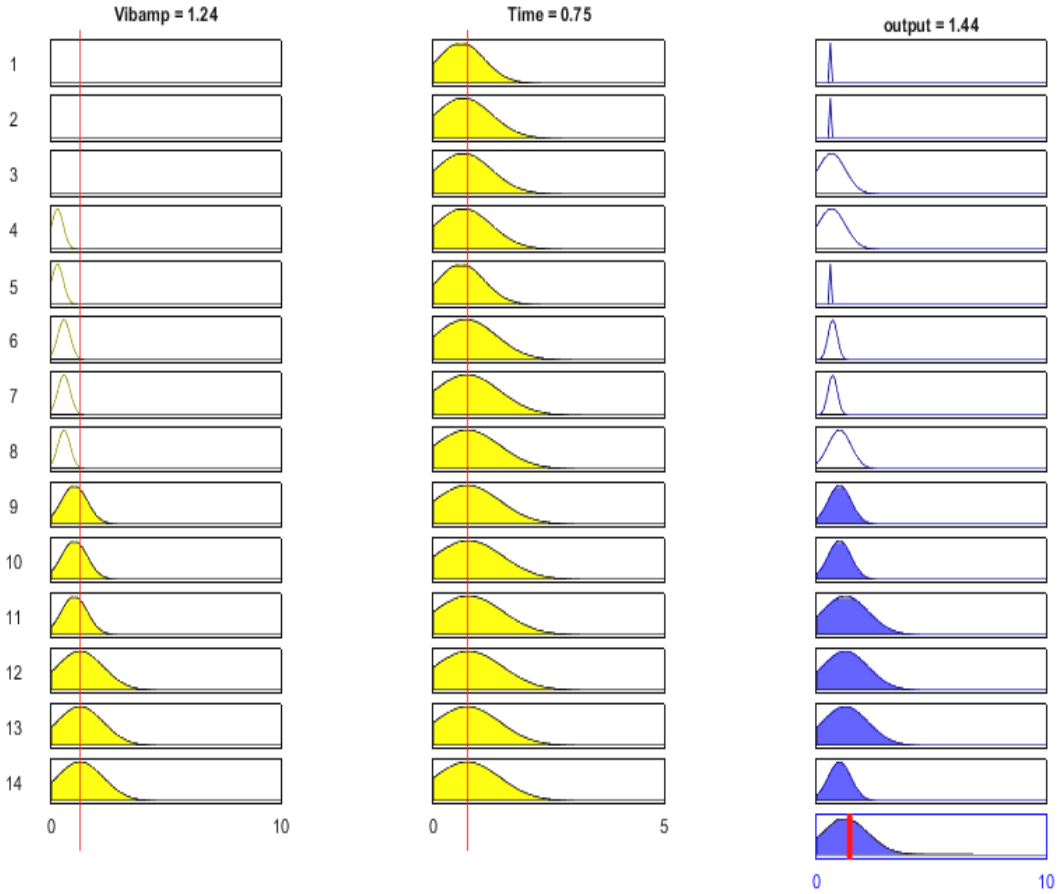
Vibamp = 1.24
Time = 0.75
output = 1.44
1
2
3
4
5
6
7
8
9
10
11
12
13
14
0
10
0
5
0
10

(d)

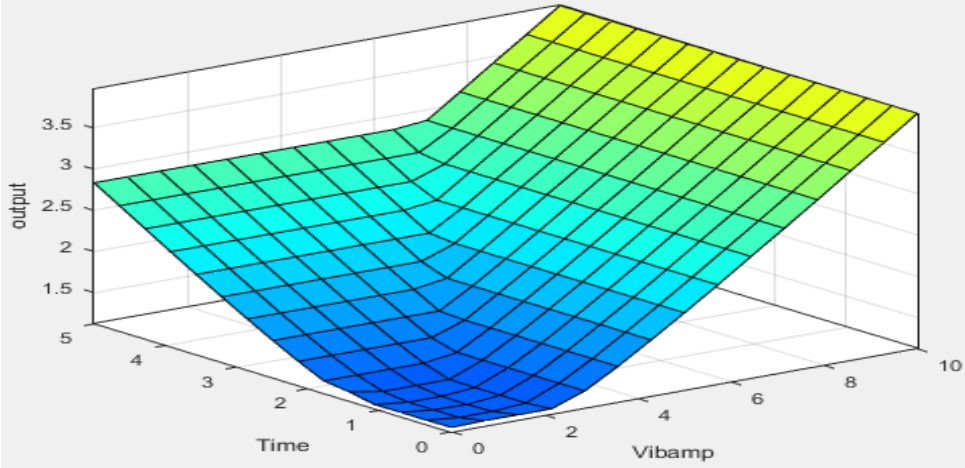

(e)

Figure 5.24 Fuzzy logic model inputs. (a) Vibration and (b) Time, (c) FLC output variables of the faulty condition case (when the drivetrain is under stress), (d) Rules, and (e) Surfaces

The same procedure (as for the previous case) was followed for the gearbox broken tooth case, in order to automate the identification of gearbox failures using a fuzzy logic model. Table 5.3 show the data extracted from figure 5.19 (b), which represents the faulty condition of the gearbox broken tooth. The inputs to the fuzzy logic model (as in figure 5.25 (a)) are the vibration amplitude and (b) the time. The output variable membership functions in this case study are shown in figure 5.25 (c), while figures 5.25 (d, e) show the developed rules and 3d surface graph of this case study.

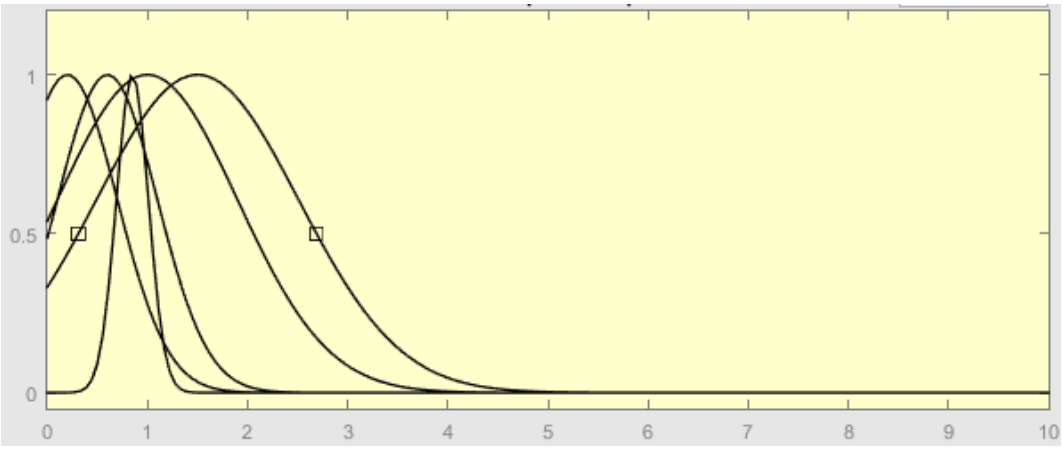

(a)

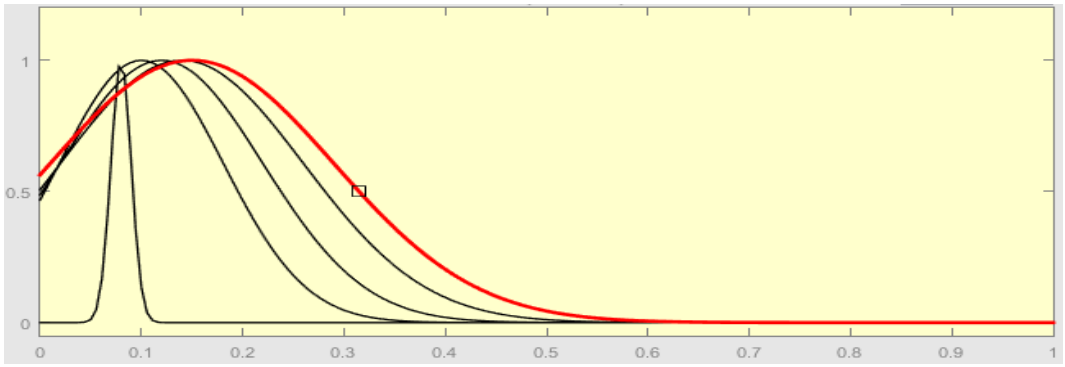
1
0.5
0
0
0.1
0.2
0.3
0.4
0.5
0.6
0.7
0.8
0.9
1

(b)

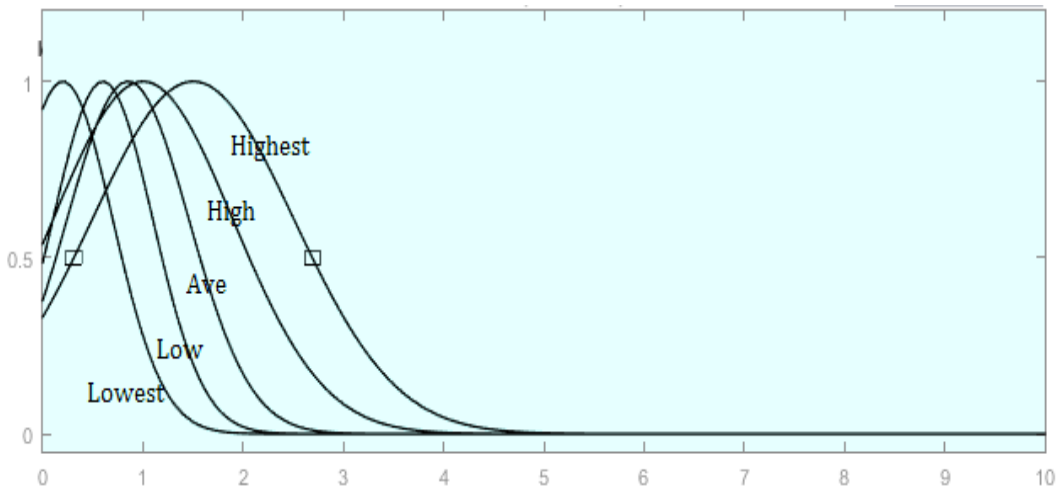
1
0.5
0
Highest
High
Ave
Low
Lowest
0
1
2
3
4
5
6
7
8
9
10

(c)

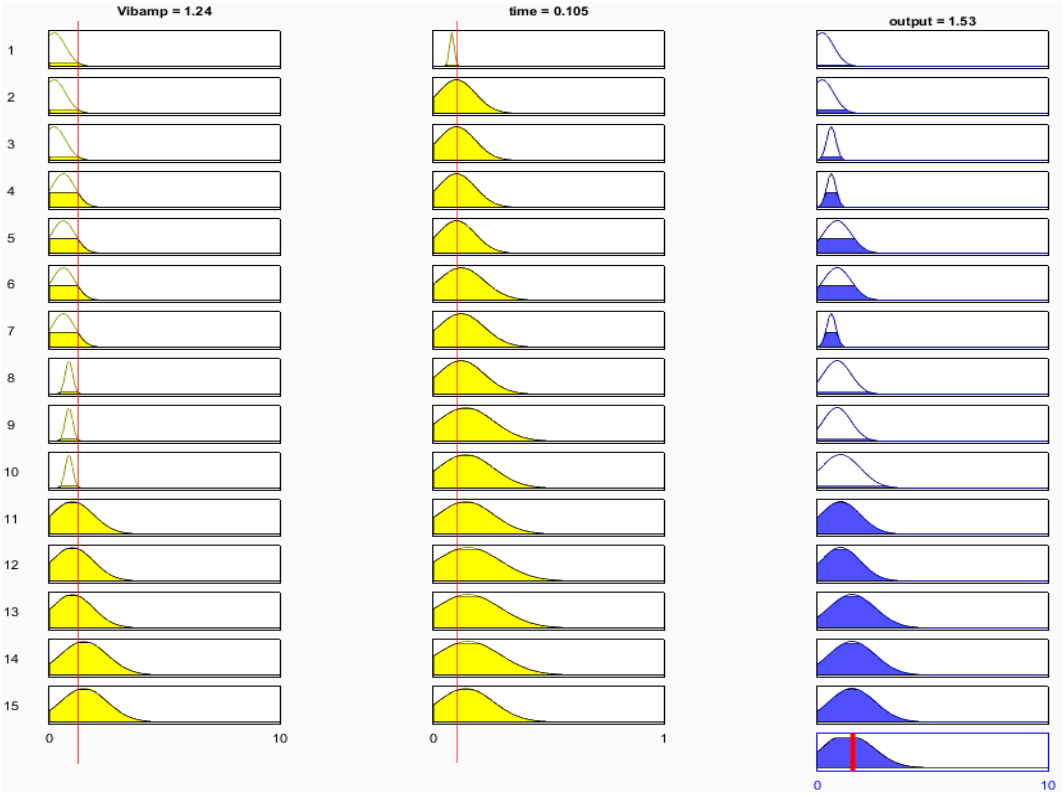

(d)

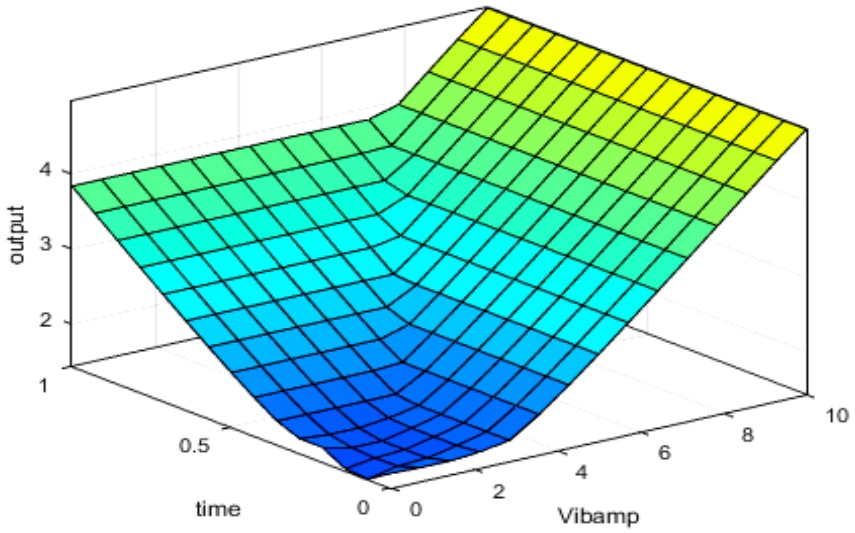

(e)

Figure 5.25 Fuzzy logic model inputs. (a) Vibration amplitude, (b) Time, (c) FLC output variables of the gearbox faulty tooth condition case, (d) Rules, and (e) Surfaces

In the case study of gear eccentricity (as was applied to the test rig), the vibration signal under faulty conditions (bent shaft) was entered into the fuzzy logic model (as mentioned in table 5.3). Figure 5.26, (a) represents the vibration amplitude input variables, lowset (bottom) to highest (top). Figure 5.26 (b) represents the time for this case study. The output membership functions of this case study can be seen in figure 5.26 (c). The set of rules and the surface reflect the condition of this case and can be seen in figure 5.26 (e, d) respectively.

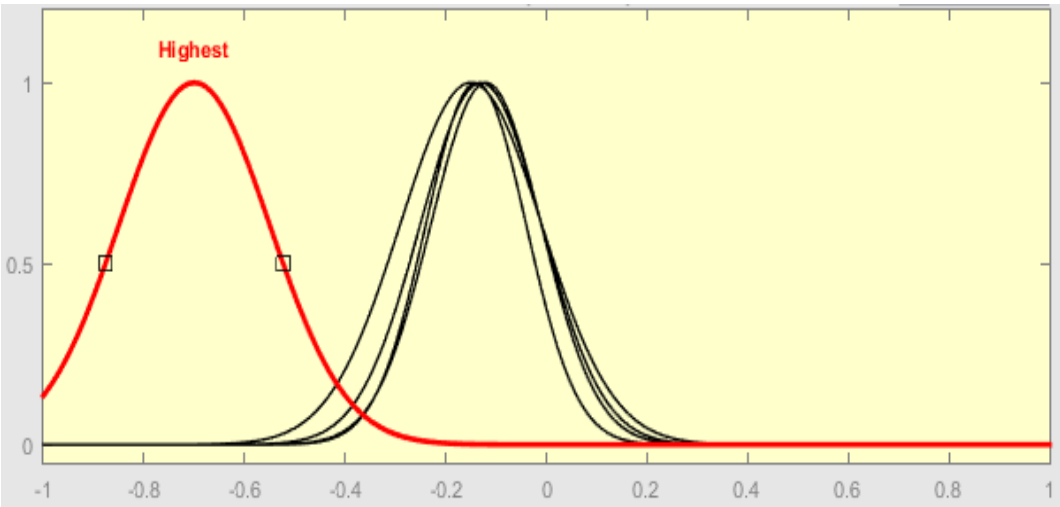

(a)

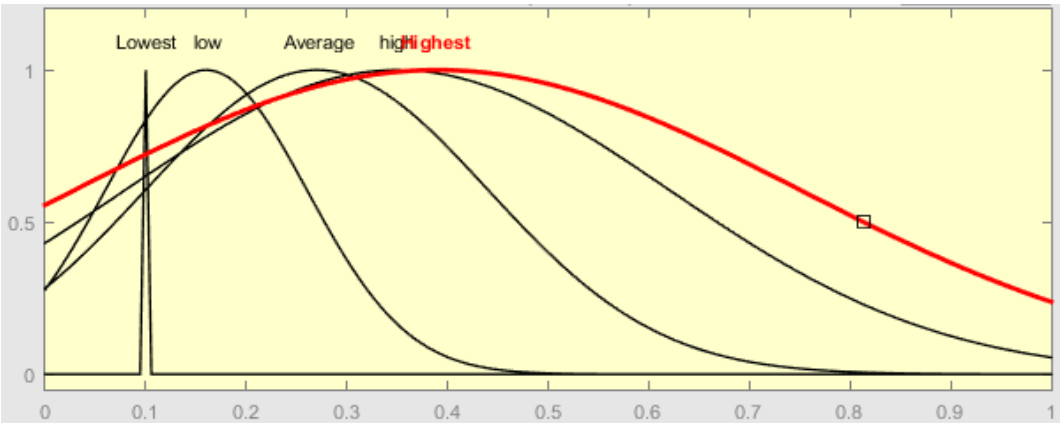

(b)

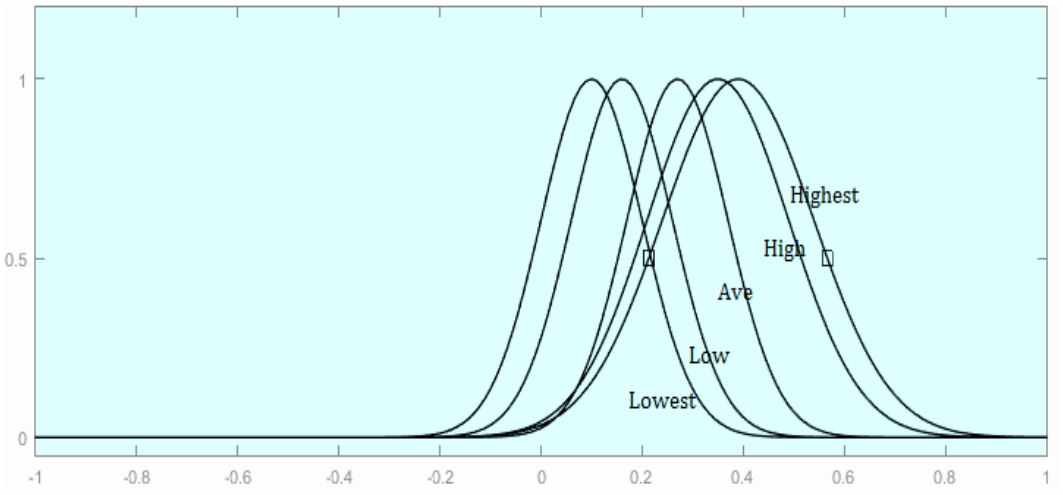
Highest
High
Ave
Low
Lowest
1
0.5
0
-1
-0.8
-0.6
-0.4
-0.2
0
0.2
0.4
0.6
0.8
1

(c)

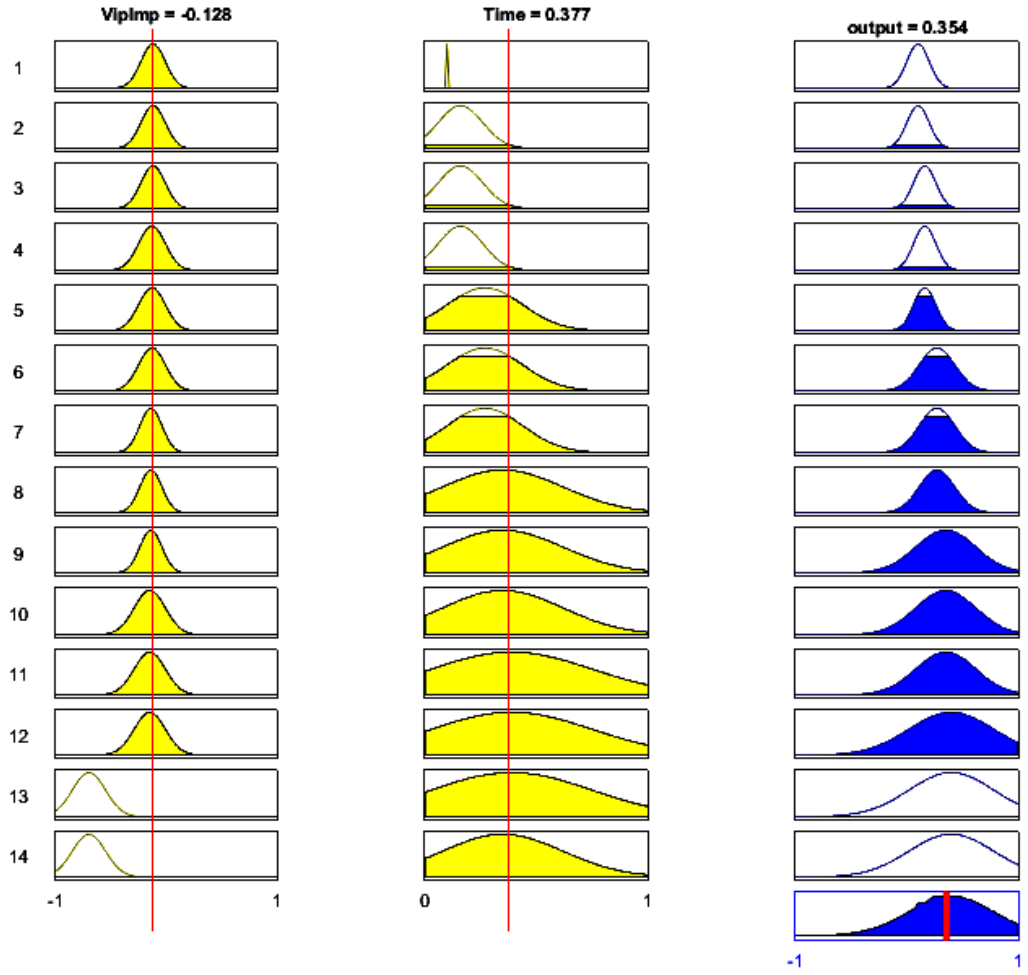
VipImp = -0.128
Time = 0.377
output = 0.354
1
2
3
4
5
6
7
8
9
10
11
12
13
14
-1
1
0
1
-1
1

(d)

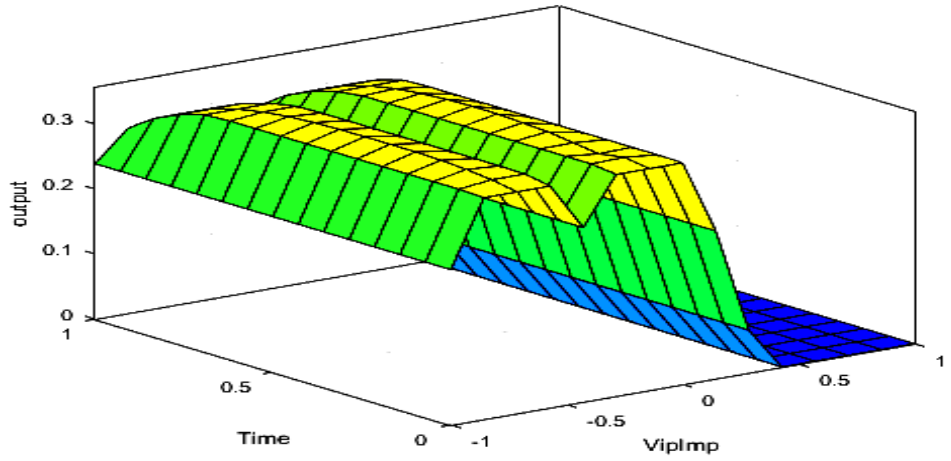

(e)

Figure 5.26 FLC input variables. (a) Vibration amplitude, (b) Time based on each level, (c) Output MF of the case, (d) Rules, and (e) Surfaces

Table 5.3 Summary of all case studies, along with recommended asset management decision

Case Study	**Vibration amplitude**	**Time(s)**	**Level**	**Asset management decision**
Drivetrain stresses	0 - 0.2	0.5- 0.6	Lowest	Normal
	0.252 - 0.265	0.61- 0.65	Low	Check req. (visual/temp.)
	0.269 - 0.55	0.66- 0.7	Average	Scheduled for maintenance
	0.56 - 1.00	0.71- 0.73	High	Must stop
	1.01- 1.25	0.74- 0.76	Highest	Out of service
Gearbox broken tooth	-0.5- 0.2	0 - 0.08	Lowest	Normal
	-0.5- 0.6	0.08- 0.1	Low	Diagnosis required
	0.61- 0.85	0.1- 0.12	Average	Broken gear identified
	0.9- 1	0.12- 0.14	High	Change the gearbox
	1.01- 1.5	0.14- 0.15	Highest	Out of service
Gear eccentricity	-0.11 – -0.12	0 – 0.1	Lowest	Normal
	-0.12– -0.13	0.1– 0.16	Low	Shaft check required
	-0.1 – -0.14	0.17– 0.27	Average	Bent shaft identified
	-0.14 – -0.15	0.27– 0.35	High	stop/fix the shaft, change it
	-0.15 – -0.7	0.36 – 0.39	Highest	Out of service

5.6 Condition Monitoring and Asset Management Decision-based WTOC

Based on the experiments conducted on the test rig, which consider different possible scenarios (as outlined in the previous case studies along with the literature review), an effective asset management decision model can be provided for reliable operation and maintenance (O&M) of the wind turbine.

To ensure a responsible decision model, all alarms (including false alarms) were passed through all required interfaces and a hardware arrangement. The decision will contribute to better power production, a reduction in unrehearsed WT power failures, will enhance the availability of the WT, as well as allowing time maintenance to be scheduled.

Calculating the probability of failure, as well the failure's significance, is critical to understanding the wind turbine operating condition (WTOC). It reveals the status of the WT, and also the highest level of performance at which it can survive before requiring scheduled maintenance. Figure 5.27 illustrates a proposed asset management and decision making strategy, which consists of different levels of failure consequences, subsequently clarified.

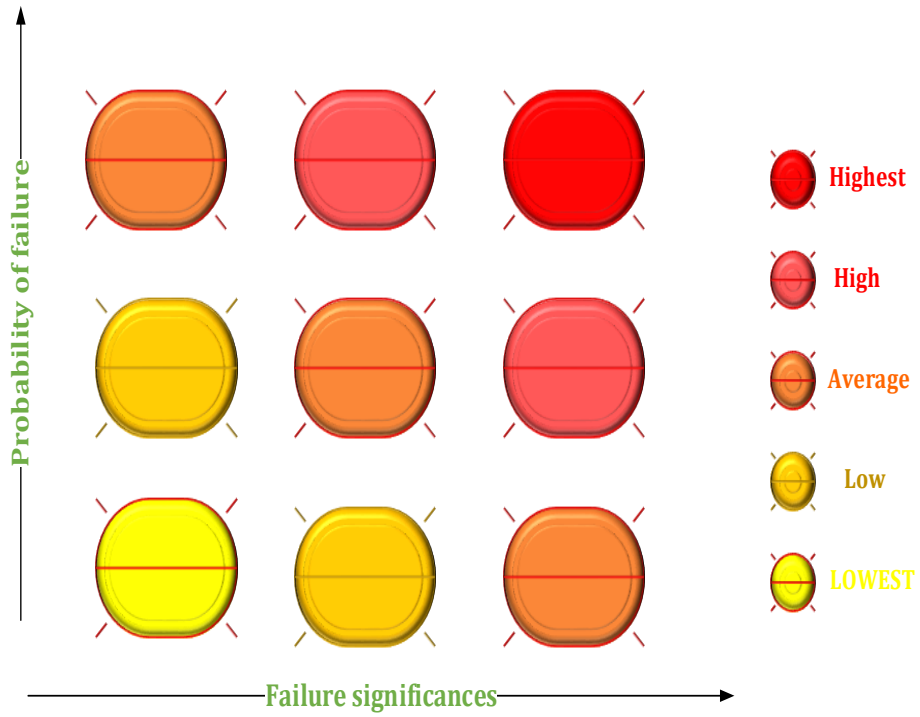

Figure 5.27 Asset management and decision-making based WTOC

Lowest: this level is the lowest risk level for both categories: failure percentage and failure significance. This alert means that the WT can easily survive until the next scheduled maintenance time without potential risk involved.

Low: this level starts at the end of the lowest level, and ends before the next level. The probability of failure here is around 30%, which means the failure is likely to take place but not highly likely. This may leave the operator divided as to what decision to make. Because the two categories (probability of failure and failure significance) are not deemed high risk, the operator is not required to make a quick decision. However, leaving the turbine connected for a long time under these conditions is not recommended.

Average: .by this stage, the probability of failure and the consequences of failure are around 60%, and the decision-maker has the opportunity to look at the grid circumstances. For instance, if the grid is suffering from a lack of productivity and therefore prone to retrospective availability of network power, an extension should be obtained.

High: at this point, it is highly recommended for the operator to take quick action within a short time frame, and ensure the WT is taken for maintenance. This zone indicates the possibility for failure, and the failure's significance, is high.

Highest: immediate action needs to be taken at this time. If the WT reaches this stage, the consequences of failure will be of the highest level and will lead to the loss of the WT. Protection systems must be activated to isolate the equipment from the network before any serious damage can occur inside the WT components.

Table 5.5 summarises the different levels of PF&FS consequences, along with the recommended action of the WT operator in order to keep the WT in service. The actions should be carried out within network power requirements and as soon as a good estimation for the time of next scheduled maintenance has been provided by the CMS (based on the WTOC). When the assets management decision-making table is applied to one of the case studies in this chapter (i.e. the removed tooth case in figure 5.19 (c)), the power output vibration levels initiate or trigger and send the commands through the interference channels to the alarms on the monitoring system. This is based on the present condition of the WT. Table 5.4 explains the case conditions along with the approximate values that the CMS requires to take action.

Table 5.4 Classification of the assets management.

Power output vib.	Lowest	Low	Average	High	Highest
Power vib. P_o	$P_o \leq 2$	$2 \leq P_o \leq 4.5$	$4.5 \leq P_o \leq 6$	$6 \leq P_o \leq 10$	$12 \leq P_o$

Table 5.5 Summary of asset management and decision-making.

PF versus FS levels	**CMS indications**	**Immediate action required**
Lowest	Yellow	No
Low	Orange	Yes/No
Average	Light Red	Yes
High	Red	Yes
Highest	Dark Red	Yes

A study shows that failure of WT components can be very costly, especially if the fault occurs on one of the WT's most important parts, such as the gearbox or the blades. Table 5.6 is taken from [157] and shows the downtime and outage of the main components due to power failure. This is shown for both onshore and offshore WTs and does not take into account potential delays due to unacceptable weather conditions. Table 5.7 illustrates the estimated cost to replace the major components of a 5 MW wind turbine, based on [157].

Table 5.6 Major Component out power failure, typical downtimes

Component outage	**No. of days downtime - onshore**	**No. of days downtime - offshore**
Gearbox	30	41
Generator	21	32
Blade	30	41
Electronics Sub.	1	2

Table 5.7 wind turbine (5MW) components replacement cost [157].

Gearbox	£ 402,000
Generator	£ 201,000
Blade	£ 166,000
Electronics Sub.	£ 10,000

Chapter 6 Conclusion and Future Work

6.1 Conclusion

In order to eliminate the detrimental impacts of conventional electricity generation technologies, the utilisation of renewable energy resources has grown rapidly. Wind turbines are a compatible target; therefore. a reliable and effective condition monitoring and fault diagnosis system (CMFDSs) is of a significant priority. This thesis proposes an improved performance of the WT by monitoring and diagnosing various mechanical failures modes within the drivetrain.

The thesis has discussed the various commercial tasks required of the condition monitoring systems currently available for wind turbines. A comprehensive literature review to summarise the current state of the art techniques in WTCMSs, including failure and diagnosis was presented in chapter 2. The importance of the WT gearbox in maintaining the overall reliability and availability of the wind turbine has also been discussed. Based on the fact that wind speed variations cause more stresses to the whole drivetrain of the WT, a condition based maintenance (CBM) system has been introduced to prevent unexpected failures.

In chapter 3, a number of common and generally applied CMS signal processing approaches are introduced, including FFT, order analysis and the wavelet transfer technique. The importance of these techniques and their significant contribution to a WTCMS, as well their advantages and disadvantages, are listed.

A test rig setup was developed to analyse the collected signals as described in chapter 4. This test rig reflects the real operational conditions that the wind turbine experiences during its lifespan. The wind turbine's main components are explained, as well as application mechanisms that involve movements and/or breaking systems.

The signals recorded from the CM test rig were processed and analysed, based on the techniques mentioned in chapter 3, using LabVIEW and Matlab software packages.

The results from different case studies showed the successful capability of the measured vibration and torque signals in detecting faulty conditions applied to the WT test rig. All the applied fault scenarios clearly show the difference between healthy and faulty conditions, especially when wavelet is used to analyse these signals. Results also show that the wavelet transfer technique (WTT) is more than capable in identifying low energy incipient faults and the flexibility of time and frequency resolutions, which are not likely to be detected using only FFT. The FFT technique is well known in frequency domain fault detection; however, it is not an effective technique when it comes to light loads, and time information can be lost in the process. In addition, the "inherent averaging process" misses essential data present within the signal.

The fuzzy logic (FLC) model was introduced to outline the results of the case studies in chapter 5, and was based on the faulty scenarios applied to the test rig setup.

Condition monitoring and asset management decision-making, based on wind turbine operating conditions, have been demonstrated. An asset management fuzzy logic-based model, for the WT operator to take proper asset action, has also been developed.

6.2 Future Work

Wind turbine condition monitoring is still under investigation and further improvements are to be carried out. Additional development of test rigs, based on practical and real data from sites, will contribute to improvements in the functionality of the CMS. The work presented in this thesis has been conducted on a small scale test rig. Further investigation on a real setup will better reflect outcomes, due to the limitations a small setup may face, such as the limited number of sensors, transducers and even reduced shaft sizes.

Wavelet families are still a challenging subject and require further investigation as to the best way to choose which one is more accurate for use with a particular concern (such as bearing damage, root teeth failure (tooth to tooth transmission error)).

An effective design is required, which merges the sensors and signal processing techniques that contribute to the improved performance of a wind turbine. The development of such a collaboration will have a potentially positive impact on the WECS.

References

[1] Y. Wenxian, P. J. Tavner, C. J. Crabtree, and M. Wilkinson, "Cost-Effective Condition Monitoring for Wind Turbines," *Industrial Electronics, IEEE Transactions on,* vol. 57, pp. 263-271, 2010.

[2] M. Molinas, J. A. Suul, and T. Undeland, "Extending the life of gear box in wind generators by smoothing transient torque with STATCOM," *Industrial Electronics, IEEE Transactions on,* vol. 57, pp. 476-484, 2010.

[3] A. Salem, A. Abu-Siada, and S. Islam, "A review of condition monitoring techniques of the wind turbines gearbox and rotor," *International Journal of Electrical Energy,* vol. 2 No 1, pp. 53-56, 2013.

[4] C. Kar and A. Mohanty, "Monitoring gear vibrations through motor current signature analysis and wavelet transform," *Mechanical systems and signal processing,* vol. 20, pp. 158-187, 2006.

[5] C. E. Council, "Clean energy Australia report 2014," 2015.

[6] K. Maki, R. Sbragio, and N. Vlahopoulos, "System design of a wind turbine using a multi-level optimization approach," *Renewable Energy,* 2011.

[7] Growth of wind turbine size, Intelligent Energy Eroup and European Wind Energy Association (EWEA), web: http://www.ewea.org , available at http://www.wind-energy-the-facts.org, access date: March 2016

[8] y. L. Bin Wu, Navid Zargari, Samir Kouro, *Power Conversion and Control of Wind Energy Systems* vol. 74. United States of America: John Wiley&Sons,Inc,Hooboken, New Jersey, 2011.

[9] R. L. Busby, *Wind Power: The Industry Grows Up*: PennWell Books, 2012.

[10] S. Heier, *Grid integration of wind energy conversion systems*: Wiley, 1998.

[11] T. Ackermann, *Wind power in power systems*: John Wiley & Sons, 2005.

[12] E. Hau, "Wind Turbines-Fundamentals, Technologies, Application, Economics," *IEEE Electrical Insulation Magazine,* vol. 19, p. 48, 2003.

[13] Y. Han and Y. Song, "Condition monitoring techniques for electrical equipment-a literature survey," *Power Delivery, IEEE Transactions on,* vol. 18, pp. 4-13, 2003.

[14] Y. Zhan, V. Makis, and A. K. Jardine, "Adaptive state detection of gearboxes under varying load conditions based on parametric modelling," *Mechanical Systems and Signal Processing,* vol. 20, pp. 188-221, 2006.

[15] R. Hyers, J. McGowan, K. Sullivan, J. Manwell, and B. Syrett, "Condition monitoring and prognosis of utility scale wind turbines," *Energy Materials: Materials Science and Engineering for Energy Systems,* vol. 1, pp. 187-203, 2006.

[16] Z. Hameed, Y. Hong, Y. Cho, S. Ahn, and C. Song, "Condition monitoring and fault detection of wind turbines and related algorithms: A review," *Renewable and Sustainable Energy Reviews,* vol. 13, pp. 1-39, 2009.

[17] Y. Amirat, M. Benbouzid, B. Bensaker, and R. Wamkeue, "Condition monitoring and ault diagnosis in wind energy conversion systems: a review," in *Electric Machines & Drives Conference, 2007. IEMDC'07. IEEE International*, 2007, pp. 1434-1439.

[18] P. Tavner, G. Van Bussel, and F. Spinato, "Machine and converter reliabilities in wind turbines," 2006.

[19] M. R. Wilkinson, F. Spinato, and P. J. Tavner, "Condition monitoring of generators & other subassemblies in wind turbine drive trains," in *Diagnostics for Electric Machines, Power Electronics and Drives, 2007. SDEMPED 2007. IEEE International Symposium on*, 2007, pp. 388-392.

[20] Y. Amirat, M. E. H. Benbouzid, E. Al-Ahmar, B. Bensaker, and S. Turri, "A brief status on condition monitoring and fault diagnosis in wind energy conversion systems," *Renewable and Sustainable Energy Reviews,* vol. 13, pp. 2629-2636, 2009.

[21] B. Lu, Y. Li, X. Wu, and Z. Yang, "A review of recent advances in wind turbine condition monitoring and fault diagnosis," in *Power Electronics and Machines in Wind Applications, 2009. PEMWA 2009. IEEE*, 2009, pp. 1-7.

[22] A. Kusiak and W. Li, "The prediction and diagnosis of wind turbine faults," *Renewable Energy,* vol. 36, pp. 16-23, 2011.

[23] P. Tavner, L. Ran, and J. Penman, *Condition monitoring of rotating electrical machines* vol. 56: IET, 2008.

[24] P. G. Steve Barber. (2004). *Case study 2: Wind Farm in Canada, Megawatt Class Turbines, Age: 3 years. Available [Cited 08 October 2015] : http://www.wwindea.org/technology/ch03/en/3_4_3.html*.

[25] J. M. Carrasco, L. G. Franquelo, J. T. Bialasiewicz, E. Galván, R. C. P. Guisado, M. Á. M. Prats, *et al.*, "Power-electronic systems for the grid integration of renewable energy sources: A survey," *Industrial Electronics, IEEE Transactions on,* vol. 53, pp. 1002-1016, 2006.

[26] "Innovative solutions for preventing white etching cracks," ed. BERLIN/SCHWEINFURT: SCHAEFFLER AG,, 2015.

[27] H. Link, W. LaCava, J. Van Dam, B. McNiff, S. Sheng, R. Wallen, *et al.*, "Gearbox reliability collaborative project report: findings from phase 1 and phase 2 testing," *Contract,* vol. 303, pp. 275-3000, 2011.

[28] D. G. Astridge, "Helicopter transmissions—Design for safety and reliability," *Proceedings of the Institution of Mechanical Engineers, Part G: Journal of Aerospace Engineering,* vol. 203, pp. 123-138, 1989.

[29] E. d. Vries, "Wind turbine gearboxes and the effort to improve their reliability," in *Wind Power*, ed. UK: Windcomms, 2010.

[30] K. Fischer, F. Besnard, and L. Bertling, "Reliability-centered maintenance for wind turbines based on statistical analysis and practical experience," *Energy Conversion, IEEE Transactions on,* vol. 27, pp. 184-195, 2012.

[31] Z. Zhang, A. Verma, and A. Kusiak, "Fault Analysis and Condition Monitoring of the Wind Turbine Gearbox," *Energy Conversion, IEEE Transactions on,* vol. 27, pp. 526-535, 2012.

[32] X. Wang, V. Makis, and M. Yang, "A wavelet approach to fault diagnosis of a gearbox under varying load conditions," *Journal of Sound and Vibration,* vol. 329, pp. 1570-1585, 2010.

[33] J. Cibulka, M. K. Ebbesen, and K. G. Robbersmyr, "Bearing Fault Detection in Induction Motor-Gearbox Drivetrain," in *Journal of Physics: Conference Series*, 2012, p. 012140.

[34] L. C. Xiaohong Yuan, "Variable amplitude Fourier series with its application in gearbox diagnosis—Part II: Experiment and application," *ScienceDirect,* vol. 19, pp. 1067-1081, 2005.

[35] J. Tang and H. Luo, "Wind Turbine Gearbox Fault Detection Using Multiple Sensors With Features Level Data Fusion," *Journal of Engineering for Gas Turbines and Power,* vol. 134, pp. 042501-1, 2012.

[36] S. J. Watson, B. J. Xiang, W. Yang, P. J. Tavner, and C. J. Crabtree, "Condition monitoring of the power output of wind turbine generators using wavelets," *Energy Conversion, IEEE Transactions on,* vol. 25, pp. 715-721, 2010.

[37] E. Wiggelinkhuizen, T. Verbruggen, H. Braam, L. Rademakers, J. Xiang, and S. Watson, "Assessment of condition monitoring techniques for offshore wind

farms," *Journal of solar energy engineering,* vol. 130, pp. 030301.1-031020.12, 2008.

[38] N. Baydar and A. Ball, "Detection of gear deterioration under varying load conditions by using the instantaneous power spectrum," *Mechanical Systems and Signal Processing,* vol. 14, pp. 907-921, 2000.

[39] R. Zimroz and A. Bartkowiak, "Two simple multivariate procedures for monitoring planetary gearboxes in non-stationary operating conditions," *Mechanical Systems and Signal Processing,* vol. 38, pp. 237-247, 2013.

[40] W. Bartelmus and R. Zimroz, "A new feature for monitoring the condition of gearboxes in non-stationary operating conditions," *Mechanical Systems and Signal Processing,* vol. 23, pp. 1528-1534, 2009.

[41] C. Stander and P. Heyns, "Instantaneous angular speed monitoring of gearboxes under non-cyclic stationary load conditions," *Mechanical Systems and Signal Processing,* vol. 19, pp. 817-835, 2005.

[42] C. Stander, P. Heyns, and W. Schoombie, "Using vibration monitoring for local fault detection on gears operating under fluctuating load conditions," *Mechanical Systems and Signal Processing,* vol. 16, pp. 1005-1024, 2002.

[43] K. S. Gaeid and H. W. Ping, "Wavelet Fault Diagnosis of Induction Motor," *cdn. intechopen. com,* 2009.

[44] F. Haghjoo and S. M. Shahrtash, "Wavelet transform based decomposition and reconstruction for on-line PD detection and measurement. Part I:

Narrow band components decomposition," *European Transactions on Electrical Power,* vol. 20, pp. 901-914, 2010.

[45] S. H. Kia, H. Henao, and S. G. A. Capolino, "Diagnosis of Broken Bar Fault in Induction Machines Using Discrete Wavelet Transform without Slip Estimation," in *Industry Applications Conference, 2007. 42nd IAS Annual Meeting. Conference Record of the 2007 IEEE*, 2007, pp. 1917-1922.

[46] W. Wang and P. McFadden, "Early detection of gear failure by vibration analysis i. calculation of the time-frequency distribution," *Mechanical systems and signal processing,* vol. 7, pp. 193-203, 1993.

[47] P. McFadden, "Examination of a technique for the early detection of failure in gears by signal processing of the time domain average of the meshing vibration," *Mechanical systems and signal processing,* vol. 1, pp. 173-183, 1987.

[48] S. Li, "Effects of centrifugal load on tooth contact stresses and bending stresses of thin-rimmed spur gears with inclined webs," *Mechanism and Machine Theory,* vol. 59, pp. 34-47, 2013.

[49] S. K. Tiwari and U. K. Joshi, "Stress analysis of mating involute spur gear teeth," in *International Journal of Engineering Research and Technology*, 2012.

[50] W. D. Mark, H. Lee, R. Patrick, and J. D. Coker, "A simple frequency-domain algorithm for early detection of damaged gear teeth," *Mechanical systems and signal processing,* vol. 24, pp. 2807-2823, 2010.

[51] M. Asmine, J. Brochu, J. Fortmann, R. Gagnon, Y. Kazachkov, C.-E. Langlois*, et al.*, "Model validation for wind turbine generator models," *Power Systems, IEEE Transactions on,* vol. 26, pp. 1769-1782, 2011.

[52] F. Combet and L. Gelman, "Novel adaptation of the demodulation technology for gear damage detection to variable amplitudes of mesh harmonics," *Mechanical systems and signal processing,* vol. 25, pp. 839-845, 2011.

[53] Y. Lei, D. Kong, J. Lin, and M. J. Zuo, "Fault detection of planetary gearboxes using new diagnostic parameters," *Measurement Science and Technology,* vol. 23, p. 055605, 2012.

[54] P. Tavner, "A survey of wind turbine condition monitoring experience in Europe," in *Wind Turbine Condition Monitoring Workshop*, 2011, pp. 19-21.

[55] O. Ozgener and L. Ozgener, "Exergy and reliability analysis of wind turbine systems: a case study," *Renewable and Sustainable Energy Reviews,* vol. 11, pp. 1811-1826, 2007.

[56] A. Staino, B. Basu, and S. R. Nielsen, "Actuator control of edgewise vibrations in wind turbine blades," *Journal of Sound and Vibration,* vol. 331, pp. 1233-1256, 2012.

[57] S. Sheng and W. Yang, "Wind Turbine Drivetrain Condition Monitoring-An Overview (Presentation)," National Renewable Energy Laboratory (NREL), Golden, CO.2013.

[58] T. Thiringer and J.-Å. Dahlberg, "Periodic pulsations from a three-bladed wind turbine," *Energy conversion, IEEE Transactions on,* vol. 16, pp. 128-133, 2001.

[59] E. Hinrichsen and P. Nolan, "Dynamics and stability of wind turbine generators," *Power Apparatus and Systems, IEEE Transactions on,* pp. 2640-2648, 1982.

[60] A. A. Salem, A. Abu-Siada, and S. Islam, "Condition Monitoring Techniques of the Wind Turbines Gearbox and Rotor," *International Journal of Electrical Energy,* vol. 2, pp. 53-56, 2014.

[61] R. Randall, "A new method of modeling gear faults," *Journal of Mechanical Design,* vol. 104, pp. 259-267, 1982.

[62] P. McFadden, "Detecting fatigue cracks in gears by amplitude and phase demodulation of the meshing vibration," *Journal of Vibration and Acoustics,* vol. 108, pp. 165-170, 1986.

[63] Z. Feng and F. Chu, "Application of atomic decomposition to gear damage detection," *Journal of Sound and Vibration,* vol. 302, pp. 138-151, 2007.

[64] Z. Feng, M. Liang, Y. Zhang, and S. Hou, "Fault diagnosis for wind turbine planetary gearboxes via demodulation analysis based on ensemble empirical

mode decomposition and energy separation," *Renewable Energy,* vol. 47, pp. 112-126, 2012.

[65] Z. Feng, M. J. Zuo, and F. Chu, "Application of regularization dimension to gear damage assessment," *Mechanical Systems and Signal Processing,* vol. 24, pp. 1081-1098, 2010.

[66] Z. Feng, M. J. Zuo, R. Hao, F. Chu, and M. El Badaoui, "Gear damage assessment based on cyclic spectral analysis," *Reliability, IEEE Transactions on,* vol. 60, pp. 21-32, 2011.

[67] G. Mandic, A. Nasiri, E. Muljadi, and F. Oyague, "Active torque control for gearbox load reduction in a variable-speed wind turbine," *Industry Applications, IEEE Transactions on,* vol. 48, pp. 2424-2432, 2012.

[68] H. Endo and R. Randall, "Enhancement of autoregressive model based gear tooth fault detection technique by the use of minimum entropy deconvolution filter," *Mechanical Systems and Signal Processing,* vol. 21, pp. 906-919, 2007.

[69] W. Wang and P. McFadden, "Application of wavelets to gearbox vibration signals for fault detection," *Journal of Sound and Vibration,* vol. 192, pp. 927-939, 1996.

[70] R. Yan and R. X. Gao, "Harmonic wavelet-based data filtering for enhanced machine defect identification," *Journal of Sound and Vibration,* vol. 329, pp. 3203-3217, 2010.

[71] Y. Lu, X. Wang, J. Tang, and Y. Ding, "Damage detection using piezoelectric transducers and the Lamb wave approach: II. Robust and quantitative decision making," *Smart Materials and Structures,* vol. 17, p. 025034, 2008.

[72] D. E. Newland, "Harmonic wavelet analysis," in *Proceedings of the Royal Society of London A: Mathematical, Physical and Engineering Sciences*, 1993, pp. 203-225.

[73] D. E. Newland, "Harmonic and musical wavelets," in *Proceedings of the Royal Society of London A: Mathematical, Physical and Engineering Sciences*, 1994, pp. 605-620.

[74] S. Mallat and W. L. Hwang, "Singularity detection and processing with wavelets," *Information Theory, IEEE Transactions on,* vol. 38, pp. 617-643, 1992.

[75] D. L. Donoho, "De-noising by soft-thresholding," *Information Theory, IEEE Transactions on,* vol. 41, pp. 613-627, 1995.

[76] J. Zhu, J. M. Yoon, D. He, and E. Bechhoefer, "Online particle-contaminated lubrication oil condition monitoring and remaining useful life prediction for wind turbines," *Wind Energy,* vol. 18, pp. 1131-1149, 2015.

[77] H. Shah and H. Hirani, "Online condition monitoring of spur gears," *International Journal of Condition Monitoring,* vol. 4, pp. 15-22, 2014.

[78] Y. Zhan and V. Makis, "A robust diagnostic model for gearboxes subject to vibration monitoring," *Journal of Sound and vibration,* vol. 290, pp. 928-955, 2006.

[79] L. Gelman, R. Zimroz, J. Birkel, H. Leigh-Firbank, D. Simms, B. Waterland*, et al.*, "Adaptive vibration condition monitoring technology for local tooth damage in gearboxes," *Insight-Non-Destructive Testing and Condition Monitoring,* vol. 47, pp. 461-464, 2005.

[80] D. R. Barron, *Engineering condition monitoring: practice, methods and applications*: Longman, 1996.

[81] G. Luo, D. Osypiw, and M. Irle, "Real-time condition monitoring by significant and natural frequencies analysis of vibration signal with wavelet filter and autocorrelation enhancement," *Journal of Sound and Vibration,* vol. 236, pp. 413-430, 2000.

[82] J. D. Smith, *Vibration measurement and analysis*: Butterworths, 1989.

[83] J. M. e Silva, "Machinery Vibration Measurements and Analysis," in *Vibration and Wear in High Speed Rotating Machinery*, ed: Springer, 1990, pp. 221-239.

[84] T. G. Habetler, "Effects of time-varying loads on rotor fault detection in induction machines," *Industry Applications, IEEE Transactions on,* vol. 31, pp. 900-906, 1995.

[85] R. G. T. De Almeida, S. A. da Silva Vicente, and L. R. Padovese, "New technique for evaluation of global vibration levels in rolling bearings," *Shock and Vibration,* vol. 9, pp. 225-234, 2002.

[86] Z. Liu, X. Yin, Z. Zhang, D. Chen, and W. Chen, "Online rotor mixed fault diagnosis way based on spectrum analysis of instantaneous power in squirrel cage induction motors," *Energy Conversion, IEEE Transactions on,* vol. 19, pp. 485-490, 2004.

[87] Z. Peng, N. Kessissoglou, and M. Cox, "A study of the effect of contaminant particles in lubricants using wear debris and vibration condition monitoring techniques," *Wear,* vol. 258, pp. 1651-1662, 2005.

[88] D. P. Walsh, "Oil Analysis 101," *Orbit,* vol. 25, pp. 50-55, 2005.

[89] L. A. Toms and A. M. Toms, *Machinery Oil Analysis: Methods, Automation and Benefits: a Guide for Maintenance Managers, Supervisors & Technicians*: Society of Tribologists and Lubrication Engineers, 2008.

[90] *Machinery Lubrication, accessed from http://www.machinerylubrication.com on June 11, 2015*.

[91] C. C. Ciang, J.-R. Lee, and H.-J. Bang, "Structural health monitoring for a wind turbine system: a review of damage detection methods," *Measurement Science and Technology,* vol. 19, p. 122001, 2008.

[92] R. Sharma and U. Madawala, "The concept of a smart wind turbine system," *Renewable Energy,* vol. 39, pp. 403-410, 2012.

[93] F. Besnard and L. Bertling, "An approach for condition-based maintenance optimization applied to wind turbine blades," *Sustainable Energy, IEEE Transactions on,* vol. 1, pp. 77-83, 2010.

[94] P. Schubel, R. Crossley, E. Boateng, and J. Hutchinson, "Review of structural health and cure monitoring techniques for large wind turbine blades," *Renewable Energy,* vol. 51, pp. 113-123, 2013.

[95] A. McIlhagger, D. Brown, and B. Hill, "The development of a dielectric system for the on-line cure monitoring of the resin transfer moulding process," *Composites Part A: Applied Science and Manufacturing,* vol. 31, pp. 1373-1381, 2000.

[96] V. Antonucci, M. Giordano, A. Cusano, J. Nasser, and L. Nicolais, "Real time monitoring of cure and gelification of a thermoset matrix," *Composites science and technology,* vol. 66, pp. 3273-3280, 2006.

[97] R. Harrold and Z. Sanjana, "Acoustic waveguide monitoring of the cure and structural integrity of composite materials," *Polymer Engineering & Science,* vol. 26, pp. 367-372, 1986.

[98] D. D. Shepard and K. R. Smith, "Ultrasonic cure monitoring of advanced composites," *Sensor Review,* vol. 19, pp. 187-194, 1999.

[99] T. Thiringer and J. Linders, "Control by variable rotor speed of a fixed-pitch wind turbine operating in a wide speed range," *Energy Conversion, IEEE Transactions on,* vol. 8, pp. 520-526, 1993.

[100] J. Wu and F. Lai, "Fatigue Life Analysis of Small Composite Sandwich Wind Tuebine Blades," *Procedia Engineering,* vol. 14, pp. 2014-2020, 2011.

[101] G. Gualtieri and S. Secci, "Wind shear coefficients, roughness length and energy yield over coastal locations in Southern Italy," *Renewable Energy,* vol. 36, pp. 1081-1094, 2011.

[102] F. R. Marzabadi, M. Soltani, and M. Masdari, "Experimental Investigation of the Leadingedge Roughness on the Boundary Layer of a Plunging Airfoil," in *27th International Congress of the Aeronautical Sciences*, 2010, pp. 1-7.

[103] R. Van Rooij and W. Timmer, "Roughness sensitivity considerations for thick rotor blade airfoils," *Journal of Solar Energy Engineering,* vol. 125, pp. 468-478, 2003.

[104] N. Ren and J. Ou, "Dust effect on the performance of wind turbine airfoils," *Journal of Electromagnetic Analysis and Applications,* vol. 1, p. 102, 2009.

[105] G. Mohammed and M. Aboelyazied, "Effect of dust on the performance of wind turbines," *Desalination,* vol. 209, pp. 209-220, 2007.

[106] L. Battisti, *Wind Turbines in Cold Climates: Icing Impacts and Mitigation Systems*: Springer, 2015.

[107] T. Laakso, H. Holttinen, G. Ronsten, L. Tallhaug, R. Horbaty, I. Baring-Gould*, et al.*, "State-of-the-art of wind energy in cold climates," *IEA annex XIX,* vol. 24, 2003.

[108] H. Seifert, "Technical requirements for rotor blades operating in cold climate," *BOREAS VI,* vol. 9, 2003.

[109] B. Tammelin, M. Cavaliere, H. Holtinnen, C. Morgan, H. Seifert, and K. Säntti, "Wind Energy in Cold Climate, Final Report WECO (JOR3-CT95-0014)," ISBN 951-679-518-6, Finnish Meteorological Institute, Helsinki, Finland2000.

[110] J. F. Maissan, "Wind power development in sub-arctic conditions with severe rime icing," *Northern Review,* 2002.

[111] H. Dobesch and G. Kury, *Basic meteorological concepts and recommendations for the exploitation of wind energy in the atmospheric boundary layer*: Zentralanstalt für Meteorologie und Geodynamik, 2006.

[112] R. X. Gao and R. Yan, *Wavelets: Theory and applications for manufacturing*: Springer Science & Business Media, 2010.

[113] D. E. Newland, *An introduction to random vibrations, spectral & wavelet analysis*: Courier Dover Publications, 2012.

[114] J. Lin, "An integrated time domain averaging scheme for gearbox diagnosis," in *Reliability, Maintainability and Safety, 2009. ICRMS 2009. 8th International Conference on*, 2009, pp. 808-812.

[115] E. Sreejith, A. Verma, and A. Srividya, "Fault diagnosis of rolling element bearing using time-domain features and neural networks," in *Industrial and Information Systems, 2008. ICIIS 2008. IEEE Region 10 and the Third international Conference on*, 2008, pp. 1-6.

[116] C. Kral, T. G. Habetler, and R. G. Harley, "Detection of mechanical imbalances of induction machines without spectral analysis of time-domain signals," *Industry Applications, IEEE Transactions on,* vol. 40, pp. 1101-1106, 2004.

[117] C. Burrus and T. W. Parks, *DFT/FFT and Convolution Algorithms: theory and Implementation*: John Wiley & Sons, Inc., 1991.

[118] K. Fyfe and E. Munck, "Analysis of computed order tracking," *Mechanical Systems and Signal Processing,* vol. 11, pp. 187-205, 1997.

[119] K. Bossley, R. Mckendrick, C. Harris, and C. Mercer, "Hybrid computed order tracking," *Mechanical systems and signal processing,* vol. 13, pp. 627-641, 1999.

[120] C. L. Nikias and J. M. Mendel, "Signal processing with higher-order spectra," *IEEE Signal processing magazine,* vol. 10, pp. 10-37, 1993.

[121] P. Saavedra and C. Rodriguez, "Accurate assessment of computed order tracking," *Shock and Vibration,* vol. 13, pp. 13-32, 2006.

[122] B. Eggers, P. Heyns, and C. Stander, "Using computed order tracking to detect gear condition aboard a dragline," *JOURNAL-SOUTH AFRICAN INSTITUTE OF MINING AND METALLURGY,* vol. 107, p. 115, 2007.

[123] R. S. Pathak, *The wavelet transform* vol. 4: Springer Science & Business Media, 2009.

[124] K. Shukla and A. K. Tiwari, *Efficient Algorithms for Discrete Wavelet Transform: With Applications to Denoising and Fuzzy Inference Systems*: Springer Science & Business Media, 2013.

[125] R. Roberts and C. Mullis, "Digital Signal Processing. Addition," ed: Wesley Publishing Company, 1987.

[126] I. Daubechies, *Ten lectures on wavelets* vol. 61: SIAM, 1992.

[127] C. K. Chui, *Wavelets: a mathematical tool for signal analysis* vol. 1: Siam, 1997.

[128] K. Gurley and A. Kareem, "Applications of wavelet transforms in earthquake, wind and ocean engineering," *Engineering structures,* vol. 21, pp. 149-167, 1999.

[129] S. Mallat, *A wavelet tour of signal processing*: Academic press, 1999.

[130] M. Misiti, Y. Misiti, G. Oppenheim, and J.-M. Poggi, "Wavelet toolbox," *The MathWorks Inc., Natick, MA,* 1996.

[131] W. G. G, "Wavelets and Other Orthogonal Systems with Application," ed: CRC Press boca raton, 1994.

[132] S. Gopalakrishnan and M. Mitra, *Wavelet Methods for Dynamical Problems: With Application to Metallic, Composite, and Nano-Composite Structures*: CRC Press, 2010.

[133] W. Yang, P. Tavner, and M. Wilkinson, "Condition monitoring and fault diagnosis of a wind turbine synchronous generator drive train," *Renewable Power Generation, IET,* vol. 3, pp. 1-11, 2009.

[134] J. A. Antonino-Daviu, M. Riera-Guasp, J. R. Folch, and M. P. M. Palomares, "Validation of a new method for the diagnosis of rotor bar failures via wavelet transform in industrial induction machines," *Industry Applications, IEEE Transactions on,* vol. 42, pp. 990-996, 2006.

[135] R. Supangat, "On-line condition monitoring and detection of stator and rotor faults in induction motors," 2008.

[136] S. Santoso, E. J. Powers, W. M. Grady, and A. C. Parsons, "Power quality disturbance waveform recognition using wavelet-based neural classifier. I. Theoretical foundation," *Power Delivery, IEEE Transactions on,* vol. 15, pp. 222-228, 2000.

[137] S. Sardy, P. Tseng, and A. Bruce, "Robust wavelet denoising," *Signal Processing, IEEE Transactions on,* vol. 49, pp. 1146-1152, 2001.

[138] M. J. Shensa, "The discrete wavelet transform: wedding the a trous and Mallat algorithms," *Signal Processing, IEEE Transactions on,* vol. 40, pp. 2464-2482, 1992.

[139] S. Santoso, E. J. Powers, W. M. Grady, and P. Hofmann, "Power quality assessment via wavelet transform analysis," *Power Delivery, IEEE Transactions on,* vol. 11, pp. 924-930, 1996.

[140] S. G. Mallat, "A theory for multiresolution signal decomposition: the wavelet representation," *Pattern Analysis and Machine Intelligence, IEEE Transactions on,* vol. 11, pp. 674-693, 1989.

[141] I. Daubechies, "The wavelet transform, time-frequency localization and signal analysis," *Information Theory, IEEE Transactions on,* vol. 36, pp. 961-1005, 1990.

[142] S. G. Khalaf and W. P. Hew, "Wavelet fault diagnosis and tolerant of induction motor: A review," *International Journal of Physical Sciences,* vol. 6, pp. 358-376, 2011.

[143] R. B. Randall, *Vibration-based condition monitoring: industrial, aerospace and automotive applications*: John Wiley & Sons, 2011.

[144] R. B. Randall and J. Antoni, "Rolling element bearing diagnostics—a tutorial," *Mechanical Systems and Signal Processing,* vol. 25, pp. 485-520, 2011.

[145] J. Antoni and R. Randall, "The spectral kurtosis: application to the vibratory surveillance and diagnostics of rotating machines," *Mechanical Systems and Signal Processing,* vol. 20, pp. 308-331, 2006.

[146] M. Lebold, K. McClintic, R. Campbell, C. Byington, and K. Maynard, "Review of vibration analysis methods for gearbox diagnostics and prognostics," in *Proceedings of the 54th Meeting of the Society for Machinery Failure Prevention Technology*, 2000, p. 16.

[147] P. McFadden, "Window functions for the calculation of the time domain averages of the vibration of the individual planet gears and sun gear in an epicyclic gearbox," *Journal of Vibration and Acoustics,* vol. 116, pp. 179-187, 1994.

[148] E. Hau, *Wind TurbinesFundamentals, Technologies,Application, Economics*: Springer Heidelberg New York Dordrecht London, 2013.

[149] "Annual Report 2012, Centre for Ships and Ocean Structures Cesos. Available: http://www.cesos.ntnu.no," NTNU-Trondheim, Norwegian University of science and Technology2012.

[150] E. Becker and P. Poste, "Keeping the blades turning: Condition monitoring of wind turbine gears," *Refocus,* vol. 7, pp. 26-32, 2006.

[151] J. Derek Smith, "Gear Noise and Vibration," ed: Marcel Dekker, Inc, 1999.

[152] M. Entezami, S. Hillmansen, P. Weston, and M. P. Papaelias, "Fault detection and diagnosis within a wind turbine mechanical braking system using condition monitoring," *Renewable Energy,* vol. 47, pp. 175-182, 2012.

[153] I. Standard, "61400-1. Wind turbines e part 1: design requirements," ed: International Electrotechnical Commission, 2005, p. 90.

[154] H. Henao, G.-A. Capolino, M. Fernandez-Cabanas, F. Filippetti, C. Bruzzese, E. Strangas*, et al.*, "Trends in fault diagnosis for electrical machines: a review of diagnostic techniques," *IEEE industrial electronics magazine,* vol. 8, pp. 31-42, 2014.

[155] A. R. Nejad, Y. Xing, Y. Guo, J. Keller, Z. Gao, and T. Moan, "Effects of floating sun gear in a wind turbine's planetary gearbox with geometrical imperfections," *Wind Energy,* vol. 18, pp. 2105-2120, 2015.

[156] M. d. S. G. Cascales, *Soft Computing Applications for Renewable Energy and Energy Efficiency*: IGI Global, 2014.

[157] D. McMillan and G. W. Ault, "Quantification of condition monitoring benefit for offshore wind turbines," *Wind Engineering,* vol. 31, pp. 267-285, 2007.

Appendix A

AC133 Series

Low & High Frequency Accelerometer, Top Exit Connector, 500 mV/g

Product Features

Designed for low speed Rotors, Main Bearings, and Gear Box Inputs, but can also be used for High Frequency Detection.

Figure A.1 Accelerometer model AC133

- 500 mV/g Sensitivity, ±10% Sensitivity
- 0.1 Hz for Low Frequency Measurements
- 10,000 Hz for High Frequency Detection

Table A.1 Accelerometer model AC133 specification

Specifications	Standard	Metric
Part Number	AC133-1D	M/AC133-1D
Sensitivity (±10%)	500 mV/g	
Frequency Response (±3dB) Frequency Response (±10%)	6-600,000 CPM 36-180,000 CPM	0,1-10000 Hz 0,6-3000 Hz
Dynamic Range	± 10 g, peak	
Electrical		
Settling Time	<2 Seconds	
Voltage Source (IEPE)	18-30 VDC	
Constant Current Excitation	2-10 mA	
Spectral Noise @ 10 Hz	1.7 µg/√Hz	
Spectral Noise @ 100 Hz	0.2 µg/√Hz	
Spectral Noise @ 1000 Hz	0.12 µg/√Hz	
Output Impedance	<100 ohm	
Bias Output Voltage	10-14 VDC	
Case Isolation	$>10^8$ ohm	

Table A.2 Accelerometer model AC133 specification (continue)

Specifications	Standard	Metric
Environmental		
Temperature Range	-58 to 250°F	-50 to 121°C
Maximum Shock Protection	5,000 g, peak	
Electromagnetic Sensitivity	CE	
Sealing	IP68	
Physical		
Sensing Element	PZT Ceramic	
Sensing Structure	Shear Mode	
Weight	3.25 oz	92 grams
Case Material	316L Stainless Steel	
Mounting	1/4-28	
Connector (non-integral)	2 Pin MIL-C-5015	
Resonant Frequency	1,080,000 CPM	18000 Hz
Mounting Torque	2 to 5 ft. lbs.	2,7 to 6,8 Nm
Mounting Hardware	1/4-28 Stud	M6x1 Adapter Stud
Calibration Certificate	CA10	

Oil Lubrication

Table A.3 Typical oil properties

Synthetic oils (lifetime lubrication)	
MAKE	TYPE
SHELL	TIVELA OIL S 320
IP	TELIUM OIL VSF 320
KLÜBER	SYNTHESO D 320 EP
BP	ENERGOL SGXP 320
TEXACO	SYNLUBE CLP 320

Table A.4 Typical oil properties

TYPICAL OIL PROPERTIES SHELL TIVELA S 320	
Volumic mass (kg/dmc) SHELL	1.069
Kinematic viscosity at 40 °C	321 cSt
Pour point	- 39 °C
Viscosity index	230
Flash point (c.o.c)	286 °C
FZG test overcomes the stage	> 12

Torque transducer specification

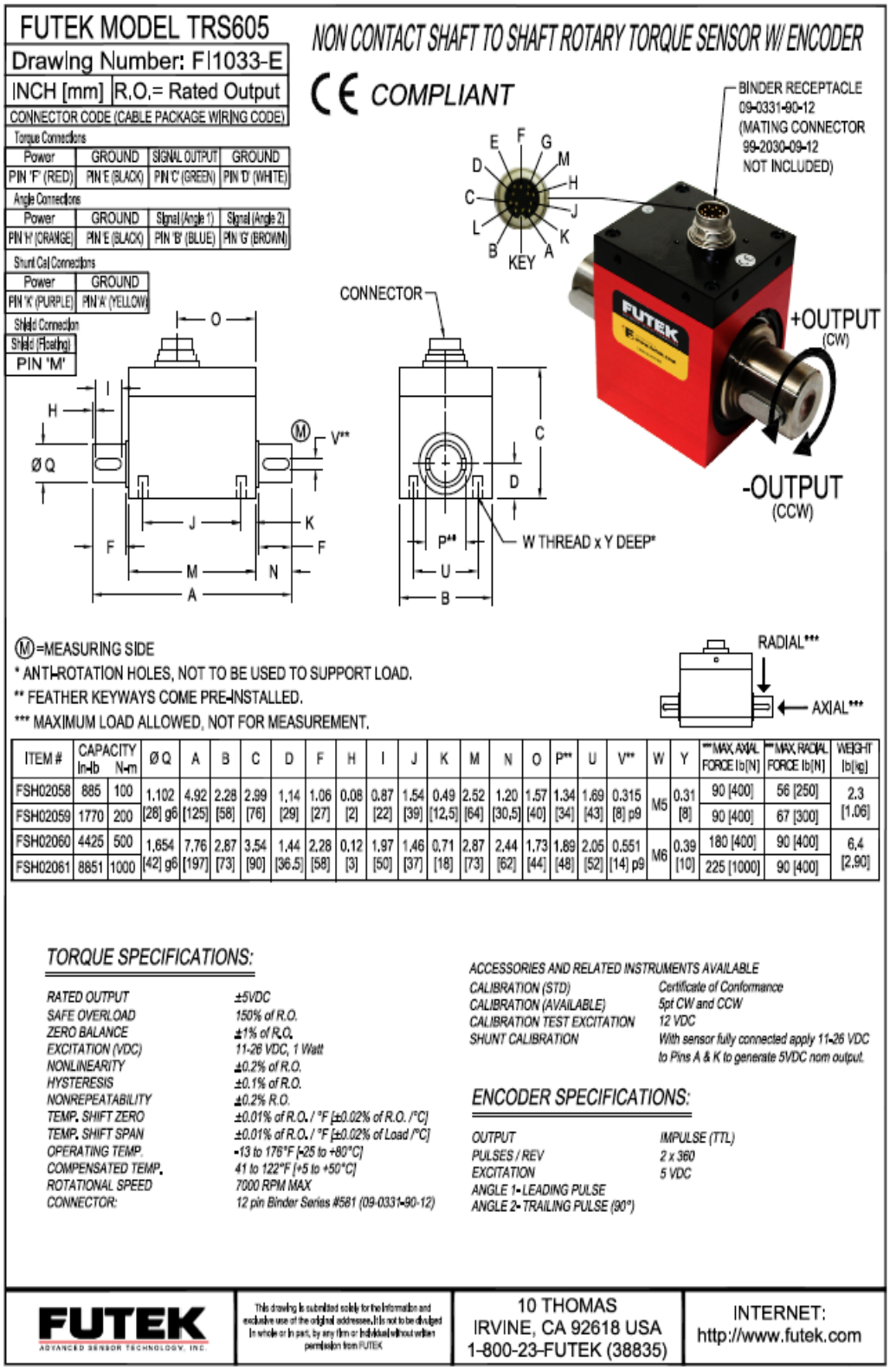

ITEM #	CAPACITY lb-in	CAPACITY N-m	ØQ	A	B	C	D	F	H	I	J	K	M	N	O	P**	U	V**	W	Y	*** MAX. AXIAL FORCE lb [N]	*** MAX. RADIAL FORCE lb [N]	WEIGHT lb [kg]
FSH02058	885	100	1.102 [28] g6	4.92 [125]	2.28 [58]	2.99 [76]	1.14 [29]	1.06 [27]	0.08 [2]	0.87 [22]	1.54 [39]	0.49 [12,5]	2.52 [64]	1.20 [30,5]	1.57 [40]	1.34 [34]	1.69 [43]	0.315 [8] p9	M5	0.31 [8]	90 [400]	56 [250]	2.3 [1.06]
FSH02059	1770	200																			90 [400]	67 [300]	
FSH02060	4425	500	1.654 [42] g6	7.76 [197]	2.87 [73]	3.54 [90]	1.44 [36.5]	2.28 [58]	0.12 [3]	1.97 [50]	1.46 [37]	0.71 [18]	2.87 [73]	2.44 [62]	1.73 [44]	1.89 [48]	2.05 [52]	0.551 [14] p9	M6	0.39 [10]	180 [400]	90 [400]	6.4 [2.90]
FSH02061	8851	1000																			225 [1000]	90 [400]	

TORQUE SPECIFICATIONS:

RATED OUTPUT	±5VDC
SAFE OVERLOAD	150% of R.O.
ZERO BALANCE	±1% of R.O.
EXCITATION (VDC)	11-26 VDC, 1 Watt
NONLINEARITY	±0.2% of R.O.
HYSTERESIS	±0.1% of R.O.
NONREPEATABILITY	±0.2% R.O.
TEMP. SHIFT ZERO	±0.01% of R.O. / °F [±0.02% of R.O. /°C]
TEMP. SHIFT SPAN	±0.01% of R.O. / °F [±0.02% of Load /°C]
OPERATING TEMP.	-13 to 176°F [-25 to +80°C]
COMPENSATED TEMP.	41 to 122°F [+5 to +50°C]
ROTATIONAL SPEED	7000 RPM MAX
CONNECTOR:	12 pin Binder Series #581 (09-0331-90-12)

ACCESSORIES AND RELATED INSTRUMENTS AVAILABLE

CALIBRATION (STD)	Certificate of Conformance
CALIBRATION (AVAILABLE)	5pt CW and CCW
CALIBRATION TEST EXCITATION	12 VDC
SHUNT CALIBRATION	With sensor fully connected apply 11-26 VDC to Pins A & K to generate 5VDC nom output.

ENCODER SPECIFICATIONS:

OUTPUT	IMPULSE (TTL)
PULSES / REV	2 x 360
EXCITATION	5 VDC
ANGLE 1- LEADING PULSE	
ANGLE 2- TRAILING PULSE (90°)	

10 THOMAS
IRVINE, CA 92618 USA
1-800-23-FUTEK (38835)
INTERNET:
http://www.futek.com

Figure A.2 Torque transducer (FUTEK model TRS605)

Electrical Block Diagram (TRD/TRH/TRS 605 model)

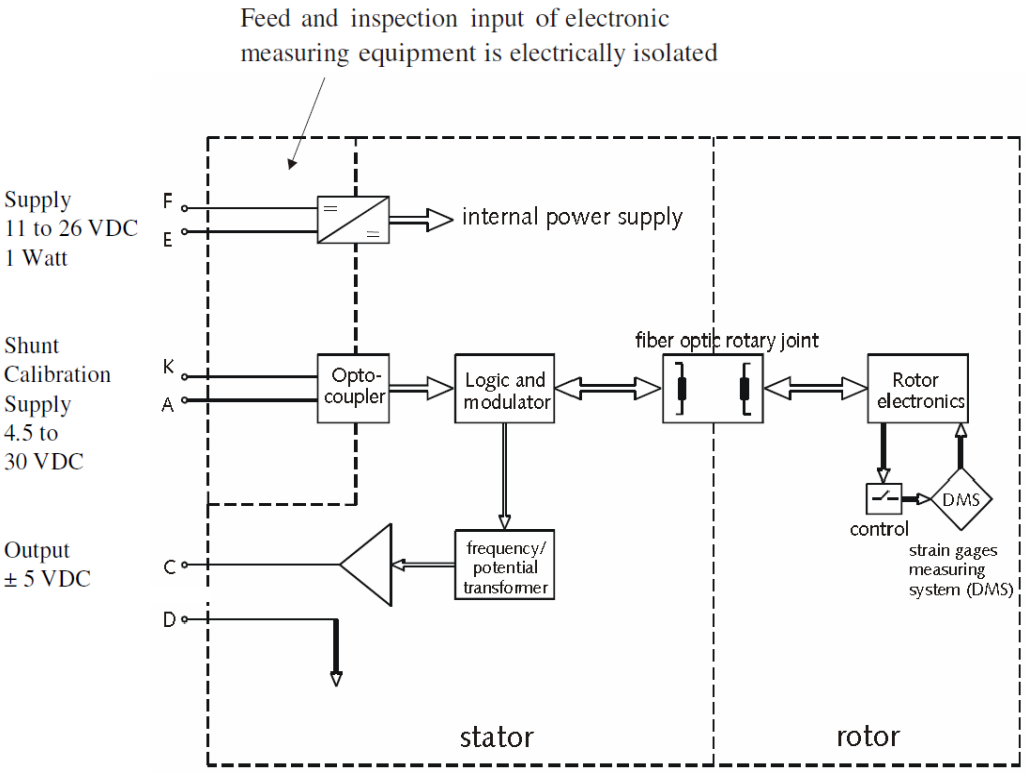

Figure A.3 Torque transducer electrical block diagram.

Figure A.4 Digital tachometer (Digitech QM1448)

Figure A.5 thermal imager Fluke Ti20